Preliminary Surficial Lineaments Mapping for the Maybelle River Area, Northeast Alberta, Using Remote Sensing Data

Alberta Energy and Utilities Board

Alberta Geological Survey

AGS

Preliminary Surficial Lineaments Mapping for the Maybelle River Area, Northeast Alberta, Using Remote Sensing Data

S. Mei, D. Pana, M. Fenton and R. Olson

May 2005

When using information from this publication in other publications or presentations, due acknowledgment should be given to the EUB/AGS. The following reference format is recommended:

Mei, S., Pana, D., Fenton, M. and Olson, R. (2004): Preliminary surficial lineaments mapping for the Maybelle River area, northeast Alberta, using remote sensing data; Alberta Energy and Utilities Board, EUB/AGS Earth Sciences Report 2004-02.

Contents

Acknowledgments

Abstract

This study attempts to

a) evaluate the applicability of RADARSAT-1 images to infer surface 'lineaments' that may reflect bedrock faults in a thick drift covered, highly vegetated area, and
b) provide new structural information that may assist ongoing uranium exploration in the Maybelle River area of northeast Alberta, using remote sensing data including RADARSAT-1 Standard Beam 1 and 7 images, a digital elevation model (DEM) extracted from RADARSAT-1 images, a DEM from Shuttle RADAR Topography Mission (SRTM) and a DEM image based on National Topographic System (NTS).

A total of 388 lineaments were identified; these range in length from 0.8 km to 23 km, with a mean length of 5.7 km. Three prominent lineament trends were recognized: (1) east-northeast, (2) northwest, and (3) north to south trending. The RADARSAT-1 images acquired by the Alberta Geological Survey (AGS) are from different incidence angles and look directions; therefore, surface topographic information can be extracted from them by applying algorithms that contrast differences caused by varying look directions and using DEM extraction methods. The processed RADARSAT-1 images contain information about surficial topography, moisture and land cover type; thus, they are superior to optical satellite images including Landsat images in lineament mapping. The methodology developed in the present study, which combines the use of both RADARSAT-1 images and DEM data derived from RADARSAT-1 images, SRTM and NTS, appears to be useful for lineament detection in thick drift covered and highly vegetated area. This methodology is also potentially applicable to other parts of northern Alberta.

1 Introduction

The Athabasca Basin in Saskatchewan hosts the largest and highest-grade uranium deposit, and the largest uranium mine in the world (Saskatchewan Geological Survey, 1994). The Alberta portion of the Athabasca Basin is approximately 8000 km^2, and much of this area has been re-staked in 2002, indicating renewed interest in uranium exploration. The 'Athabasca unconformity type' uranium deposits occur in the vicinity of the basement unconformity, with ore bodies localized within either or both the Early Proterozoic crystalline basement and the uppermost Early to lowermost Middle Proterozoic Athabasca Group. Previous studies of core by the Alberta Geological Survey (AGS) indicate

a) the main stratigraphic units of the Athabasca Group associated with the uranium deposits in Saskatchewan can be traced into Alberta (Collier, 2004; Ramaekers, 2004); and

b) lithological units of the sub-Athabasca crystalline basement and their geochemical characteristics in the Alberta portion are very similar to the highly prospective Wollaston Fold Belt, which underlies the eastern portion of the Athabasca Basin in northeast Saskatchewan (Pana et al., 2004). The most recent (early 2000s) exploration activities for uranium in Alberta have mainly focused on the Maybelle River area (Figure 1).
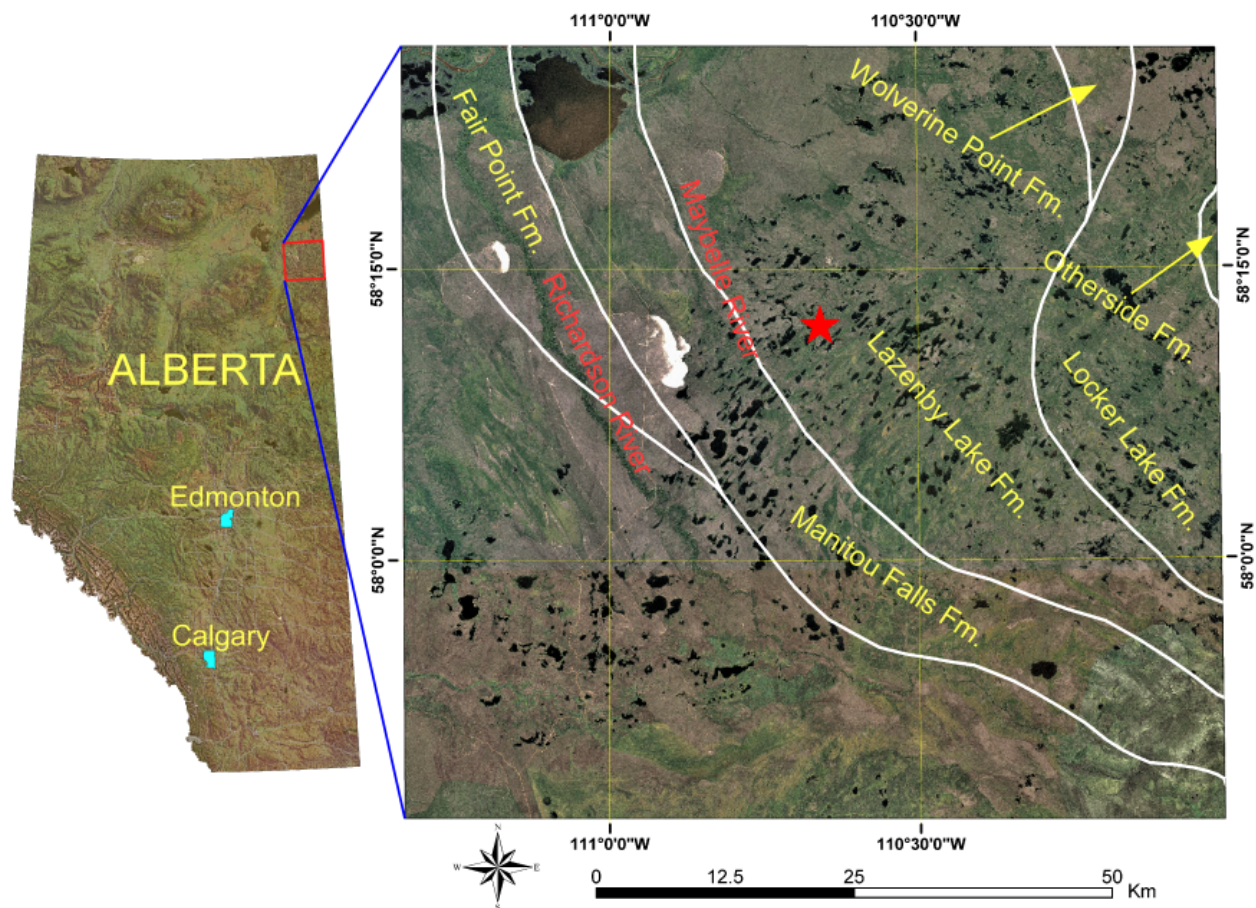
Figure 1. Study area with simplified stratigraphic formation boundaries of the Athabasca Group. The red star indicates the approximate location of the Maybelle uranium zone based on the intersection in drill hole MR-39, which assayed 23% U$_3$O$_8$ across 5 m core length. The two white areas represent active sand dunes.

As part of a strategy to map the surficial and structural geology in northern Alberta, AGS acquired RADARSAT-1 Standard Beam 1 and 7 images in both ascending and descending passes and derived the principal component images from these four beam positions (Grunsky, 2002a, 2002b). Principal component analysis (PCA) is a classical statistical method that produces images (components) that are a linear combination of the input images (Richards, 1986; Gupta, 1991). Previous studies have shown that principal component images derived from radar imagery, acquired by European Remote Sensing (ERS-1) and Canadian Centre of Remote Sensing (CCRS) C-SAR and of different incident angles, look direction, frequencies and polarizations are very useful for highlighting structural features in the Canadian Shield (Masuoka et al., 1988; Harris et al., 1994; Moon et al., 1994), where the drift cover is relatively thin over the bedrock. While most studies have focused on the use of radar for delineating the geological structure, radar imagery has also been used for mapping surficial geology (Graham and Grant, 1994).

Previously, Misra et al. (1991) used Landsat multispectral scanner (MSS), Thematic Mapper (TM) and Seasat satellite radar images to prepare a lineament map of the entire western plains of Alberta, Saskatchewan, part of British Columbia and a portion of the Northwest Territories. In that study, lineaments were visually interpreted on the remotely sensed imagery, and two main lineament trends were identified: one trends northwest and the other northeast. These lineaments were interpreted to be a reflection of basement structures in north-central Alberta dominated by the Peace River Arch comprising a zone of Devonian crustal thinning and arching (Ross, 1990). The RADARSAT-1 principal component imagery acquired by the AGS has been used for structural mapping in the central Alberta Foothills (Paganelli and Rivard, 2002) and the Buffalo Head Hills area (Eccles et al., 2001; Paganelli et al., 2003), and land cover and terrain mapping (Grunsky, 2002b). Paganelli et al. (2003) also identified a northwest- and northeast-trending lineament conjugate set and two additional north-northeast- and east-northeast-trending lineament sets from the Buffalo Head Hills area, which is covered by thick drift and highly vegetated. In that study, the lineaments were interpreted visually based on principal component 1, 2, 3 and 4 images derived from RADARSAT-1 standard beam 1 and 7, ascending and descending images. Card et al. (2003) used DEM derived from Shuttle Radar Topography Mission (STRM) for regional lineament analysis of the western Athabasca Basin within Saskatchewan.

AGS has compiled surficial lineaments previously interpreted from satellite images and old photos for Alberta (AGS, 2003; AGS, 2004, working files by Pana and Waters). The lineaments have been digitized and stored in GIS format. The previously interpreted lineaments for the Maybelle river area, as shown in Figure 2, are not adequate in light of accuracy and detail for the ongoing uranium exploration.

The present study has two objectives:

1. further evaluate the applicability of the existing RADARSAT-1 images of AGS for structural mapping in an area of thick drift covered, such as the Maybelle River area

2. attempt to provide supplementary structural information to assist industry in their ongoing exploration for uranium in the Maybelle River area

In contrast to the Canadian Shield north of Lake Athabasca, the Maybelle River area is blanketed by thick sandy drift (Bayrock, 1970a, 1970b) and is moderately to highly vegetated. The selected study area (Figure 1) includes an area from 57^045' north latitude to 58^026' north latitude and from 111^020' west longitude to 110^0 west longitude. In addition to the existing AGS RADARSAT-1 imagery and newly generated principal component images, DEM images were extracted from the RADARSAT-1 images. DEM from Shuttle RADAR Topography Mission (SRTM) and a DEM image based on National Topographic System (NTS) maps at the 1:250,000 scale, were also used for lineaments detection and comparison.
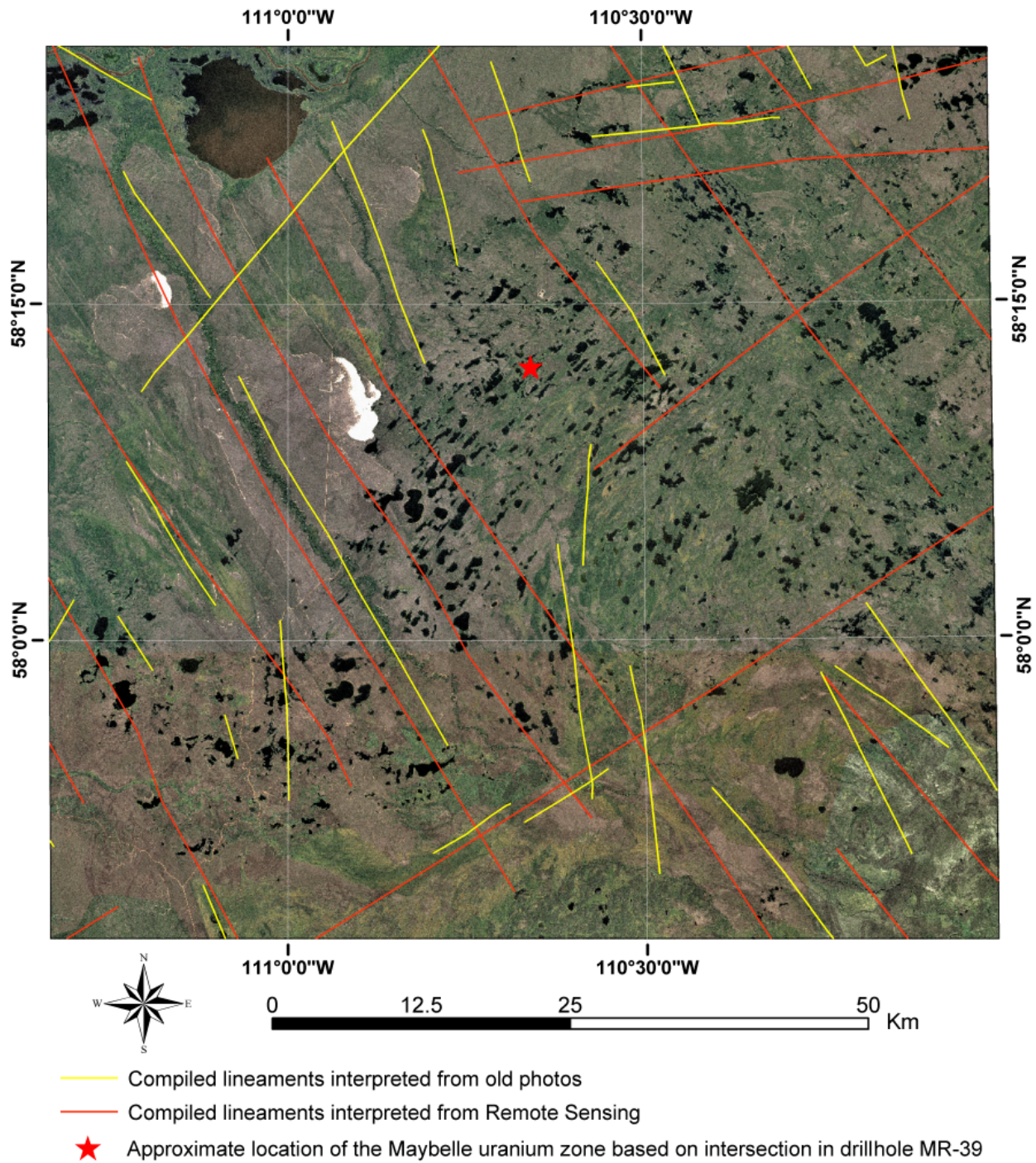
Figure 2. Compiled lineaments interpreted from old photos (AGS, working file by Pana and Waters) and old remote sensing data (Misra et al., 1991; AGS, 2003).

2   Regional Geology

The bedrock within the study area includes Early Proterozoic crystalline basement of the Taltson Magmatic Zone, the overlying late Early Proterozoic to early Middle Proterozoic Athabasca Group and Devonian rocks. The northeastern half of the study area is underlain by nearly flat-lying quartzose sandstone and minor conglomerate of the Athabasca Group (Figure 1), which unconformably overlies the Early Proterozoic crystalline rocks. The eastern part of the southwestern half of the study area is underlain by Early Proterozoic rocks, which include granitic rocks, granite gneiss of various types, quartzite, schist and amphibolite. The western part of the southwestern half of the study area is underlain by mainly Devonian carbonate and evaporate sedimentary rocks. In general, bedrock within the study area is extensively covered by Pleistocene glacial deposits and recent alluvial deposits. The main exception is at the Marguerite River area, which is in the central-southernmost part of the study area. At this locale, granite and gneiss of probably Early Proterozoic crop out on the stoss sides of hills and knolls.

The surficial geology was mapped by Bayrock (1970a, 1970b). Pleistocene deposits include aeolian sands, glacial moraine (i.e., lodgement and other till types), glacio-lacustrine and glacio-fluvial deposits. The central part of the study area is underlain by well-defined drumlins and flutings (Figure 3). Bayrock (1970a) mapped this area as thick to very thick outwash sand and gravel that had been subsequently overridden by a glacier advance. Surrounding this location is a large area stretching from the eastern part of the study area to the southwest (Figure 3), which was mapped as ice-contact deposits (Bayrock, 1970a, 1970b). This area comprises a complex of kame moraines, eskers, Moulin kames and crevasse fillings of sand and gravel to coarse boulder gravel. The kame deposits range between 30 and 180 metres thick, forming a series of northwest-trending end moraines in continuation with the Cree Lake Moraine of northwestern Saskatchewan (Bayrock, 1970a). The ice-contact deposits are flanked by level to gently undulating outwash sand and gravel on both the north and south sides (Figure 3). In general, the glacial deposits thicken towards the north. The rest of the study area, mainly to the west, is dominated by medium-grained quartzitic sand in sheet and dune forms. The northwestern corner of the study area is underlain by recent deltaic sediments. Most of the surficial deposits described above are mantled by lakes, organic deposits, including marshes, swamps, bogs and fens in poorly drained areas, and jack pine forest in well-drained highlands.

Some insights can be gained in the glacial history of the study area by draping the surficial geological map over the RADARSAT-1 principal component 3 (PC3) image (Figure 3). The PC3 image processed for this area highlights geomorphological features and has proven useful for surficial mapping (M.M. Fenton and J.G. Pawlowicz, personal communication, 2003). On the PC3 image, drumlins and flutings are well defined in the central part of the study area. This area was mapped as Unit 3 by Bayrock (1970a) for NTS 74L and Unit 6 by Bayrock (1970b) for NTS 74E. The PC3 image also shows that the ice-contact deposits, which were mapped as Unit 2 by Bayrock (1970a) for NTS 74L and Unit 5 by Bayrock (1970b) for NTS 74E, drape over the drumlins and fluted unit. An esker cuts through the drumlins and fluted unit in the western part. The well developed drumlins and flutings, and the interpreted genetic relations among different units (see below), suggest that the drumlins and fluted unit is very likely to be the Fluted Moraine (MF) Class based on the new glaciogenetic scheme the AGS has recently developed for northern Alberta surficial mapping (Roger Paulen, personal communication, 2004). However, ground truthing needs to be carried out in the Maybelle River area to confirm whether this suggested interpretation is correct.

Surrounding the drumlins and fluted unit are ice-contact deposits; these are characterized by a series of north-west–trending ridges on the PC3 image. This confirms that the eastern part of this unit forms
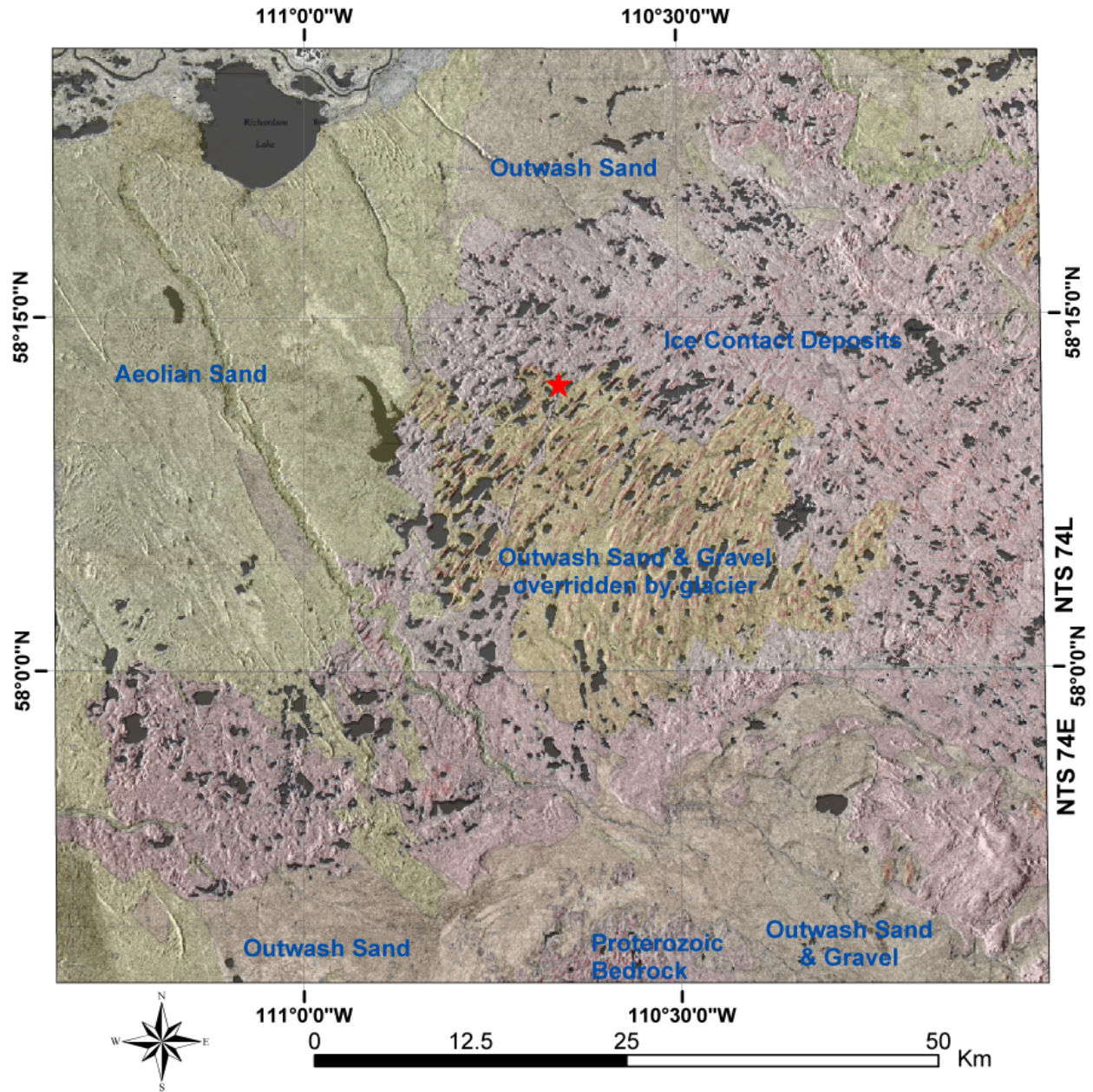
Figure 3. Surficial geological map draped over RADARSAT-1 principal component 3 image. Surficial geology is from Bayrock (1970a, 1970b). The red star indicates the approximate location of the Maybelle uranium zone based on the intersection in drillhole MR-39.

a series of north-west–trending moraines in continuation with the Creek Lake Moraine in northwestern Saskatchewan. A west-facing escarpment or ridge is clearly seen in the northeast of the study area on the PC3 image. It probably represents a major component of this end moraine complex. As mentioned previously, the ice-contact deposits unit is shown to drape over the drumlins and fluted unit (Figure 3). This indicates that the drumlins and fluted unit were formed during a glacier advance through the area and the ice-contact unit was deposited as end moraine later, during the overall melting back of the glacier. Finally, it is obvious that the glacier was retreating from southwest to northeast.

The outwash sand to the north and south of the ice-contact deposits, is mapped as Unit 5 for NTS 74L by Bayrock (1970a) and Unit 7 and 8 for NTS 74E by Bayrock (1970b). Hints of outwash channels can be seen on the PC3 image, confirming Bayrock's (1970a) assignment. This unit is shown to drape over the ice-contact deposits unit in both the northern and southern parts of the study area. This indicates that the outwash sand unit was deposited after the ice-contact deposits unit.

It is clear on the PC3 image that the aeolian deposits, mapped as Unit 9 for NTS 74L by Bayrock (1970a) and Unit 12 for NTS 74E by Bayrock (1970b), drape over the ice-contact deposits unit and the outwash sand unit, indicating that the aeolian deposits took place after the glacier deposition.

3 Methodology

Surficial lineaments are linear features that can be picked out as lines in aerial or space imagery (Heddi et al., 1999; Casas et al., 2000). They appear as lines or are evident because of contrasts in terrain or ground cover on either side. Angular breaks in drainage patterns, straight stream segments, linear cliffs or escarpments, or abrupt changes in vegetation, land cover type, or moisture patterns may all indicate lineaments. The causes for lineaments can be geological, man-made or some unknown factors. Of the most interest to geologists are those related to faults and joints of bedrock. In areas of none or very thin surficial material cover and/or less vegetation, these structural lineaments can be visible in several ways. Being zones of weak structure, they may be scoured out by glacial action or opened up and enlarged by erosion. Some may even become small valleys or filled by water to become elongated lakes. Groundwater may invade and gouge the fragmented rock or seep into the joints, causing periodic dampness. Vegetation can then develop in this moisture-rich soil, so that at certain times of the year linear features are enhanced. All of these conditions can be detected either visually or digitally in aerial or space imagery. A good example is an area north of Athabasca Lake, as shown in Figure 4. In this area, the structural lineaments of the Proterozoic crystalline Shield rocks are clearly shown on the PC3 image.

In dramatic contrast to the area north of Athabasca Lake, most of the study area is covered by thick glacial drift (Bayrock, 1970a, 1970b). As a result, the structural lineaments from the bedrock of the Athabasca Group would have been mostly masked by the glacial deposits. This is confirmed by examining an area, including a south-central portion of the study area (Figure 5). In this area, Possibly Proterozoic bedrock is exposed in the central part and covered by surficial material in the surrounding area. The bedrock structural lineaments are clearly displayed in the exposed area, but stop and disappear in the surrounding area, which is covered by Pleistocene and Quaternary sediments.

Nonetheless, even with the thick drift, a preliminary examination of the available images for the study area shows there are in fact numerous surficial lineaments. Most of these lineaments can be attributed to glacial processes, including fluting, crevasse filling, end moraine margins and meltwater channels. In contrast, some other lineaments are more obviously caused by wind (e.g., linear sand dunes), streams and fire tracks. From Figure 3 it can be observed that the lineaments represented by linear sand dunes
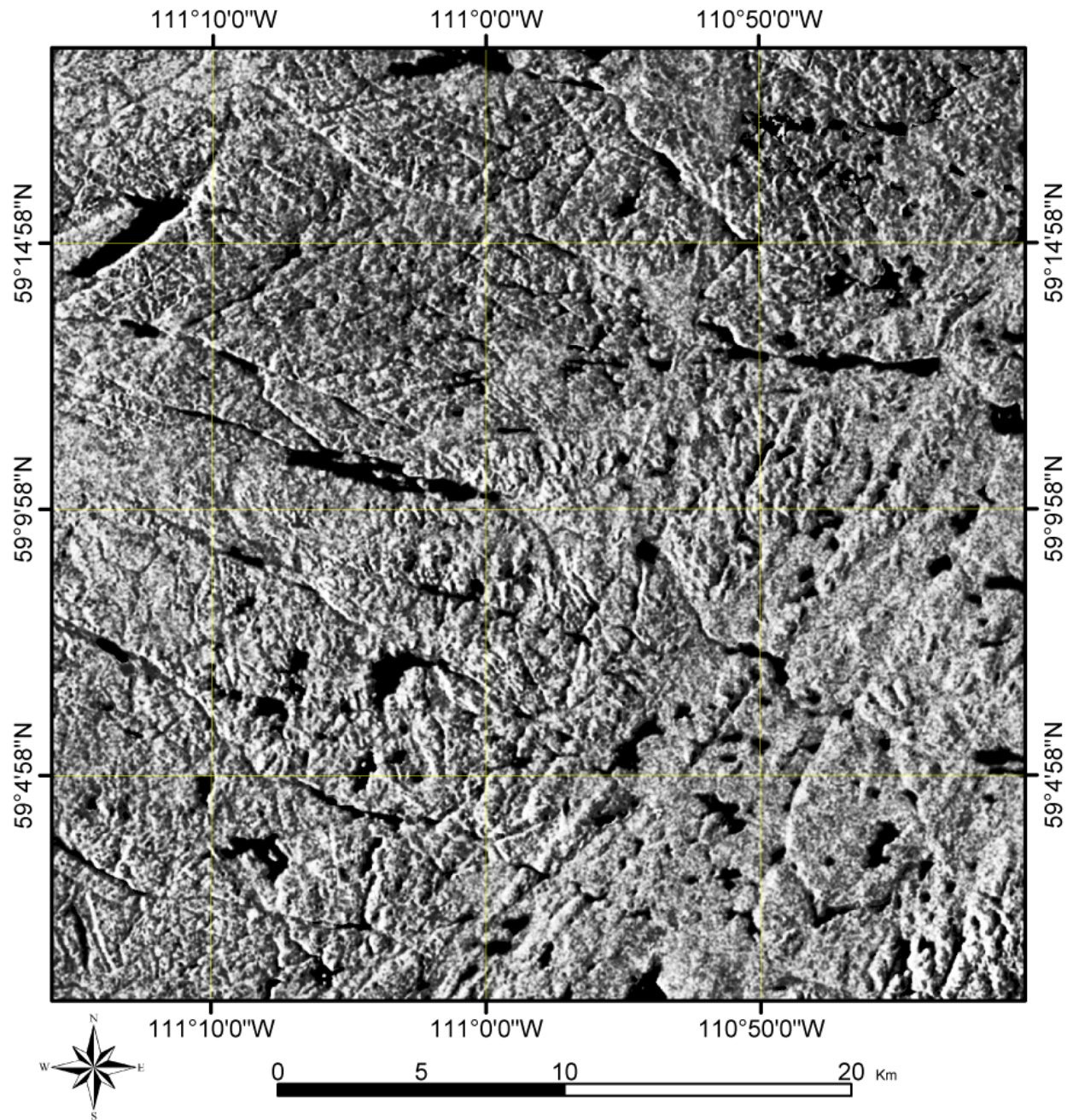
Figure 4. RADARSAT-1 principal component 3 image showing numerous bedrock lineaments of an area north of Athabasca Lake.
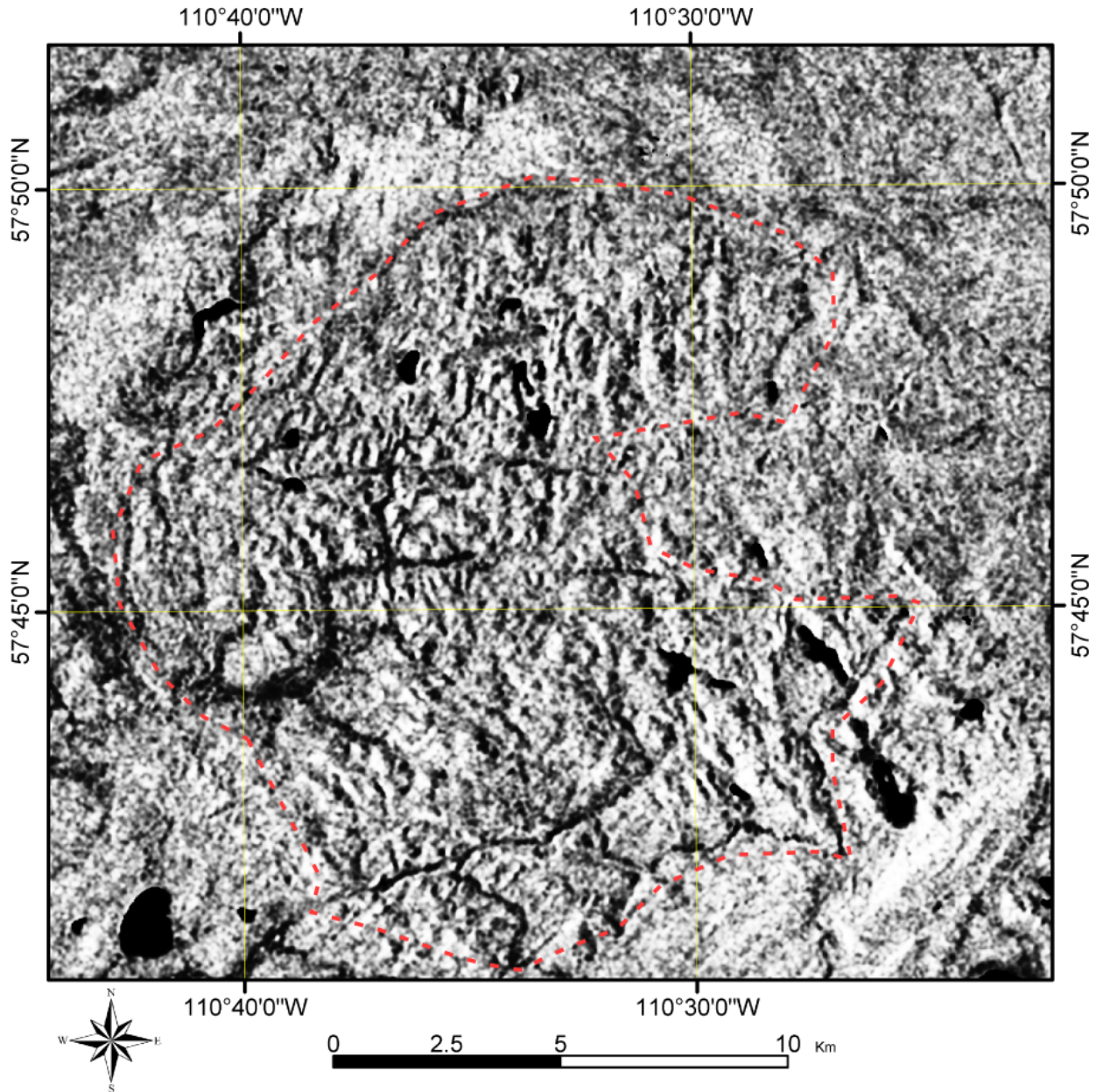
Figure 5. RADARSAT-1 principal component 3 image showing numerous bedrock lineaments of an area south of the study area. The bedrock area is highlighted with red dashed lines.

are trending northwest; the flutings and drumlins trend southwest, which also indicates the ice flow direction; the end moraine complex contains lineaments that mostly trend northwest; and finally, crevasse ridges trend in two dominant directions: southwest and northwest. These lineaments, in contrast to the lineaments recognizable in Figure 4, appear not to be related to the bedrock structure. Paganelli et al. (2003) carried out a similar study for the Buffalo Head Hills area, north-central Alberta. In that study, lineaments interpreted from RADARSAT-1 principal component images were compared with lineaments compiled from structural data from oil and gas wells, aeromagnetic depth-solution analysis, and a structural interpretation derived from compiled two and three dimensional seismic sections (Pryde, 2000). However, a close examination of Paganelli et al.'s (2003) map with surficial lineaments interpreted from the principal component 2 image (Paganelli et al., 2003, Figure 18B) and the map with subsurface

structural lineaments (Paganelli et al., 2003, Figure 18A) indicates that almost none of the individual lineaments matches on the two maps, although the general trend of lineament patterns on the two maps show some similarity, as Paganelli et al. (2003) suggested. This indicates that in areas covered by thick glacier sediments, such as are common in many parts of northern Alberta, lineaments interpreted from satellite images of optical reflectance and microwave backscatter are probably not the direct expressions of bedrock structures.

It is also possible that major faults, joints or weak structural zones in bedrock somehow penetrated through or left expressions on the overlying drift cover. Possible mechanisms for propagation and preservation of regional lineament patterns include fault reactivation, structurally influenced paleo-erosion, paleo-deposition, salt dissolution, differential compaction and differential crustal uplift caused by melting of the glacier. As well, they may have had influence on the courses of meltwater channels, rivers and the linear arrangement of lakes. For example, the weak structural zones, scoured by the advancing glacier, tend to trap stagnant ice blocks during glacier retreat, and thus, tend to cause a linear arrangement of lakes, kettle holes or kames due to the prior existence of stagnant ice. As a result, surficial lineaments, which may have resulted from glacier advance and retreat, fluvial process and weathering, could reflect a pattern similar to the underlying bedrock structure.

The present study was focused on those lineaments that possibly have a bedrock origin. Based on the previous discussion, it can be reasoned that the direct expressions of the major faults or joints will be subtle in topographic difference (i.e., shallow), wide and over a longer distance if they can be traced, unlike the younger surficial lineaments caused by glacier, wind affects, fire and fluvial processes that tend to be distinct, short and narrow. Based on this rationale, the methodology attempts to highlight and detect the subtle expressions of major bedrock faults or joints, as opposed to those lineaments of surficial or non-bedrock genetic origin.

Grunsky (2002b) and Paganelli et al. (2003) demonstrated that principal component 2 and 3 images, derived from RADARSAT-1 standard beam 1 and 7, in both ascending and descending passes, highlight topography features. In the present study, the same combination of RADARSAT-1 standard beam 1 and 7 images were enhanced by using various techniques, including contrast stretching, band rationing and algebra, and principal components analysis (PCA). Edge detection and edge enhancements were also performed on the processed images. However, it was found that various false colour composite images of the processed single band images would be more useful for lineament analysis than the individual single band image. Topographic information was also extracted from the RADARSAT-1 images, using the stereo capability of RADARSAT-1 imagery for extracting DEM (Leberl, 1990; PCI Geomatica, 1997; Paillou and Gelautz, 1999; Toutin and Gray, 2000). In addition, DEMs generated from SRTM and NTS are included in the present study. Sunshade relief images were generated for the DEMs from SRTM and NTS. In order to avoid introducing bias in lineament interpretation, two sunshade relief images were created for each of the DEMs using sun azimuths 90 degrees apart.

Objective or statistical methods for consistently identifying linear features have proven difficult to develop. It appears much reliance has been placed on pattern recognition by humans. In the present study, linear features were visually identified based on image colour, texture, tone and pattern, and then plotted using heads-up, on-screen digitizing. Landsat 7 Enhanced Thematic Mapper (ETM) images are used as supplementary data for discrimination of the non-structural surficial lineaments from those that possibly have a bedrock origin, and only those lineaments that could be possibly interpreted as geological structure were included. Following identification of the lineaments, a rose diagram was plotted and lineament trends were recognized.

4   Image Data and Image Processing

4.1   RADARSAT-1 Images

This study uses the RADARSAT-1 images to extract topographic information for lineament analysis. The processes include applying principal component analysis and different algorithms to the RADARSAT-1 images and DEM extraction from the RADARSAT-1 images. The AGS acquired RADARSAT-1 images over northern Alberta (north of 55 degrees north latitude) with two looking angles: Standard Beam 1 (S1) (20-27 degree) and Standard Beam 7 (S7) (45-49 degree); and two looking directions: east for ascending pass and west for descending pass. RADARSAT International (RSI) refers to this type of imagery as Synthetic Aperture Radar Georeferenced Fine resolution (SGF) images (RADARSAT International, 1999). SGF images have been converted to ground range and are multi-look processed. Each Standard Beam image is a composite of four looks. This composite increases the signal-to-noise ratio at the expense of the spatial resolution. The imagery is provided at a nominal resolution of 12.5 m (close to the single look spatial resolution), although the true spatial resolution of the averaged four-look image is closer to 25 m. The imagery is calibrated, but remains oriented in the direction of the orbit path. It is sampled in unsigned, 16-bit integer format and written in Committee of Earth Observation Satellites (CEOS) standard format. The strategy of acquiring S1 and S7 imagery was done to contrast the radar responses based on two incidence angles and two look directions. The images were obtained in a dry autumn (September to December 1999) and, thus, provided ideal conditions of no to little deciduous foliage or snow.

4.2   RADARSAT-1 Principal Component Images Processed by RGI

The acquired SGF scene images were individually orthorectified and then tiled into 25, 1:250 000 scale NTS map areas covering all of northern Alberta north of latitude 55°N (Grunsky, 2002a, 2002b; Mei, 2004a to 2004y). This results in four RADARSAT-1 images from the four beam positions for each NTS map area: i.e., Standard Beam 1 ascending image (S1A), Standard Beam 1 descending image (S1D), Standard Beam 7 ascending image (S7A) and Standard Beam 7 descending image (S7D). As well, the four RADARSAT-1 images for northern Alberta were processed using Principal Component Analysis (PCA). As a result, the first four principal component images were generated for each NTS map area.

The orthorectification, mosaic and principal component analysis were carried out by Resource GIS and Imaging Ltd. (RGI) (now renamed PhotoSat) using processing methods and software developed by RGI and run within the ER Mapper processing environment. Orthorectification was performed using digital elevation data provided by the Resource Data Division (RDD) of the Alberta Department of Sustainable Resource Development. The digital elevation data used had a 100-metre resolution. Ground control points (GCPs) were collected from 1:20 000 Alberta Access Vectors and an Alberta mosaic of orthorectified Indian remote sensing satellite (IRS) images, also provided by RDD. An average root mean-square error of 20 m is obtained for the orthorectification.

Then, the orthorectified images were mosaicked. For the S1 mosaics, the near-nadir sides of the images were favoured in the mosaic process. For the S7 mosaics, the off-nadir sides of the images were favoured. This maximized the incidence angle difference between the S1 and S7 mosaics. Radiometric differences between adjacent images were minimized using two-dimensional, piecewise linear gain and offset adjustment functions, which were interactively adjusted to achieve an optimum balance.

PCA is a statistical method evaluating correlation among the signals from the S1A, S1D, S7A and S7D image data, and generates resultant principal component images. It is a linear transformation, which rotates the axes of image space along lines of maximum variance. The rotation is based on the orthogonal

eigenvectors of the covariance matrix generated from a sample of image data from the input channels. The output from this transformation is a new set of image channels containing the principal component images.

The covariance eigenvectors were determined by RGI using a 10 000 columns by 20 000 rows window of the four beam mode images (Table 1). The window is located between $113^0 42'25.2436"$ W to $111^0 33'59.8916"$ W and $55^0 37'30.3879"$ N to $57^0 50'36.5615"$ N, which is out of the present study area. During the PCA, the S7 ascending image was used to mask the lakes to remove them from the calculation of the covariance eigenvectors. The S1 ascending image was multiplied by 1.35, and the S1 descending image was multiplied by 1.60 to match the means of the S1 and S7 ascending/ descending images. An ER Mapper std_dev_1.6 filter is applied to each of the four beam position images. After PCA, a value of 11 000 was added to PC3 values and 5 000 to PC4 values to bring all of the image values into the positive range. Then, the dataset was converted into unsigned, 8-bit integer format, and the pixel size remained at 12.5 m.

Table 1. Covariance eigenvectors of principal component analysis used by RGI

Input Image	PC1	PC2	PC3	PC4
S1A	0.152	0.866	0.465	-0.102
S1D	0.501	0.347	-0.759	0.230
S7A	0.594	-0.275	0.451	0.607
S7D	0.611	-0.233	0.068	-0.754

The four principal component images evaluated for the study area were created from the principal component images generated by RGI for NTS 74E and 74L (Mei, 2004c, 2004d). First, the image dataset for NTS 74E and 74L were mosaicked. Then, the image dataset for the study area was subset from the mosaicked image dataset (Figures 6–9).

4.3   RADARSAT-1 Principal Component Images and Other Images Processed in this Study

The existing four principal component images processed for the study area by RGI are based on covariance eigenvectors derived from an area outside the study area (Table 1). For a consistent evaluation, PCA was applied to the orthorectified images of the study area (Figures 10–13), based on covariance eigenvectors directly derived from the input images of the study area. Before PCA, an Enhanced Frost Speckle Filter in PCI Geomatica was applied to remove high frequency noise (speckle), while preserving high frequency features (edges). For the filter, a kernel of nine pixels by nine pixels was used. The derived covariance eigenvectors are shown in Table 2.

Table 2. Covariance eigenvectors of principal component analysis used by this report

Input Image	PC1	PC2	PC3	PC4
S1A	0.34934	0.91519	-0.15382	0.12937
S1D	0.36340	-0.11450	-0.50647	-0.77351
S7A	0.59107	-0.06462	0.77355	-0.21925
S7D	0.62971	-0.38099	-0.34848	0.58041
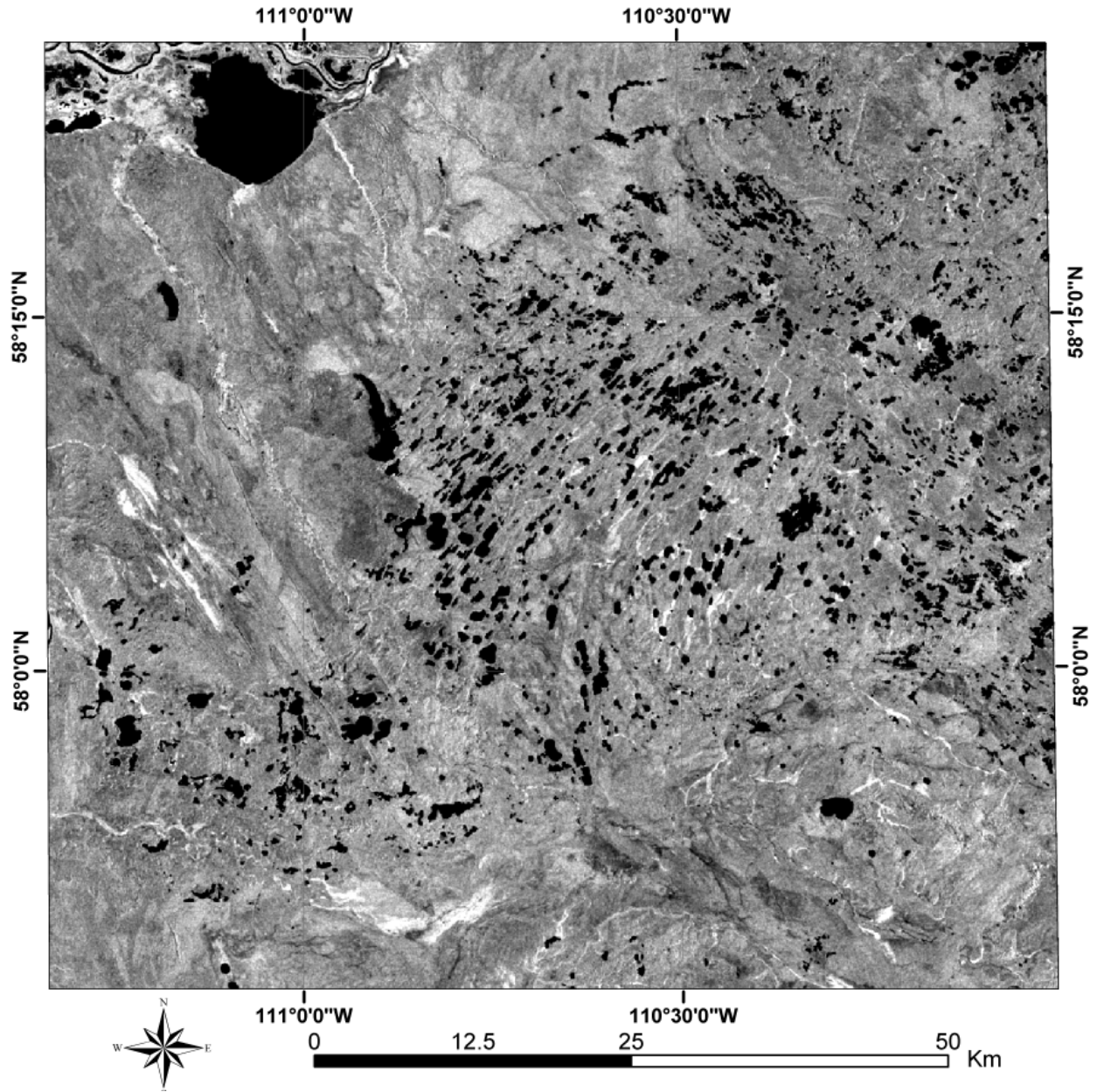
Figure 6. Principal Component 1 Image processed by Resource GIS and Imaging Ltd.
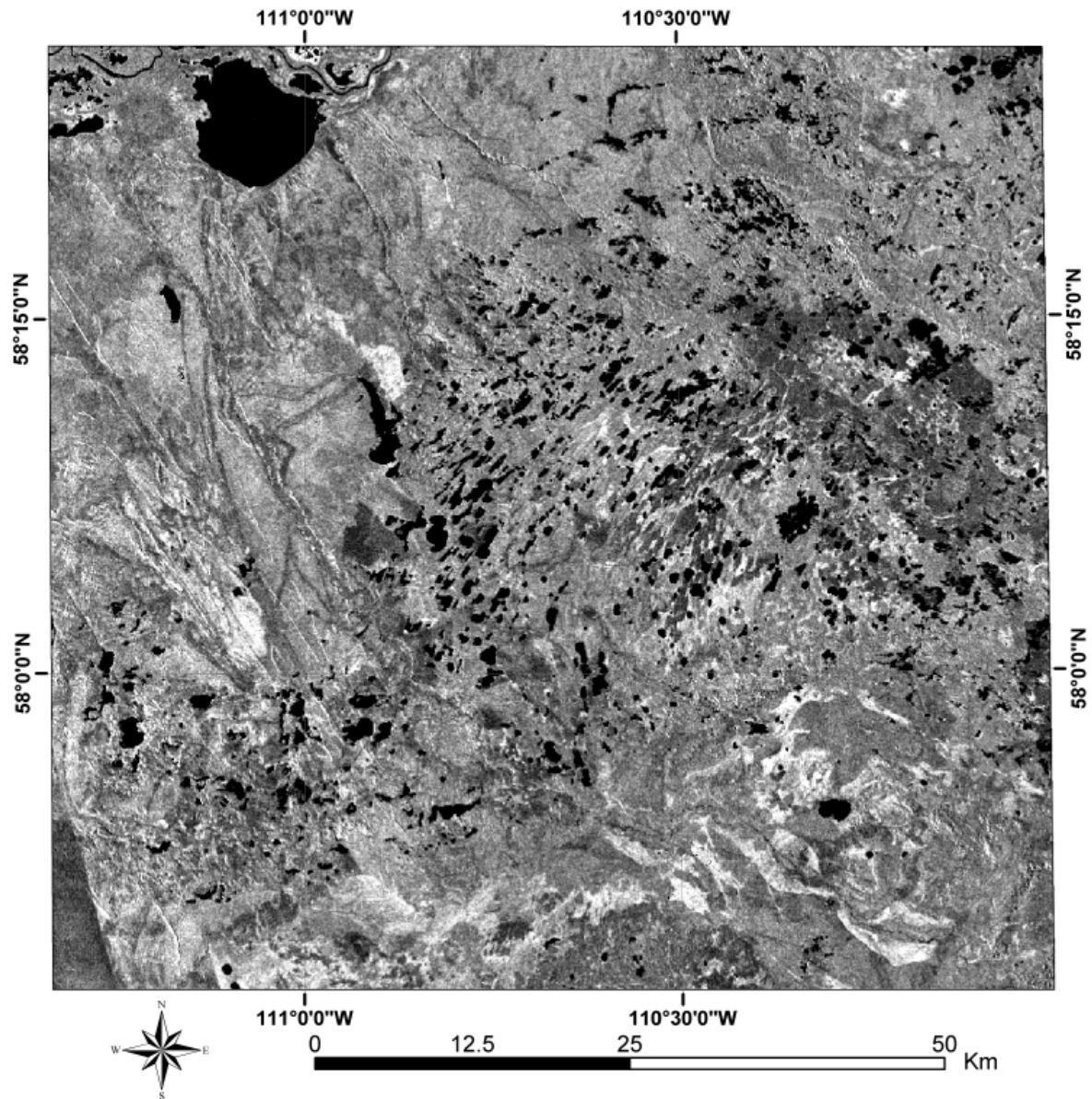
Figure 7. Principal Component 2 Image processed by Resource GIS and Imaging Ltd.
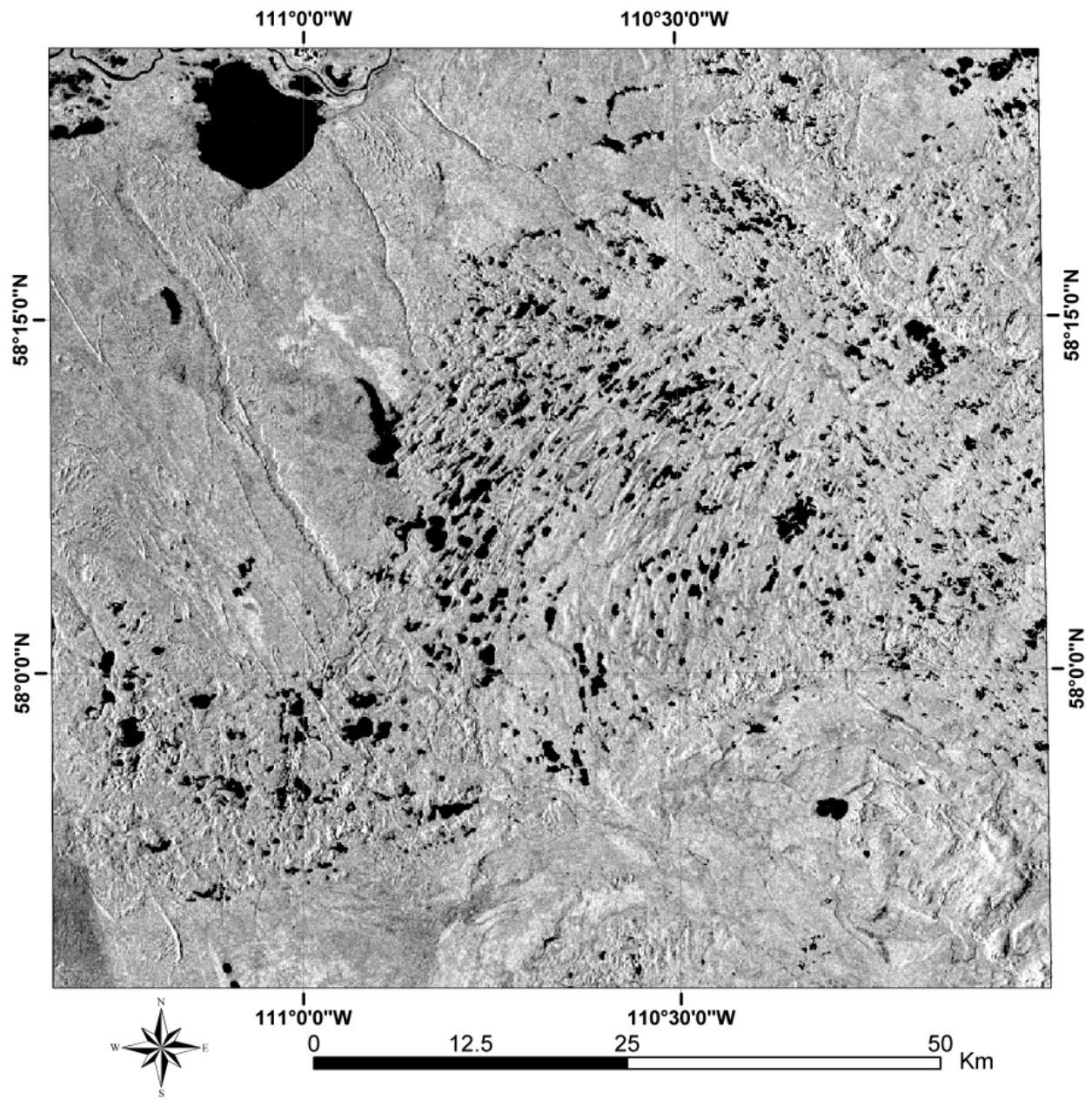
Figure 8. Principal Component 3 Image processed by Resource GIS and Imaging Ltd.
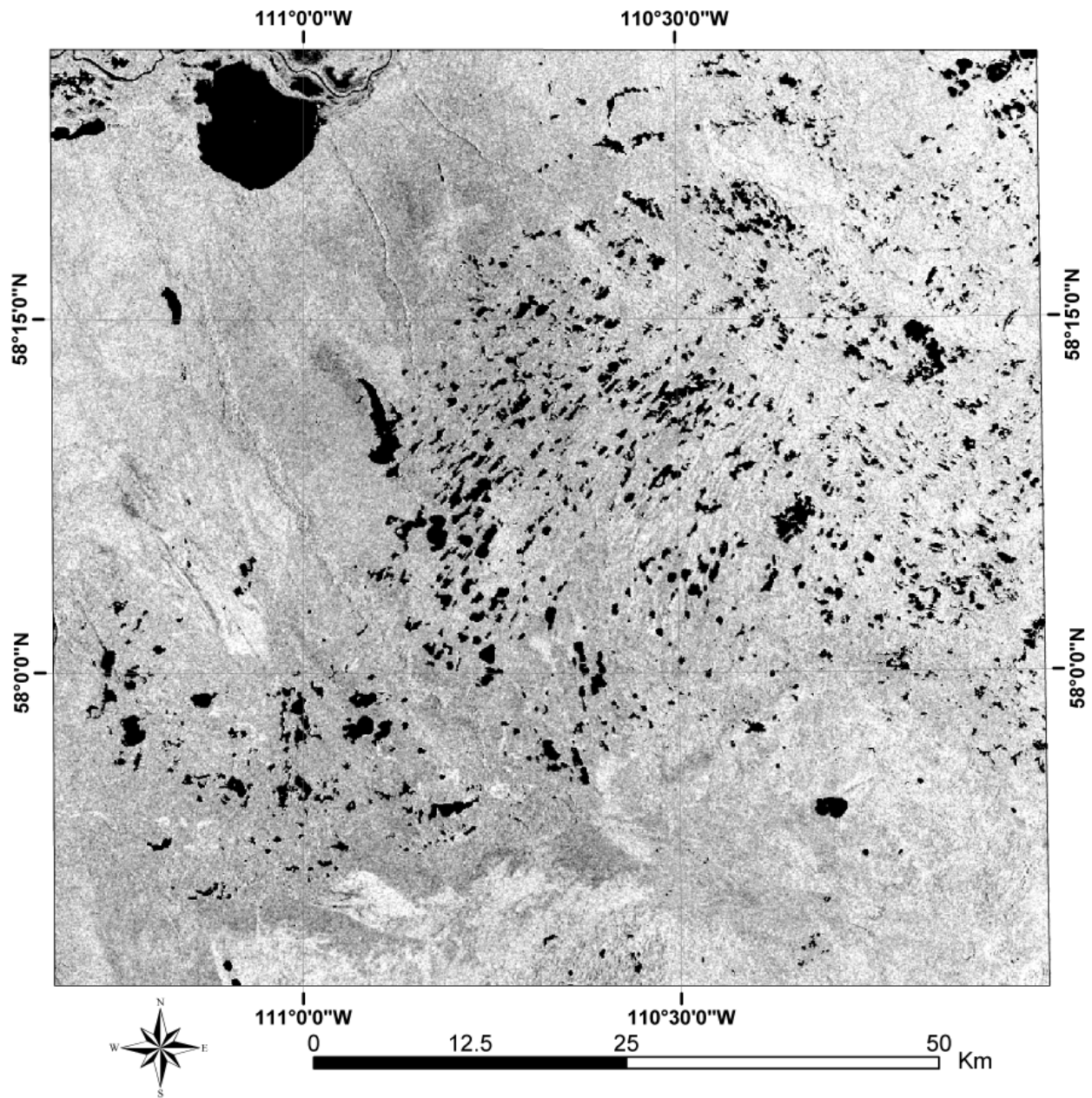
Figure 9. Principal Component 4 Image processed by Resource GIS and Imaging Ltd.
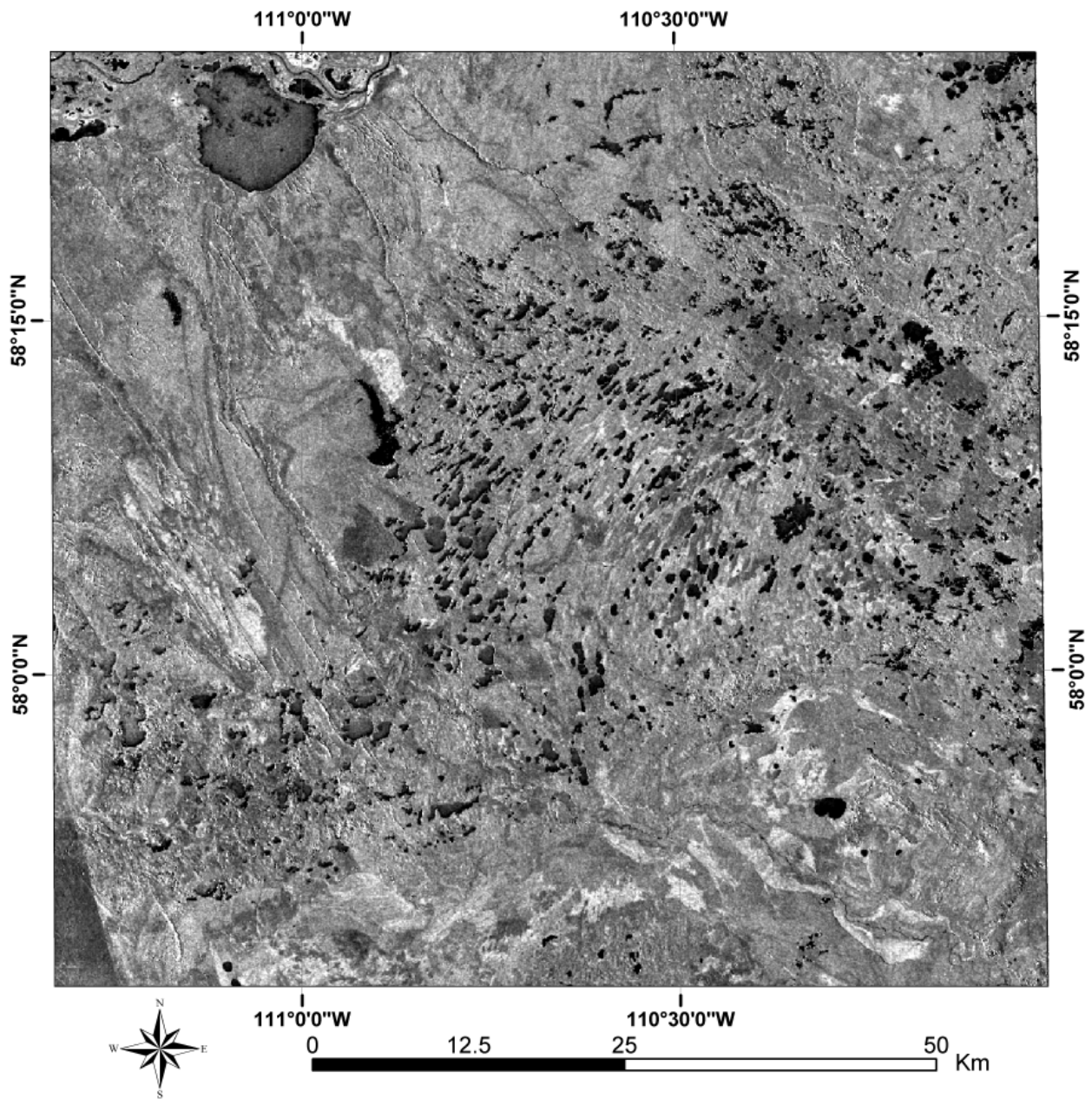
Figure 10. RADARSAT-1 Standard Beam 1 ascending pass image (S1A) with enhanced frost-removal transformation using a 9 x 9 kernel.
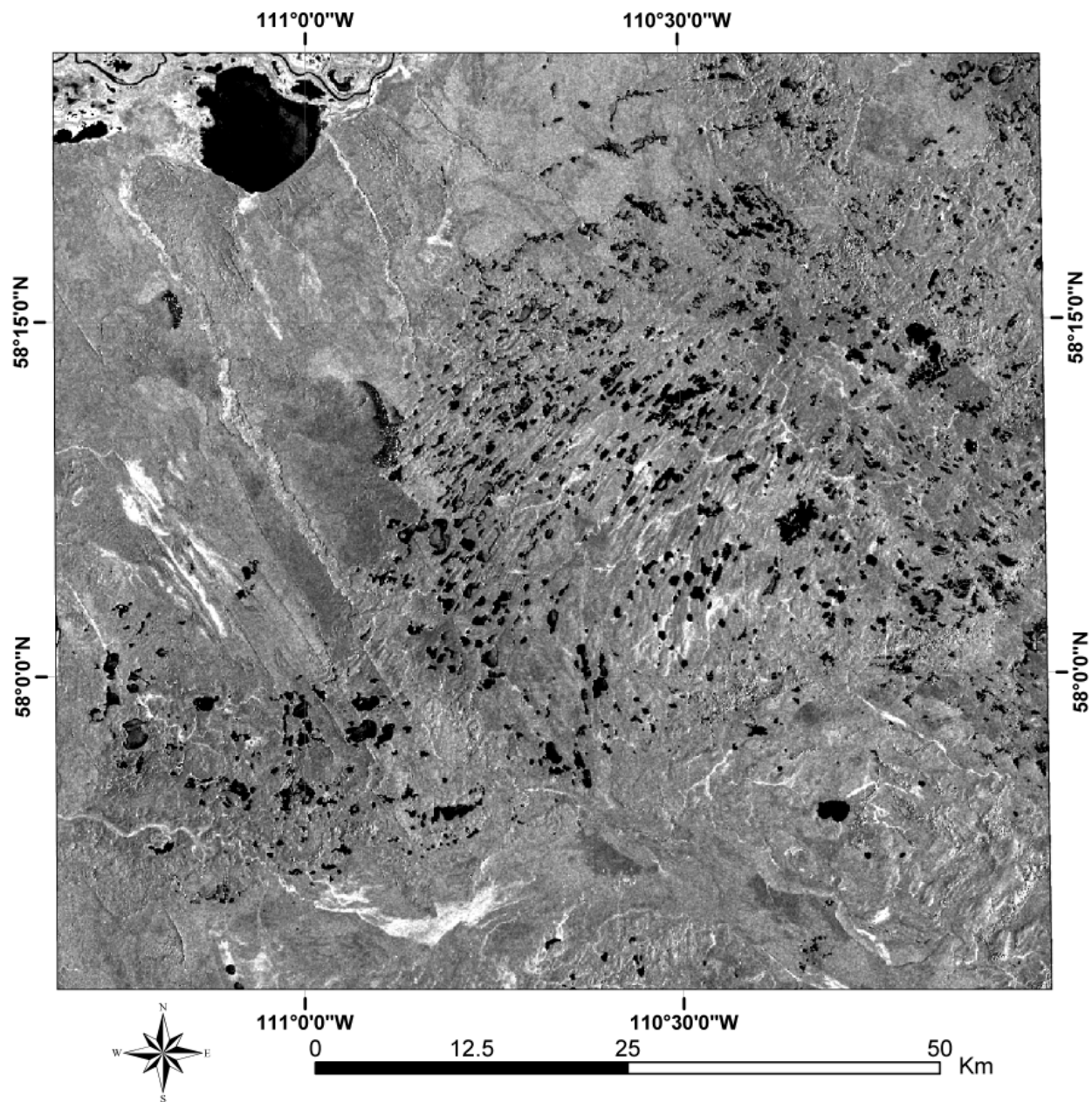
Figure 11. RADARSAT-1 Standard Beam 1 descending pass image (S1D) with enhanced frost-removal transformation using a 9 x 9 kernel.
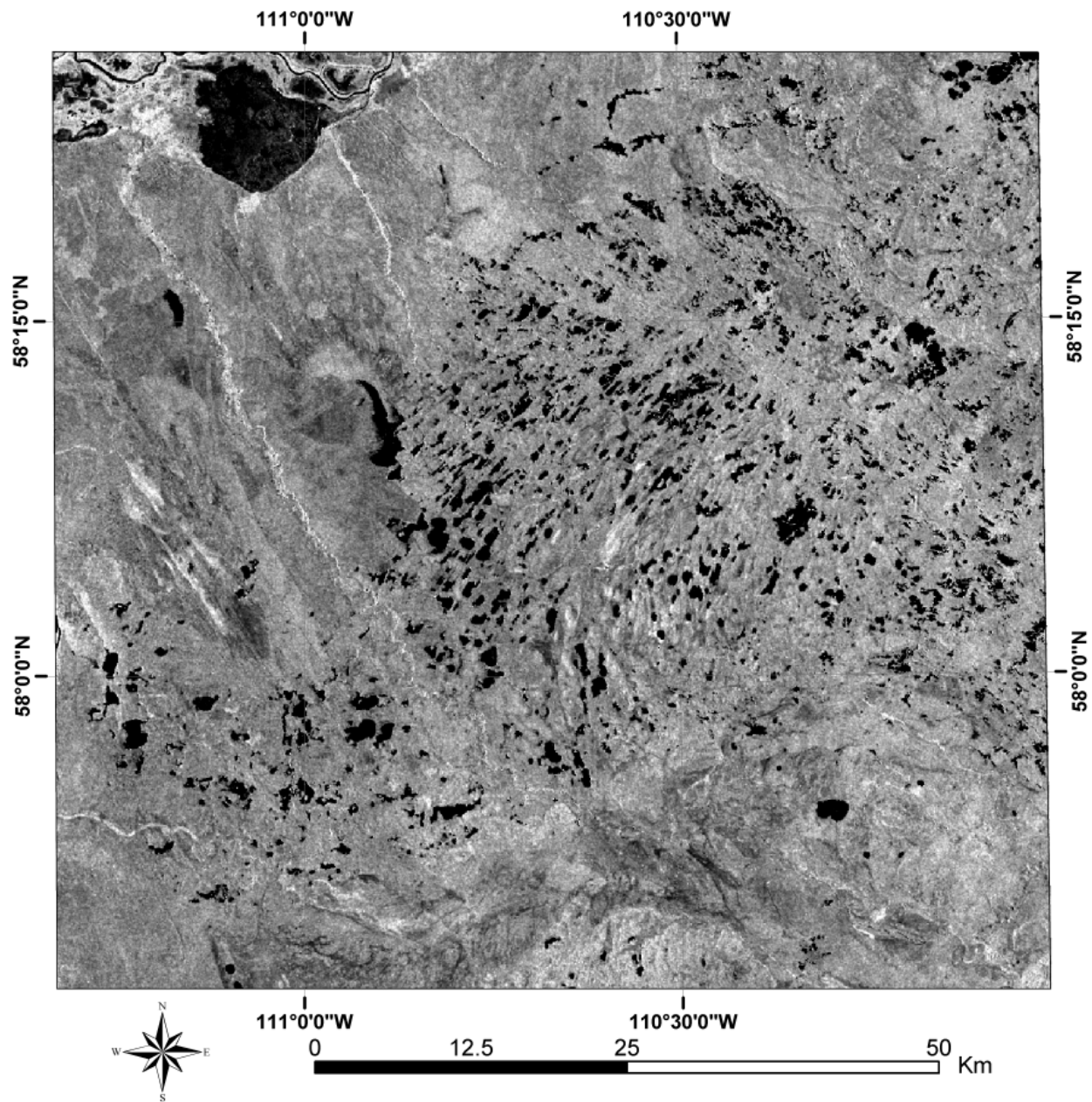
Figure 12. RADARSAT-1 Standard Beam 1 ascending pass image (S7A) with enhanced frost-removal transformation using a 9 x 9 kernel.
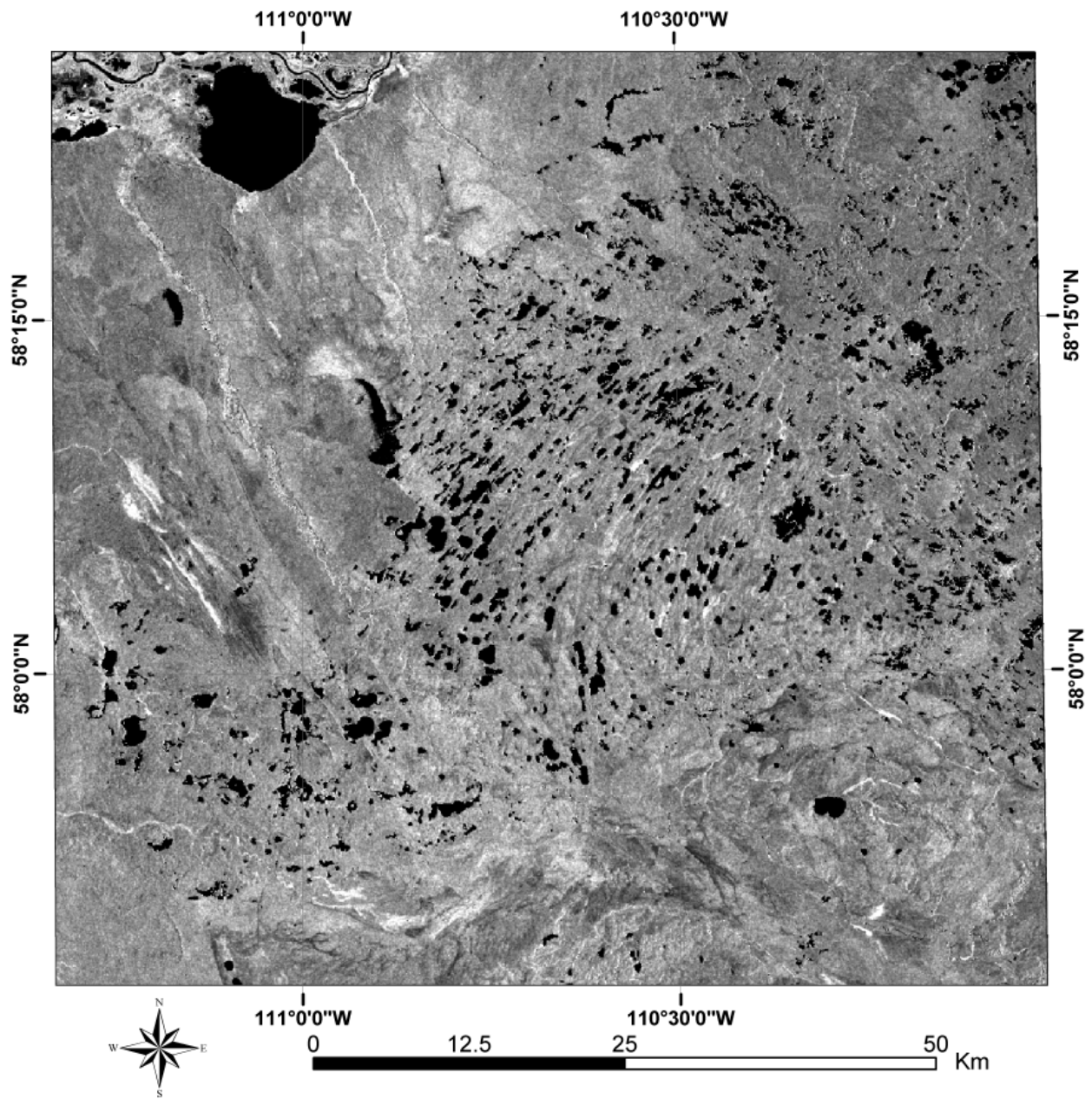
Figure 13. RADARSAT-1 Standard Beam 1 descending pass image (S7D) with enhanced frost-removal transformation using a 9 x 9 kernel.

The resultant four PC images are shown in Figure 14–17. The application of PCA and the resultant component images are dependent on the images being processed, and specific to each study area (Grunsky, 2002b). The PC1 image contains positive contributions from all the input images (Grunsky, 2002b; Paganelli et al., 2003; Tables 1 and 2). It highlights differences in land cover type (Grunsky, 2002b). The PC2 and PC3 images are found to highlight differences in topography (Grunsky, 2002b; Paganelli et al., 2003). Grunsky (2002b) concluded that the discrimination of topographic features using the PC3 image is superior to any other optical commercial satellite imagery with similar spatial resolution. Areas of drumlins, sand dunes, eskers, crevasse ridges, embankments and other prominent topographic features typically are more clearly shown on PC2 and PC3 images than on the other PCA images (e.g., compare Figure 8 with Figures 6, 7 and 9; and Figures 15 and 16 with 14 and 17). This is because PC2 and PC3 images are dominated by the contrast between the look directions (Grunsky, 2002b; Paganelli et al., 2003; Tables 1 and 2). The slop facing the sensor tends to result in a higher radar backscatter, and the slop facing away from the sensor tends to result in a low radar backscatter. As a result, the contrast between the look directions contributes to an enhanced sunshade relief effect on PC2 and PC3 images. The PC4 image is characterized by the contrast between the look directions of one beam mode (S1 or S7) that is offset by the contrast between the look directions of the other beam mode. Consequently, the PC4 image contains much less topographic information than the PC2 and PC3 images.

A close examination of the correlation eigenvectors used by Grunsky (2002b), Paganelli et al. (2003), RGI (Table 1) and covariance eigenvectors in this paper (Table 2) indicates that the contrast between the look directions in PC2 and PC3 images is offset by one of the input images. The contrast between images from opposite look directions is found to highlight linear features. To maximize the contrast between the look directions, different linear transformations and band rationing were applied to the orthorectified RADARSAT-1 images for the study area; this resulted in ten processed images (Figures 18–26). In the captions of these images, S1A stands for the Standard Beam 1 ascending pass image, S1D stands for the Standard Beam 1 descending pass image, S7A stands for the Standard Beam 7 ascending pass image and S7D stands for the Standard Beam 7 descending pass image.

A visual comparison of all PCA and processed images indicates that the processed images of contrast in looking direction (Figures 20–27) have a comparable and, in some cases, even better effect in highlighting topographic features, compared to the PC2 and PC3 images (Figures 7, 8, 15 and 16). Various pseudocolour composite images (Figures 28–31) were created using the processed images. These images were used for visual lineament interpretation.

4.4   DEM Extraction from RADARSAT-1 Images

Eight RADARSAT-1 SGF images from Standard Beam 1 and 7, in both ascending and descending passes (Table 3), were used for DEM extraction for the study area. A program named CDSAR in PCI Geomatica was used to automatically extract the CEOS file on the CD and save both the orbital and database ground control points (GCPs) information into two segments. The orbital information was used for DEM extraction using PCI Geomatica OrthoEngine. These internal GCPs are useful when the user cannot obtain any GCPs from the field.

The DEM extraction process creates a DEM from stereo pairs of images, which are two or more images of the same area taken from different viewpoints. PCI Geomatica OrthoEngine uses image correlation to extract matching pixels in the two images and then uses the sensor geometry from the computed math model to calculate x, y and z positions (PCI Geomatica, 1997). In the process, the input images are first converted into epipolar pairs. Epipolar images are stereo pairs reprojected so the left and right images have a common orientation, and matching features between the images appear along a common
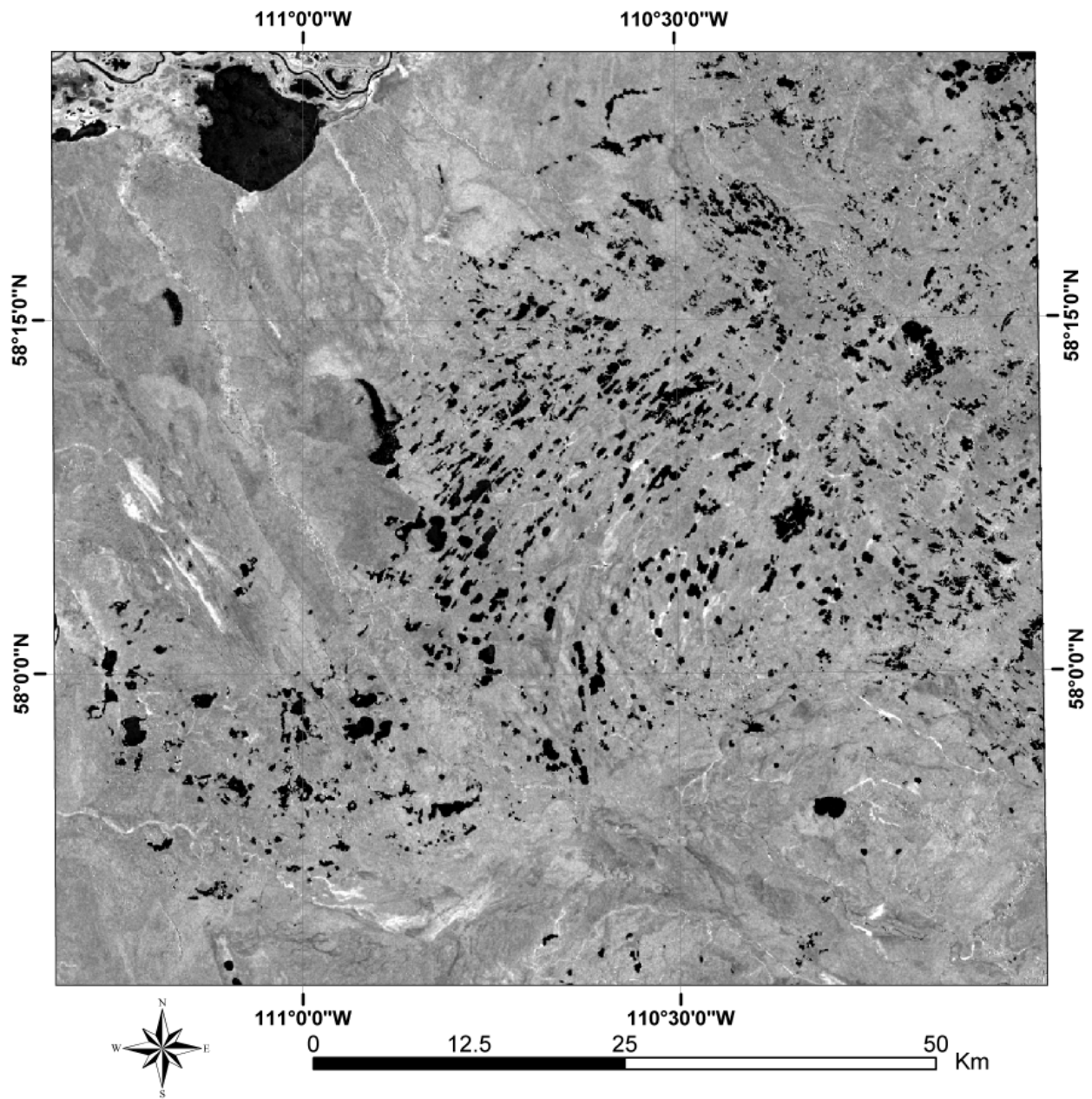
Figure 14. Principal Component 1 Image processed for the study area.
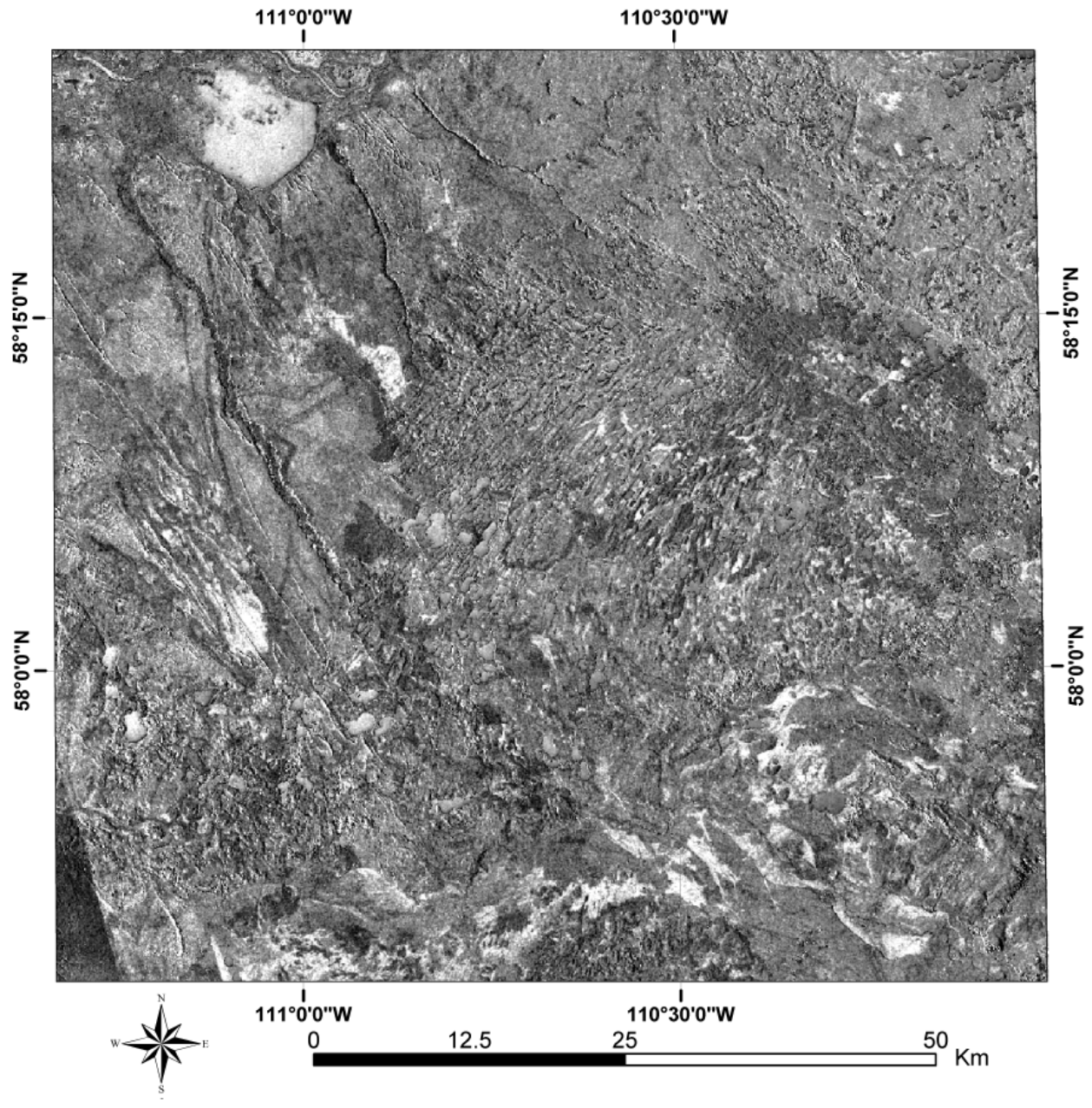
Figure 15. Principal Component 2 Image processed for the study area.
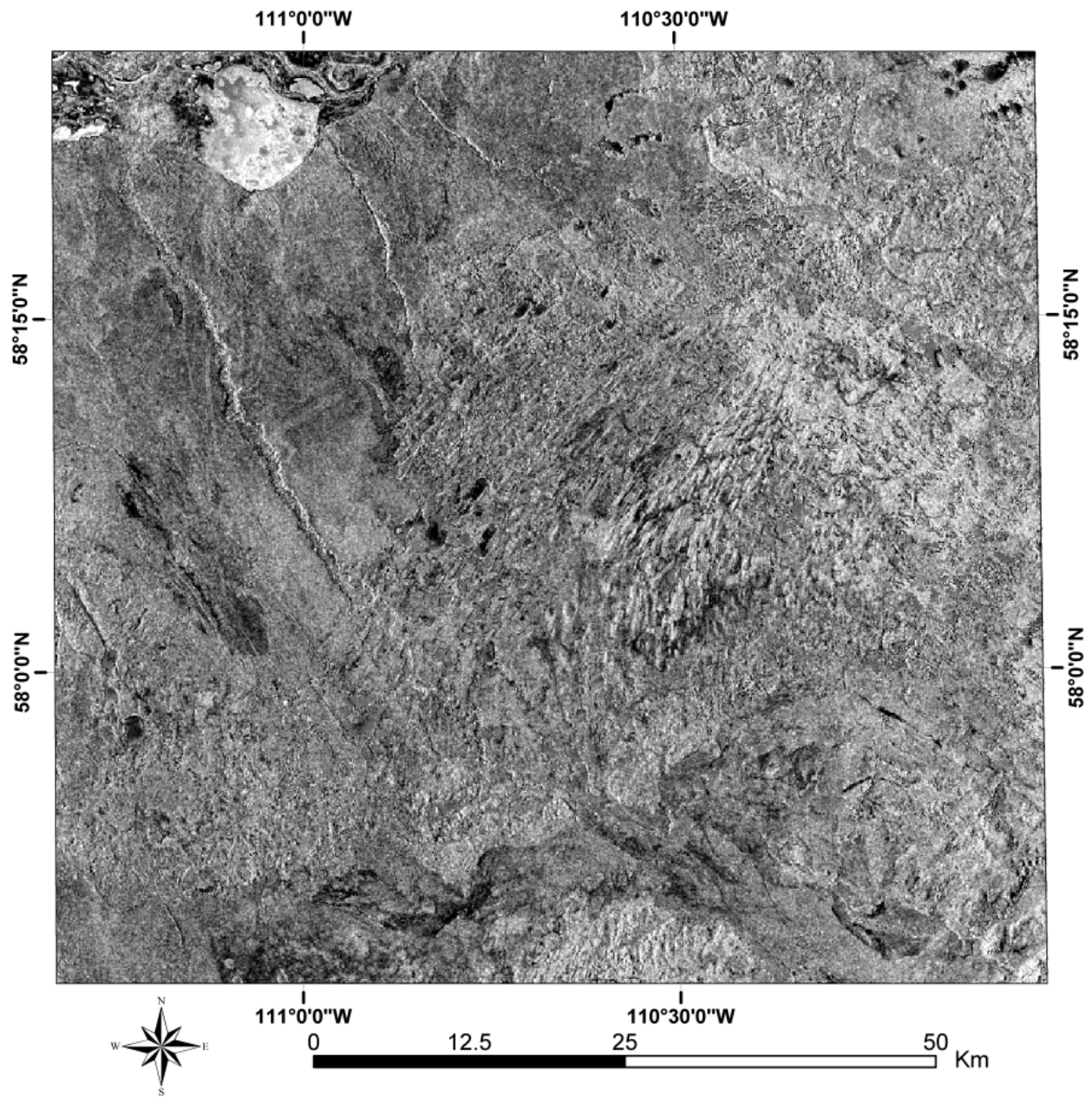
**Figure 16. Principal Component 3 Image processed for the study area.**
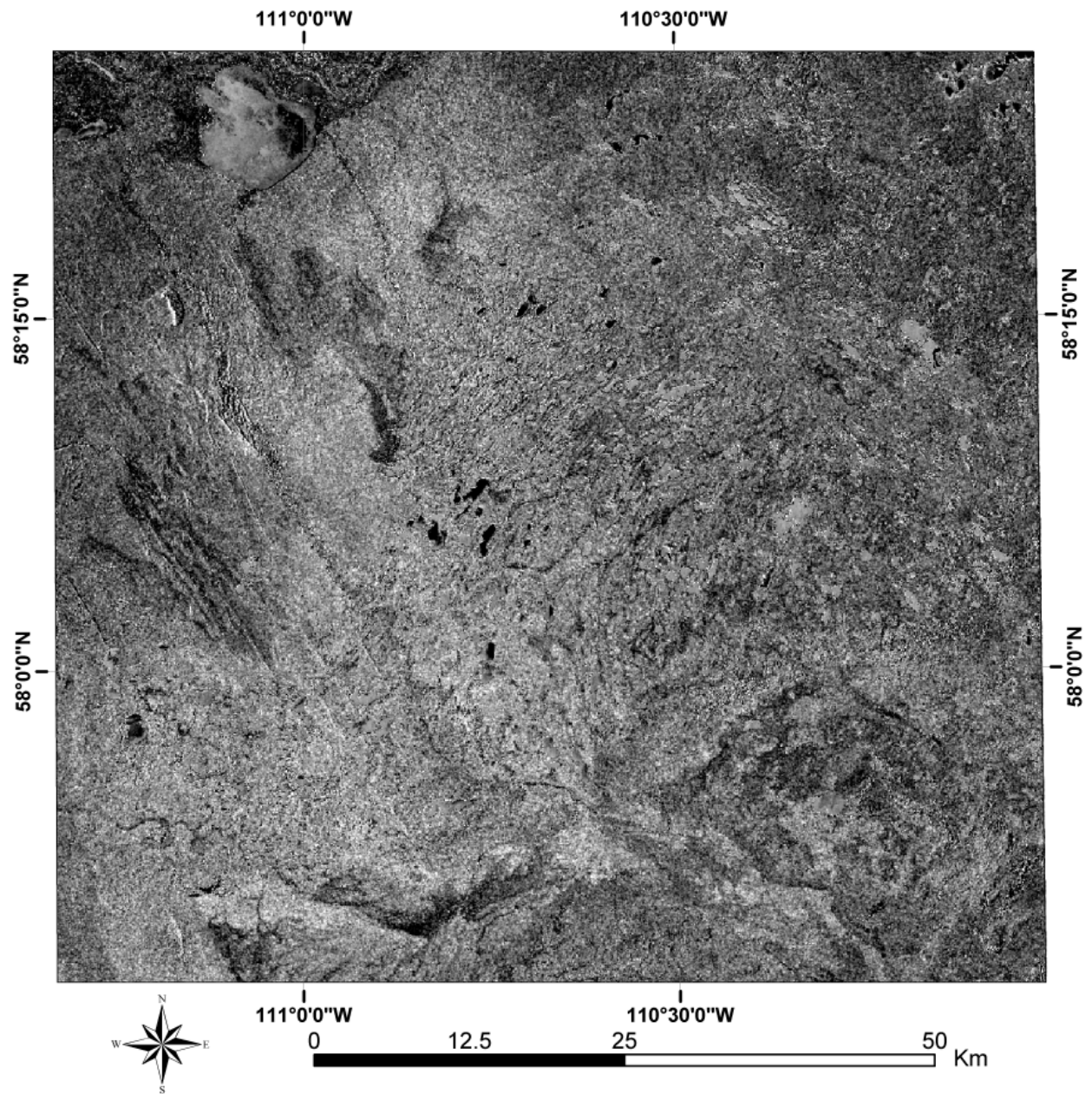
Figure 17. Principal Component 4 Image processed for the study area.
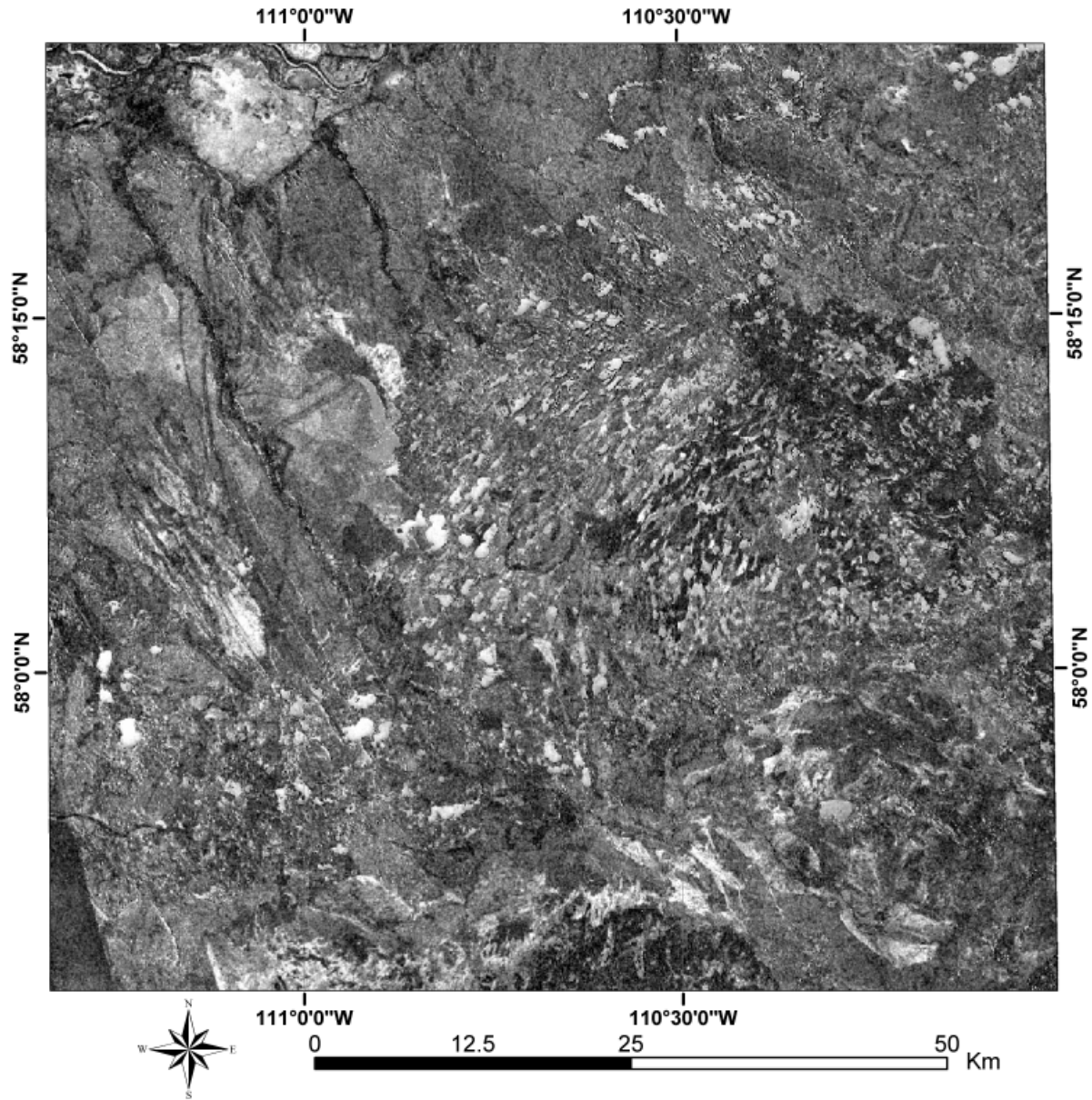
Figure 18. Image processed using an algorithm (S1A – S7A) for the study area.
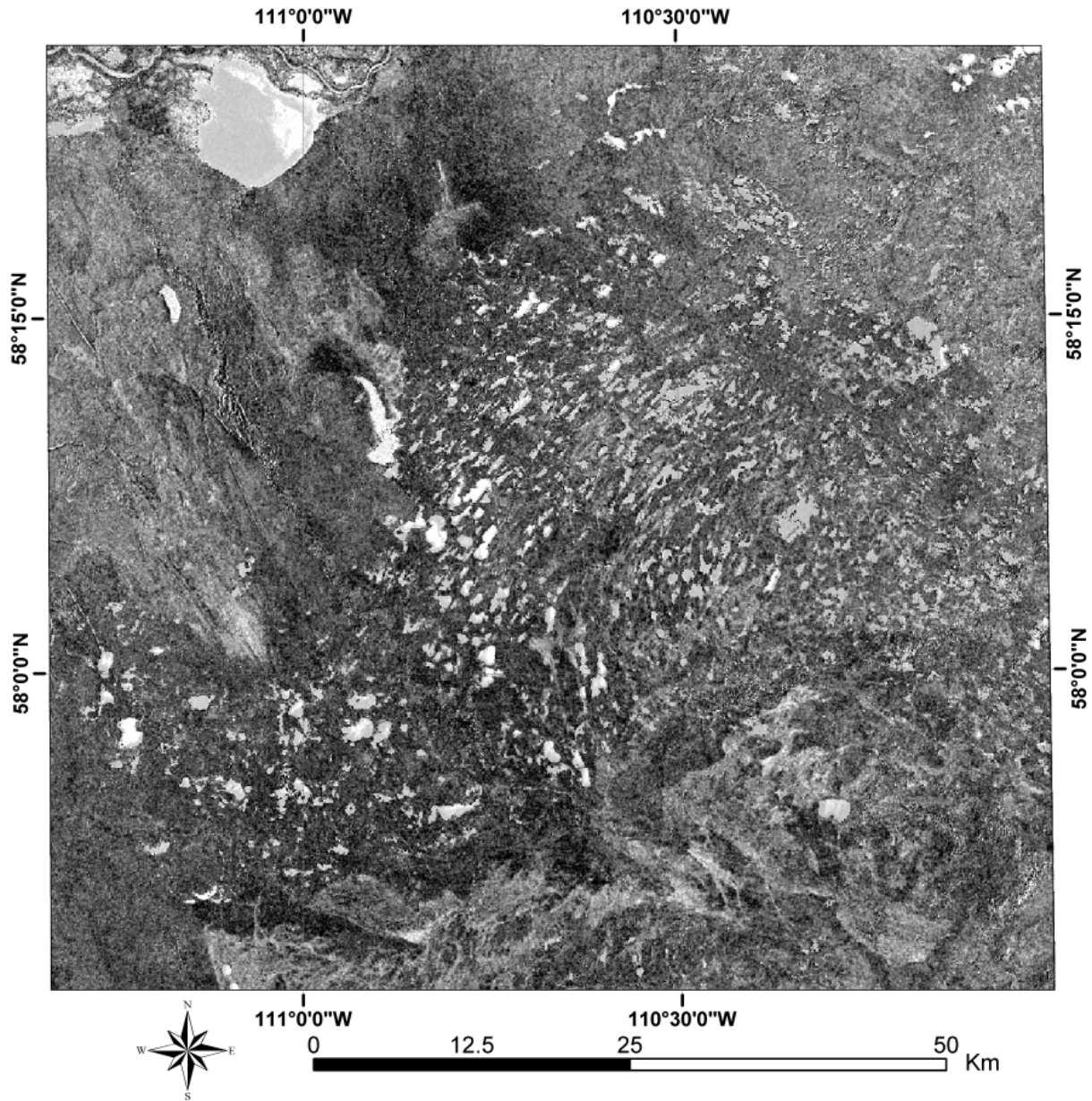
Figure 19. Image processed using an algorithm (S1D - S7D) for the study area.
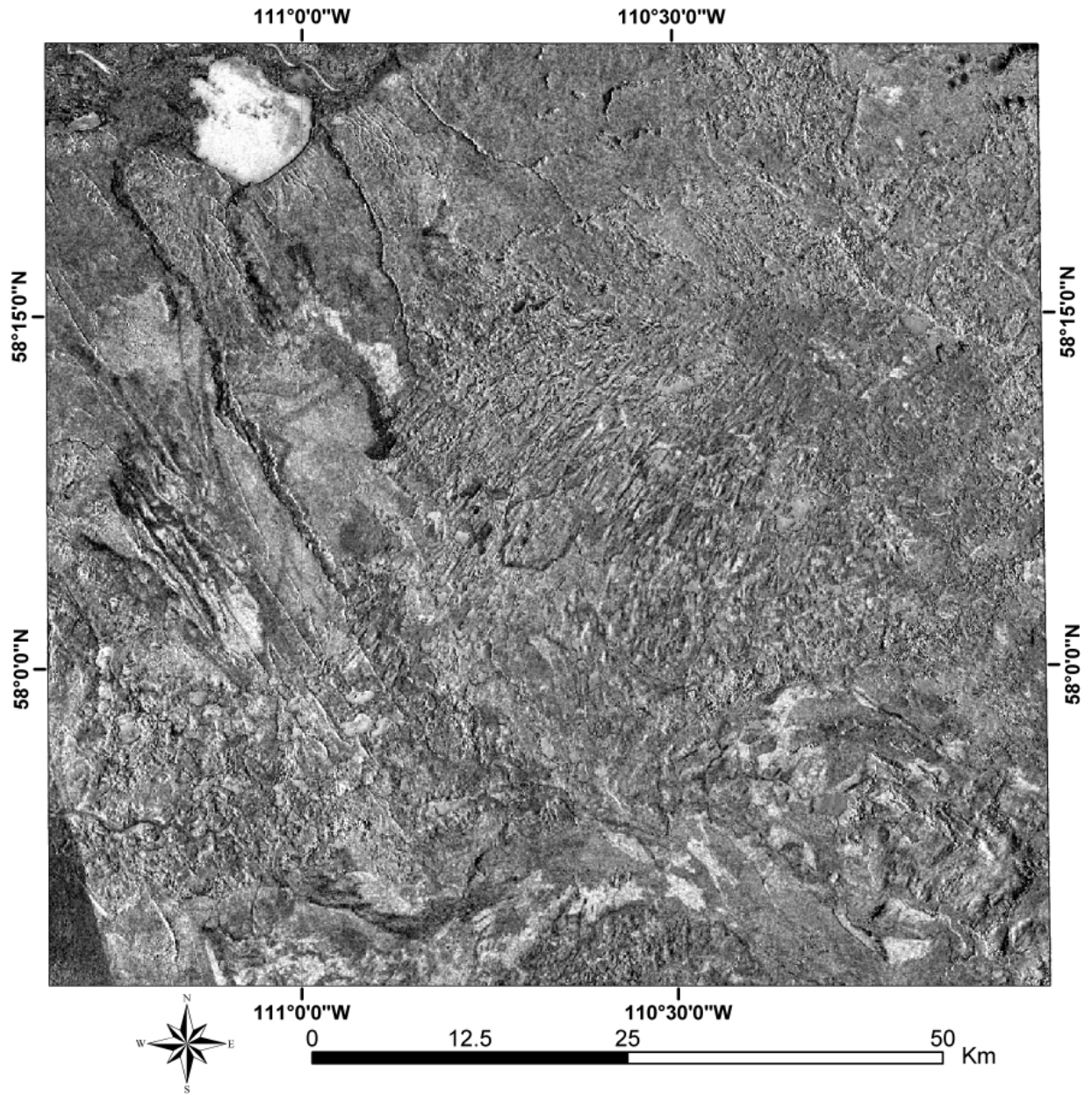
Figure 20. Image processed using an algorithm (S1A-S1D) for the study area.
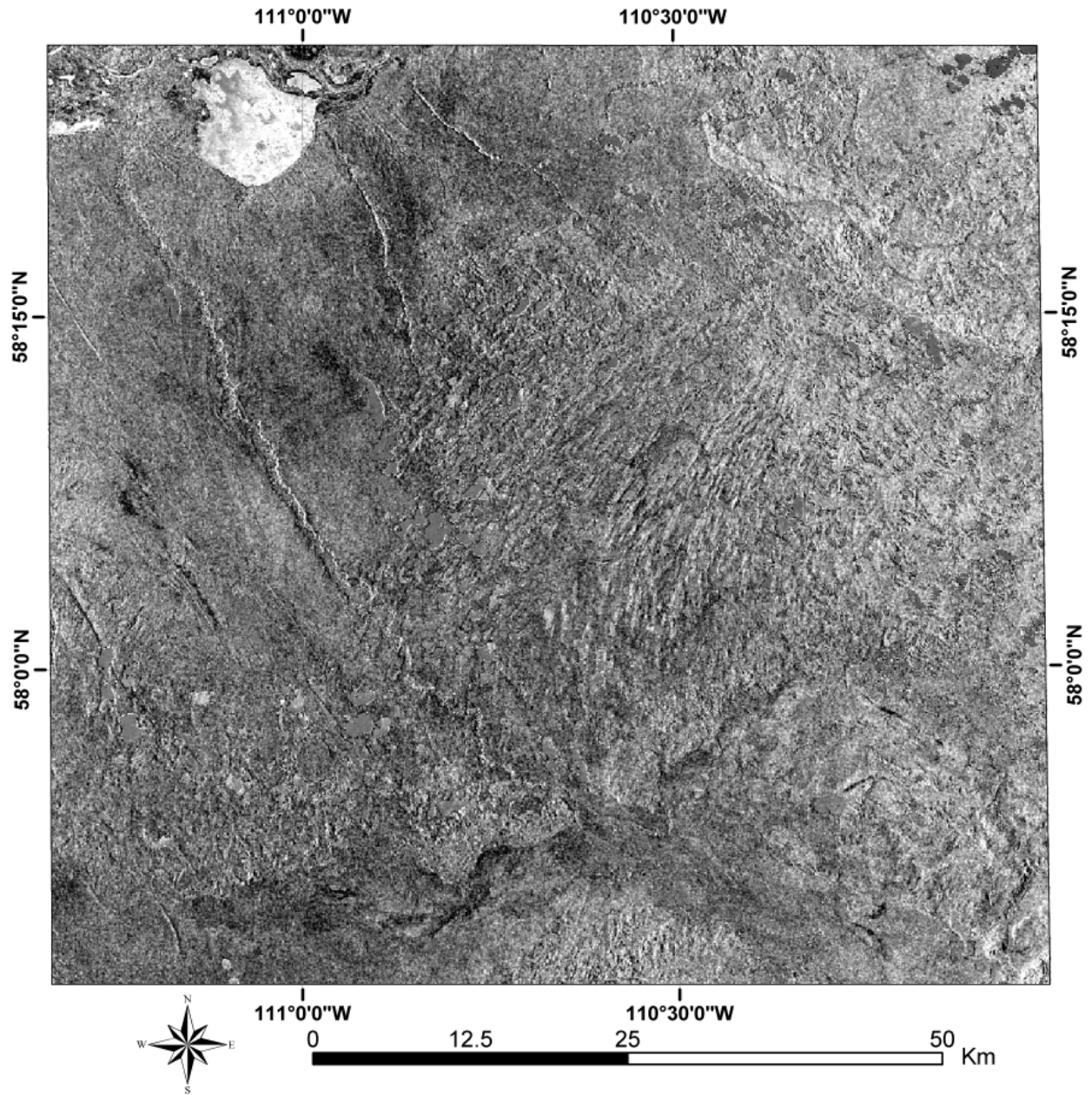
Figure 21. Image processed using an algorithm (S7A-S7D) for the study area.
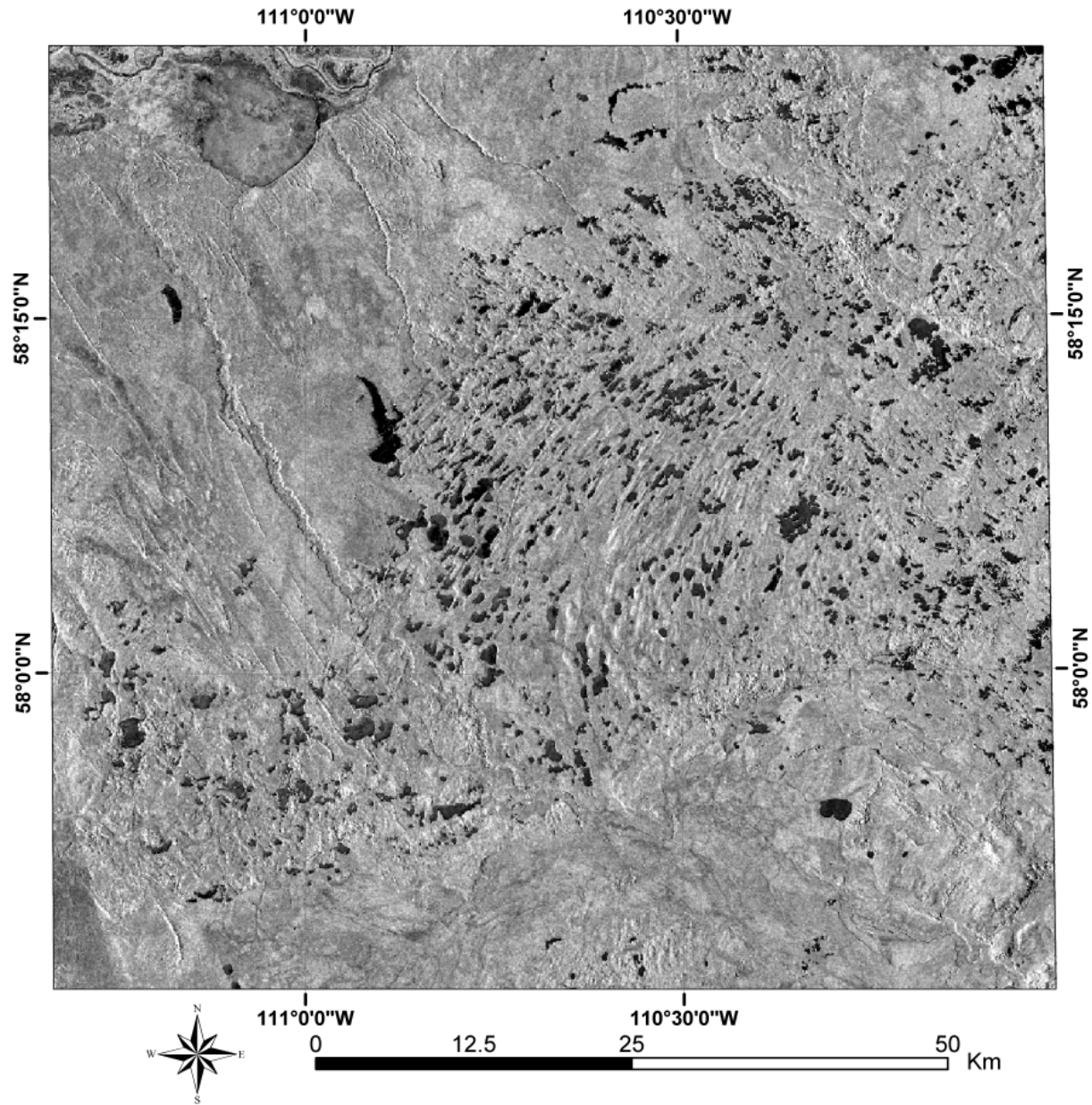
Figure 22. Image processed using an algorithm (S1A + S7A - S1D) for the study area.
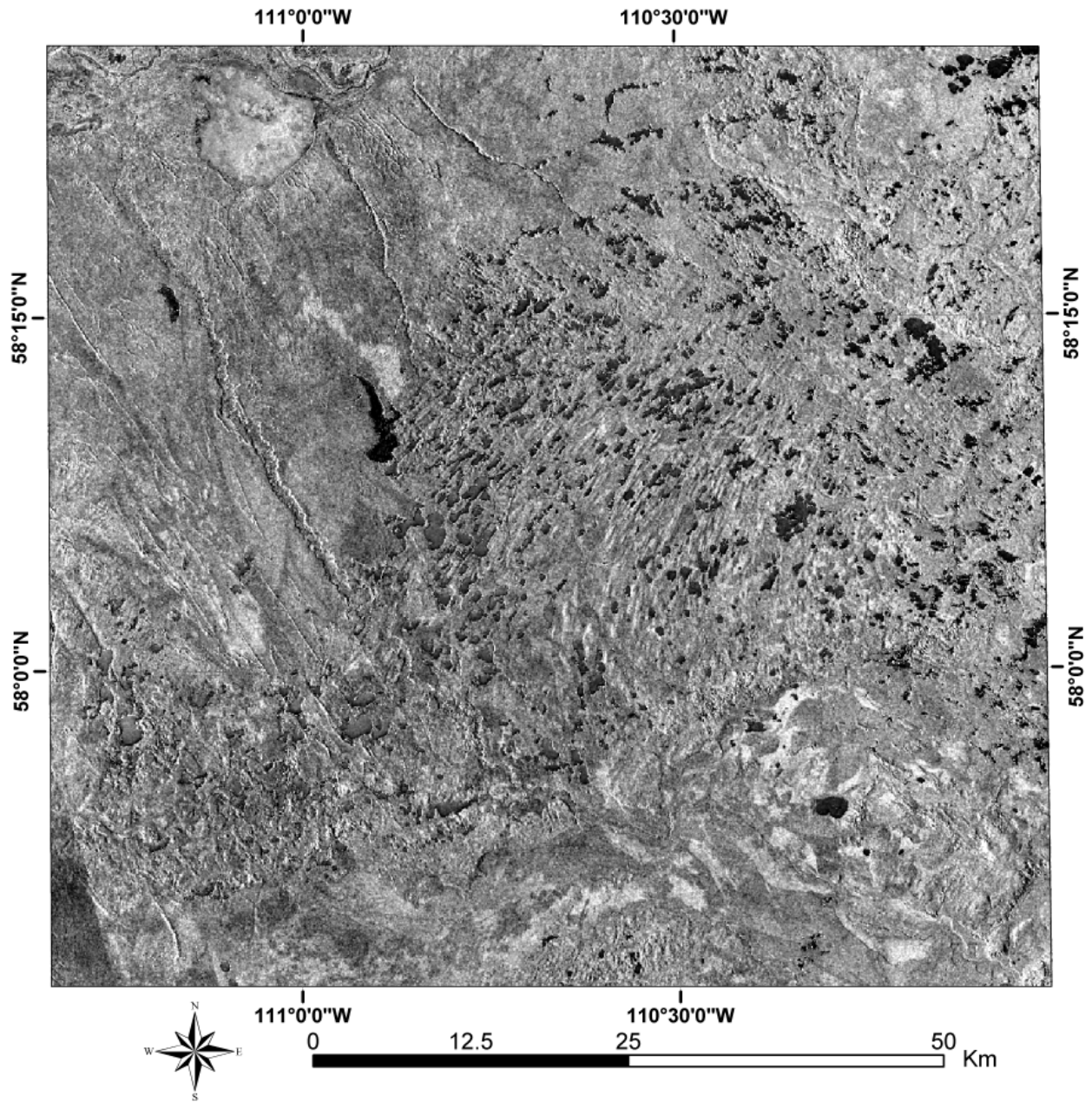
Figure 23. Image processed using an algorithm (S1A + S7A - S7D) for the study area.
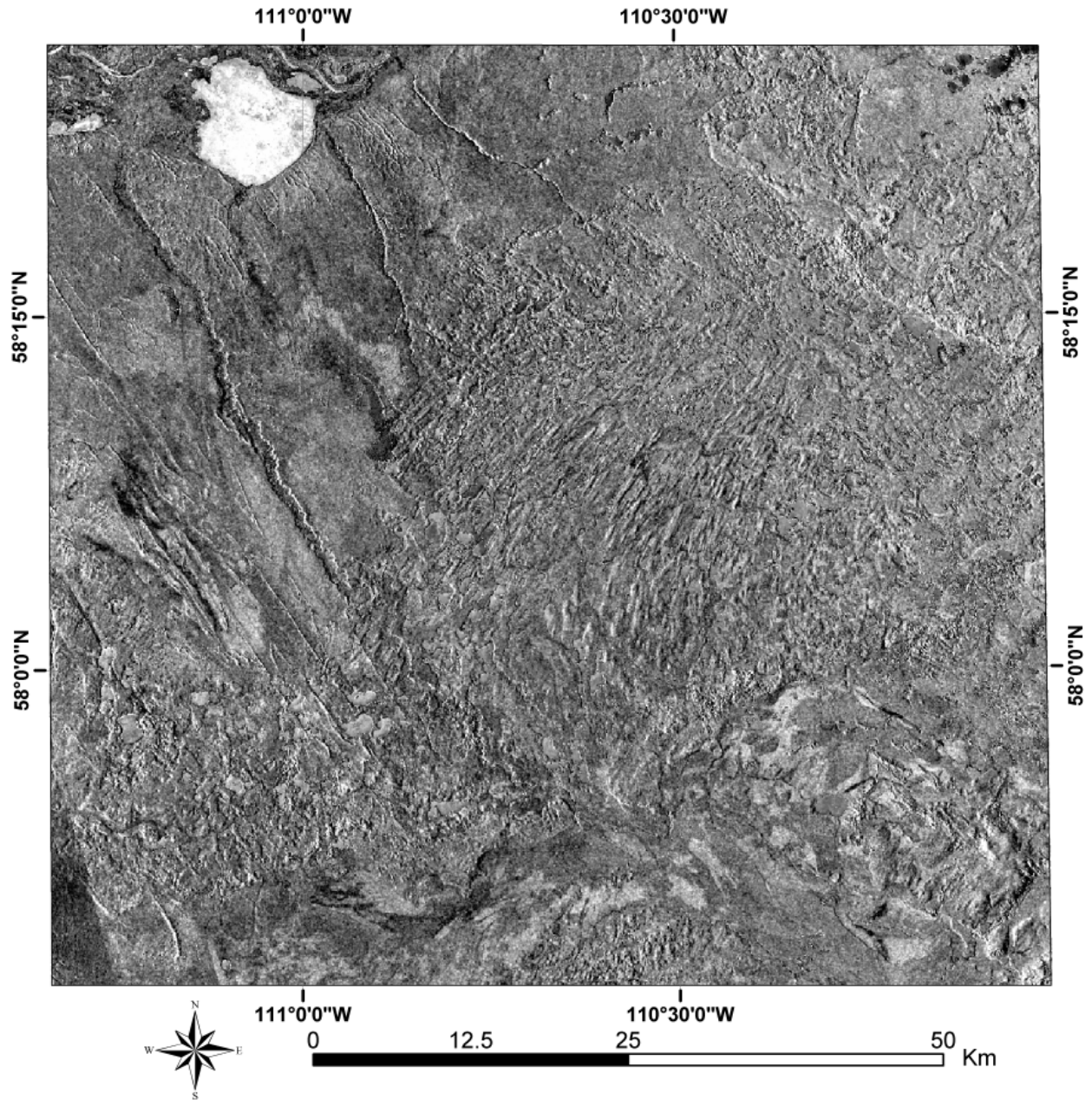
Figure 24. Image processed using an algorithm ((S1A + S7A)-(S1D + S7D)) for the study area.
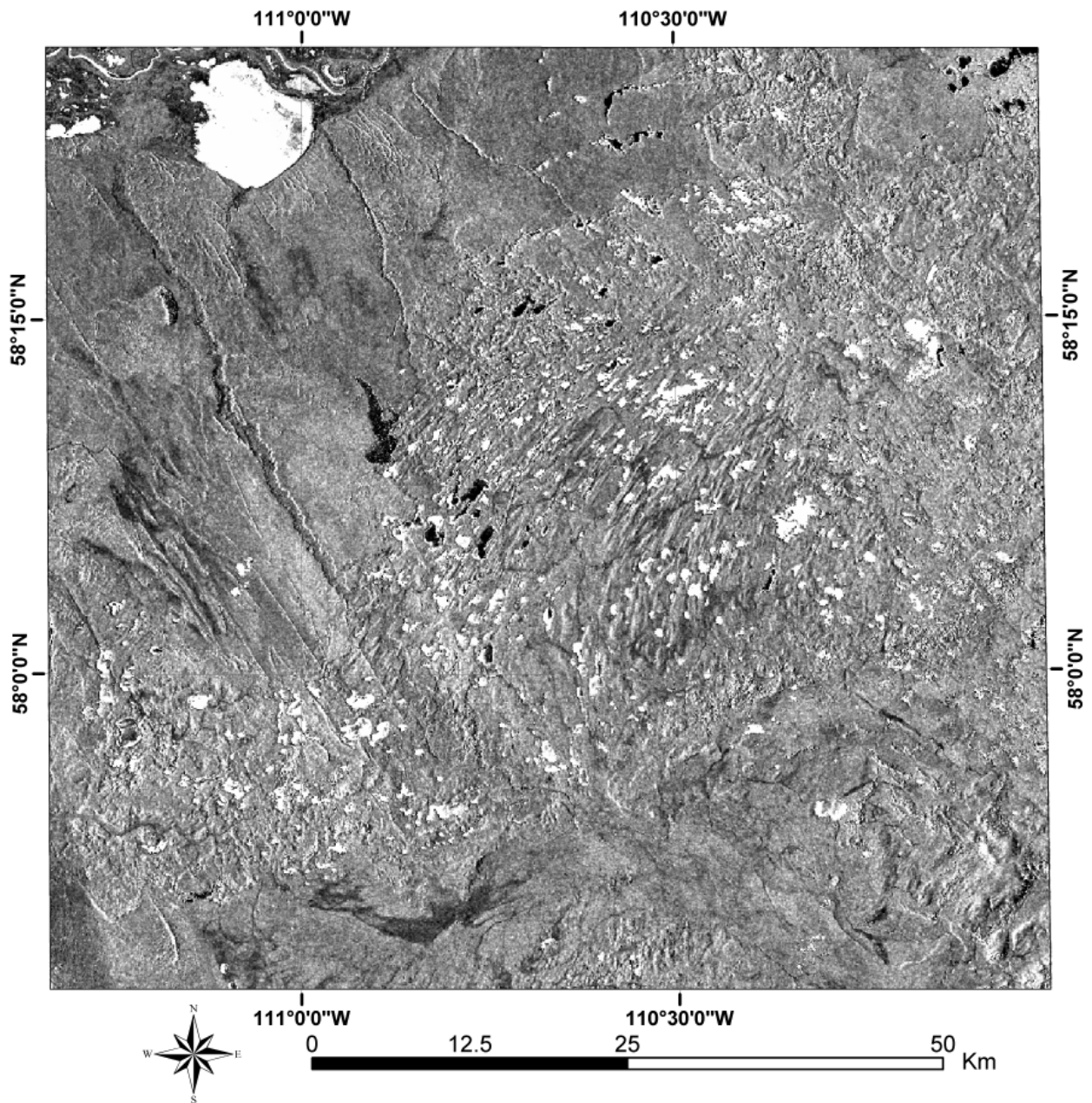
Figure 25. Image processed using an algorithm ((S1A + S7A)/S1D) for the study area.
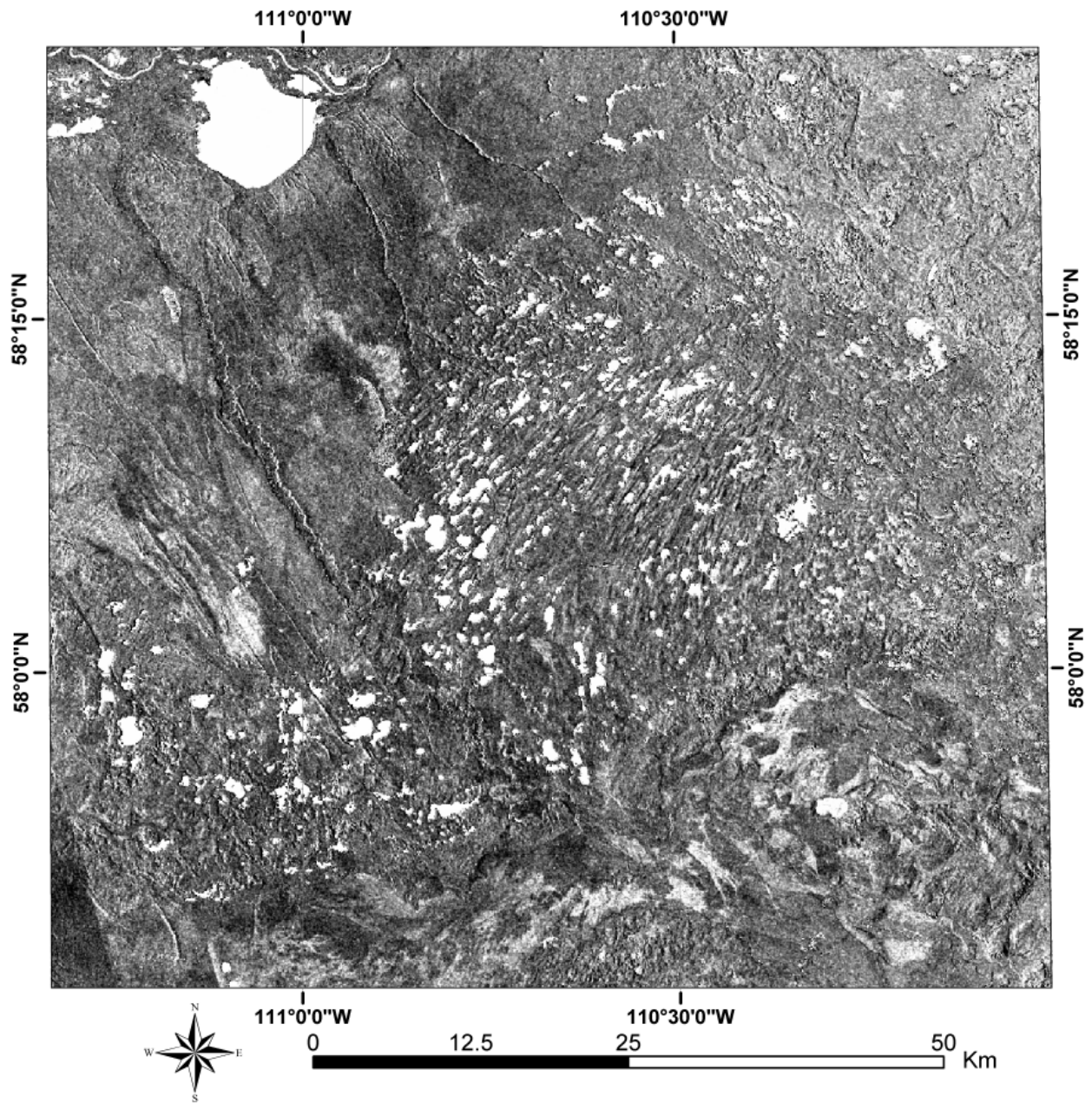
Figure 26. Image processed using an algorithm ((S1A + S7A)/S7D) for the study area.
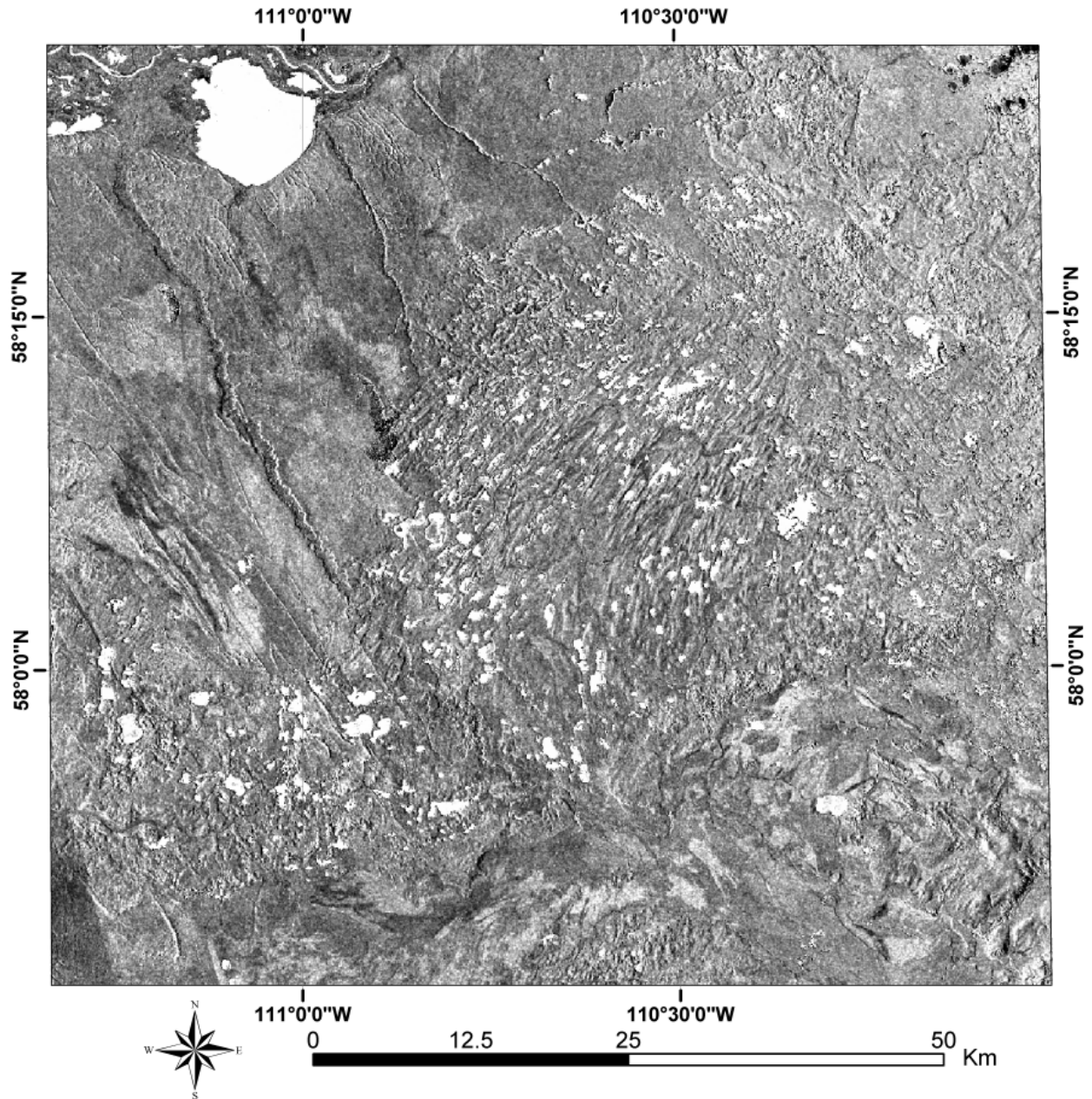
Figure 27. Image processed using an algorithm ((S1A + S7A)/(S1D + S7D)) for the study area.
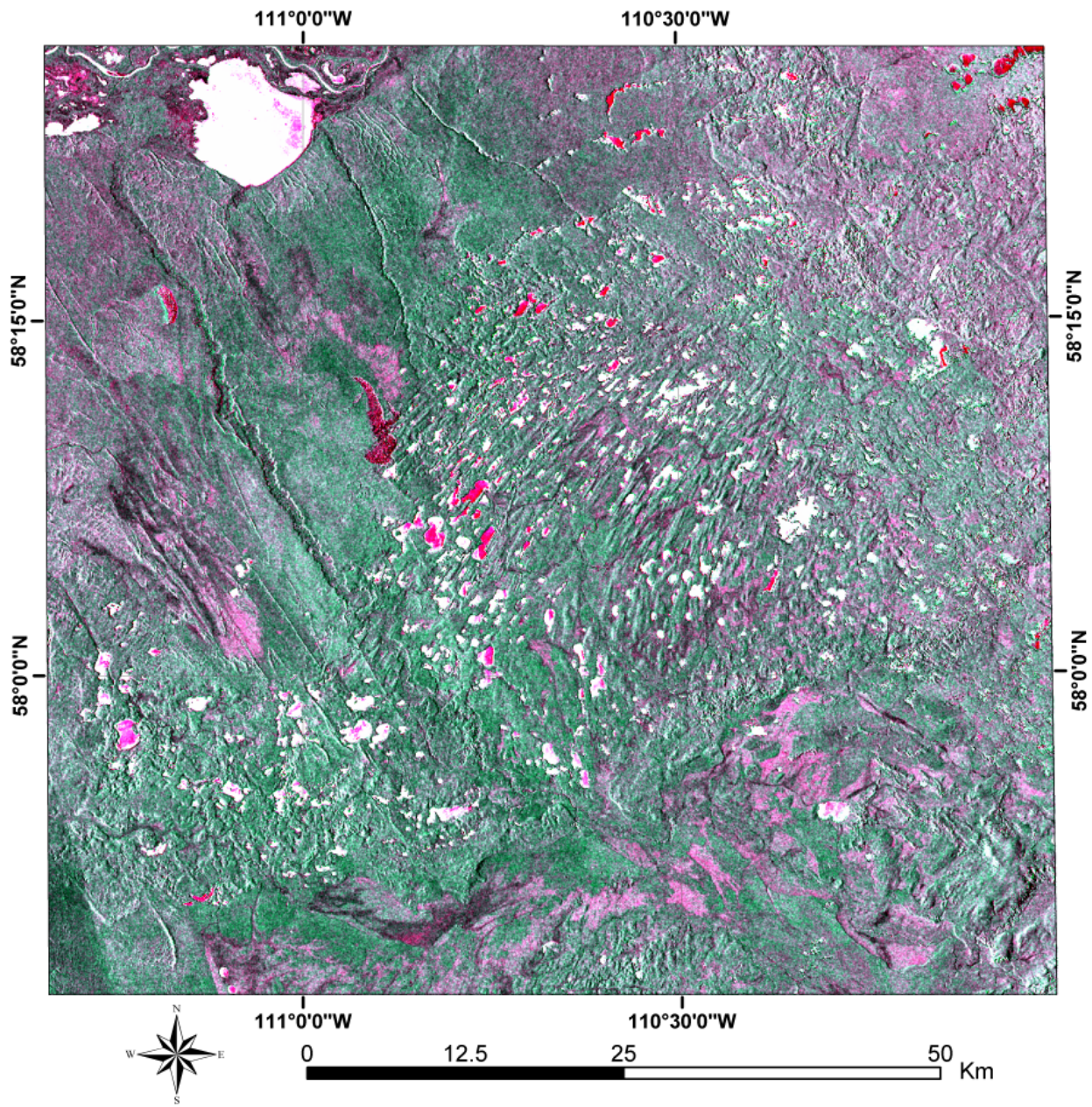
Figure 28. Pseudocolour composite image using (S1A + S7A)/S7D as red, (S1A + S7A)/S1D as green, and (S1a + S7A)/ (S1D + S7D) as blue.
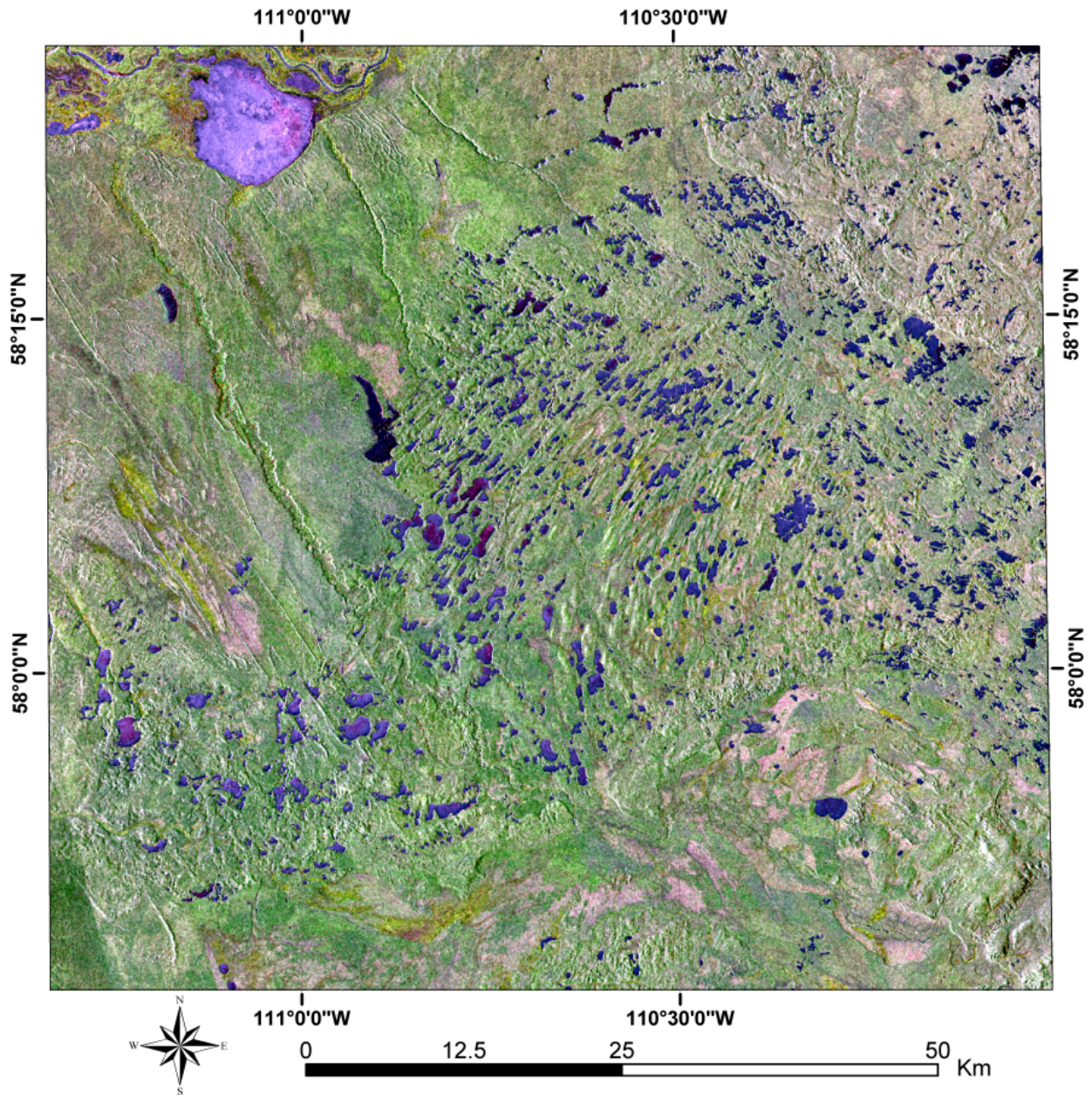
Figure 29. Pseudocolour composite image using (S1A + S7A) - S7D as red, (S1A + S7A) - S1D as green, and (S1A + S7A) - (S1D + S7D) as blue.
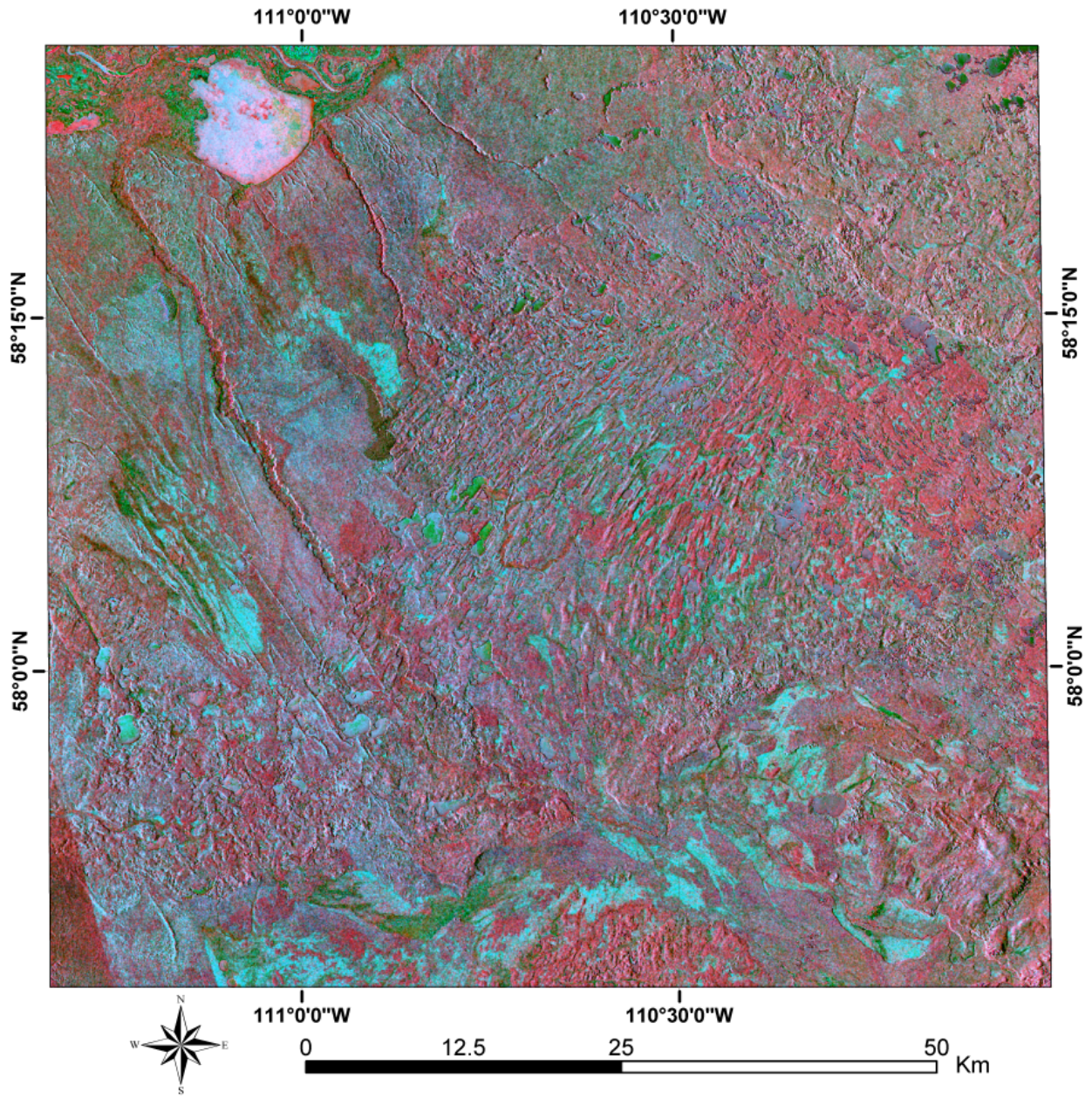
Figure 30. Pseudocolour composite image using PC3 as red, PC2 as green, and (S1A - S1D) as blue.
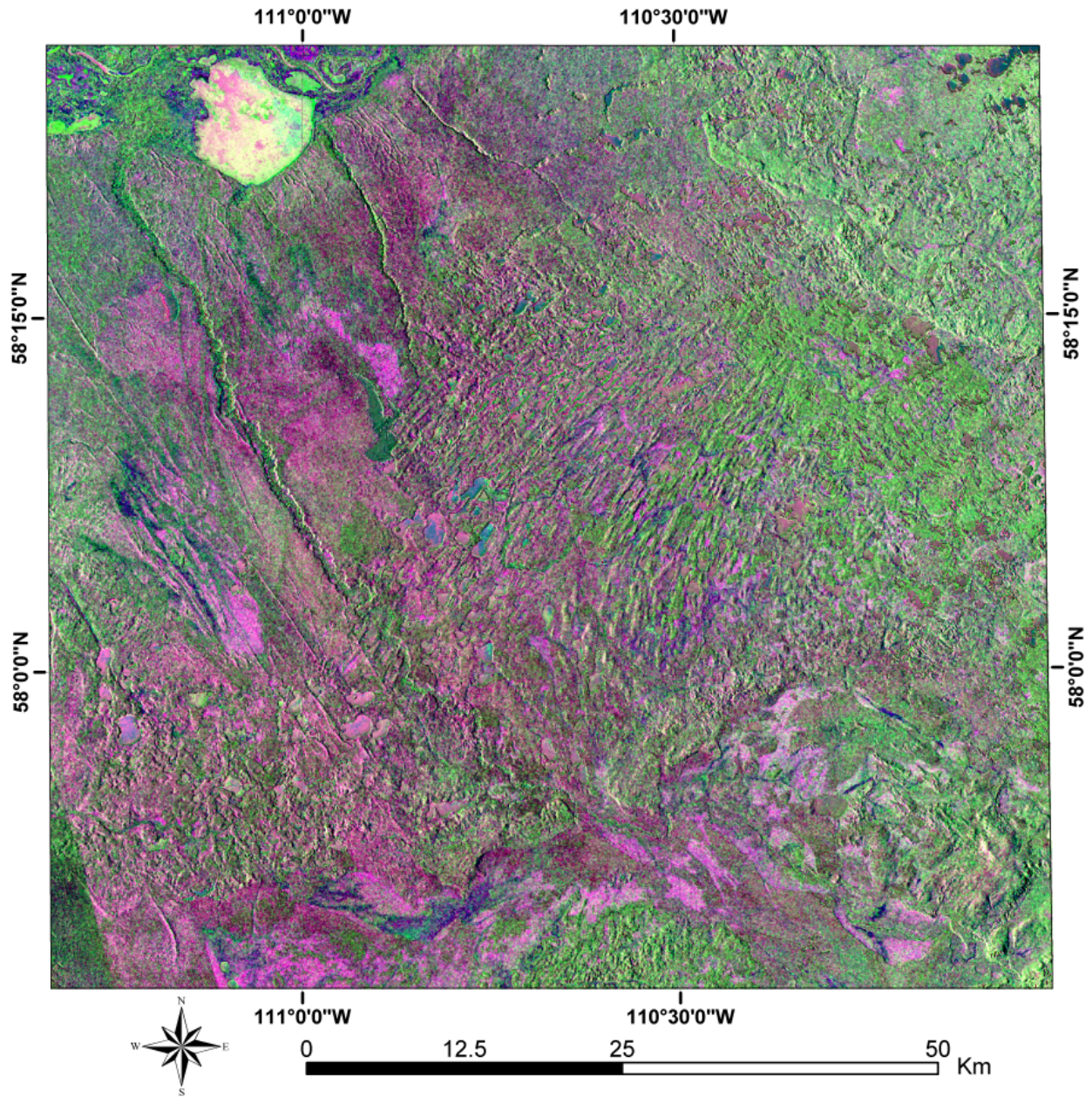
Figure 31. Pseudocolour composite image using S1A - S1D as red, S7A - S7D as green, and PC2 as blue.

Table 3. List of the RADARSAT-1 SGF images used for DEM extraction.

Scene ID	Beam	Path	UL_LAT	UL_LONG	UR_LAT	UR_LONG	LR_LAT	LR_LONG	LL_LAT	LL_LONG
M0196917	S1	ASC	58:35:25.54N	111:41:10.61W	58:50:28.23N	109:46:02.45W	57:55:39.28N	109:21:11.66W	57:40:51.52N	111:13:20.74W
M0196916	S1	ASC	57:46:13.07N	111:16:02.23W	58:01:02.24N	109:23:36.07W	57:06:10.63N	108:59:36.40W	56:51:35.42N	110:49:12.23W
M0195851	S1	DES	58:22:29.69N	111:30:45.42W	58:07:41.70N	109:37:47.85W	57:13:05.13N	110:04:59.87W	57:27:38.89N	111:55:04.32W
M0195850	S1	DES	59:11:55.27N	111:07:59.91W	58:56:53.56N	109:12:18.05W	58:02:21.10N	109:40:31.58W	58:17:07.58N	111:33:11.38W
M0199053	S7	ASC	58:41:05.88N	111:37:08.77W	58:49:27.60N	109:41:59.46W	57:54:50.30N	109:28:46.59W	57:46:28.31N	111:20:58.92W
M0199052	S7	ASC	57:51:43.27N	111:22:32.08W	58:00:05.19N	109:30:03.93W	57:05:27.88N	109:17:05.44W	56:57:05.36N	111:06:45.95W
M0195871	S7	DES	58:20:12.96N	111:25:13.44W	58:11:53.79N	109:31:57.84W	57:17:16.68N	109:47:50.82W	57:25:36.37N	111:38:15.50W
M0195870	S7	DES	59:09:32.89N	111:13:15.09W	59:01:13.84N	109:17:15.20W	58:06:37.70N	109:33:32.34W	58:14:56.93N	111:26:31.74W

axis. Two epipolar pairs were created for the ascending pass and two for the descending pass, and a 4 x 4 average filter was applied in the process. Epipolar DEMs are then extracted from the overlap between the epipolar pairs for ascending and descending passes, respectively. The extracted epipolar DEMs are not georeferenced. Finally, the epipolar DEMs were georeferenced into UTM 12 with an ellipsoid of WGS84, and mosaicked. This resulted in two DEMs, one from the ascending images and the other from the descending images (Figures 32 and 33). Only the GCPs included with the SGF images were used for georeference, due to time limitations. The DEMs extracted represent relative elevation, and the horizontal accuracy has not been fully evaluated. Toutin (1999) reported an elevation error of 11 metres with 90% of confidence for low terrain relief, 27 metres for moderate terrain relief and 14 metres for high terrain relief, using the same side Standard Beam 1 and 7 images and automatic image matching. The accuracy of the extracted DEMs in the present study is estimated to be 27 metres as recorded for moderate terrain relief by Toutin (1999). Areas of miscorrelation occur as black holes in the resultant DEMs (Figures 32 and 33). Most were found to correspond to very flat areas, including lakes, sand sheets and wetlands. Colour balancing was not applied during mosaicking of extracted DEMs. Some differences between scenes persisted into the final analysis (Figure 33). However, the effects of these artifacts can be ignored during the visual interpretation of lineaments.

4.5 DEM Based on the National Topographic System

The Digital Elevation Model (DEM) from the National Topographic System (NTS) (Figure 34) was purchased from Geometric Canada, Natural Resources Canada in November 1998. The source format is in Canadian Digital Elevation Data (CDED). It is based on the NTS maps at the 1:250,000 scale. Other complementary sources include elevation data, aerotriangulation control points and geodetic control points. Grid spacing is based on the geographic coordinates at a spacing of three arc seconds. In metres, the spacing is about 93 metres in the north-south direction and varies from approximately 30 to70 metres in the west-east direction, depending on latitude. The CDEM data consist of elevation data in metres relative to mean sea level based on the NAD83 horizontal reference datum. Since all data came from scanning NTS map sheets at 1:250 000 scale and since conversion errors are cumulative, sometimes the data quality might be somewhat lower than that of the source product. The CDED were compiled from all the hypsographic and hydrographic elements on the original 1:250 000 map. Supplementary control points from Geodetic Survey and Aerial Survey Database are added in the process to enhance accuracy. The accuracy also depends on the original map from which the data are scanned. Source from http://maps.nrcan.gc.ca/search/ntsquery.html (last accessed August 2004) indicates the DEM has a 250-metre horizontal accuracy and a 25-metre vertical accuracy for the area south of 58 degrees north latitude, and a 125-metre horizontal accuracy and a 25-metre vertical accuracy for the area north of 58 degrees north latitude.
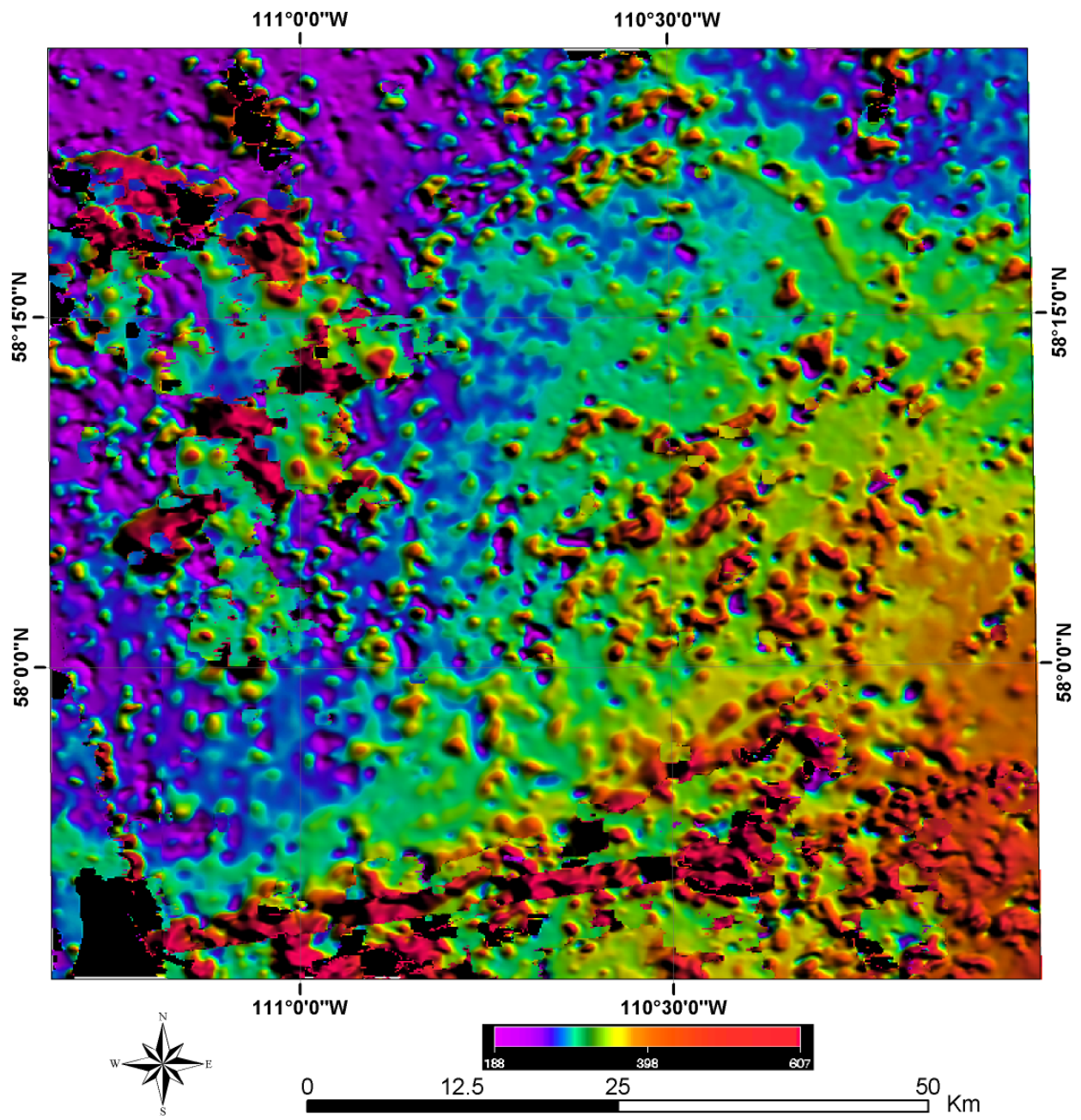
Figure 32. Relative DEM extracted from RADARSAT-1 Standard Beam 1 and 7 image pairs from ascending pass.
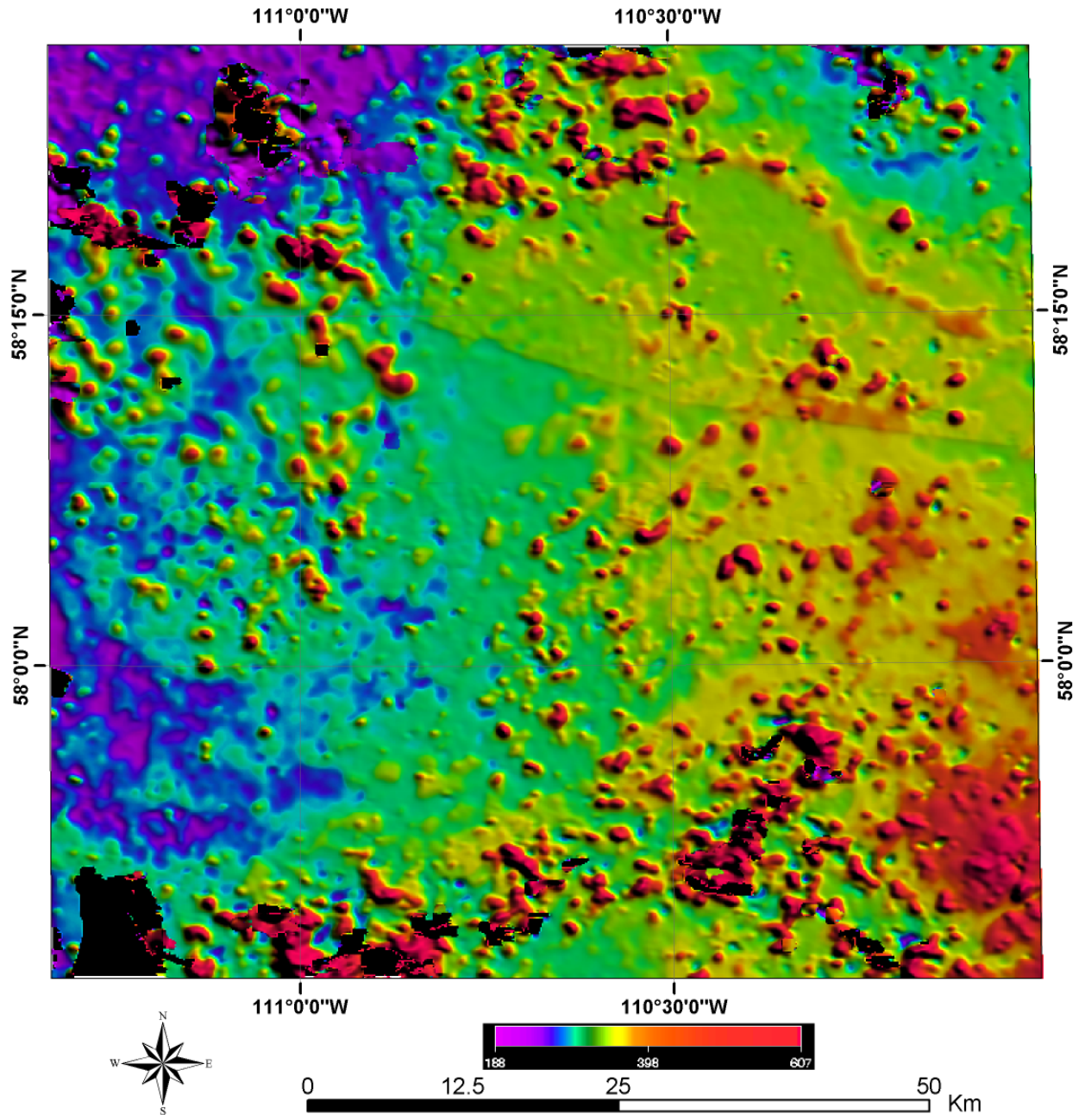
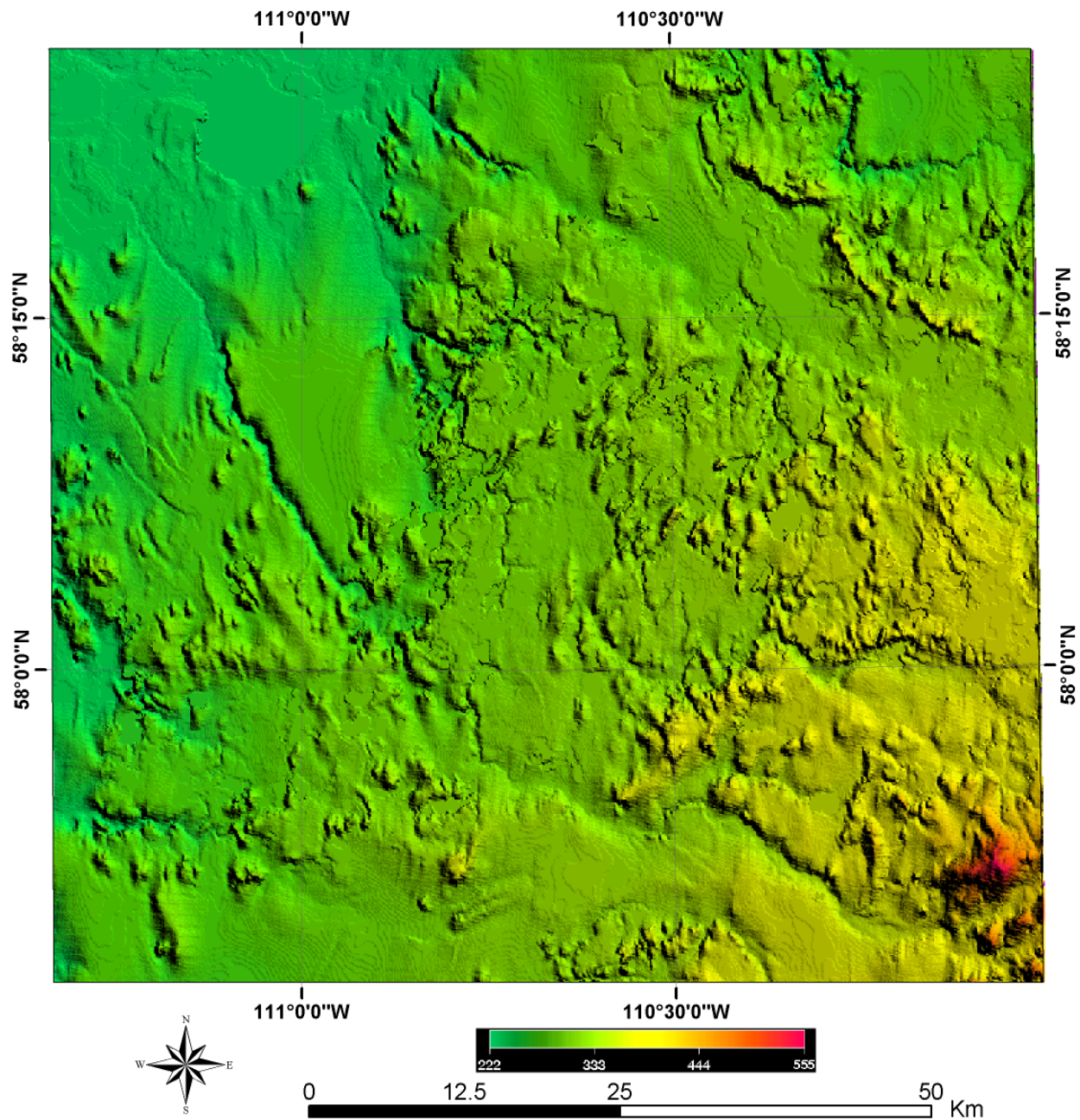**Figure 33. Relative DEM extracted from RADARSAT-1 Standard Beam 1 and 7 image pairs from descending pass.**

Figure 34. DEM from NTS displayed in pseudocolour combined with sunshade relief with an azimuth of 45 degrees and a sun elevation of 45 degrees.

4.6 DEM From Shuttle Radar Topography Mission

The Shuttle Radar Topography Mission (SRTM) aboard the Space Shuttle Endeavour was launched on February 11, 2000. The objective of the SRTM is to obtain elevation radar data on a near-global scale and generate the most complete high-resolution digital topographic database of the Earth. To date, it has generated a digital topographic map for 80 per cent of the Earth's land surface (between 61 degrees north and 56 degrees south latitude), at 30-metre pixel resolution with data points spaced every 1 arc second of latitude and longitude (approximately 30 metres). The mission objective is to produce digital topographic map products with less than or equal to 20 m absolute horizontal circular accuracy, less than or equal to16 m absolute vertical height accuracy and less than or equal to 10 m relative vertical height accuracy. These accuracies are quoted at the 90% level, consistent with National Map Accuracy Standards of USA. Extensive DEM data from a single source, as with SRTM, are especially desirable because they are consistent and comparable across large areas, whereas other high resolution DEMs are derived from variable sources. The SRTM DEM at 30-metre pixel size are averaged into 90-metre pixel size (3 arc second) and have become available for North America and South America. The SRTM DEM data (Figure 35) for the study area have a 50-metre x 90-metre pixel size and were ordered from http://seamless.usgs.gov/.

A comparison of the SRTM DEM (Figure 35), NTS DEM (Figure 34) and RADARSAT-1 DEM (Figure 33) indicates the SRTM is superior to the other two DEMs in depicting topographic details. The RADARSAT-1 DEM shows some features that cannot be clearly seen from the NTS DEM. A comparison of the SRTM DEM and the processed RADARSAT-1 images (Figures 28–31) indicates the processed RADARSAT-1 images depict most of the surficial roughness that can be seen in the SRTM DEM. In addition, the processed RADARSAT-1 images contain additional land cover type and moisture information.

4.7 Landsat Image

The Landsat 7 image (Figure 1) used here is a subset for the study area clipped from the Alberta mosaic of Landsat 7 Enhanced Thematic Mapper (ETM) plus, produced by Photosat (www.photosat.ca). The Landsat 7 image is a natural colour image mosaicked from cloud-free images taken in the summer of 2001, sharpened with the panchromatic band (15-metre resolution) and then re-sampled into 12.5-metre pixel size. This image mainly serves as an alternative to field ground-truthing. It is used to differentiate such surficial lineaments as linear sand dunes, land cover boundaries, fire tracks, roads, etc., from those lineaments that could have a bedrock origin.

4.8 Scanned Surficial Maps

The surficial maps for NTS 74E and 74L by Bayrock (1970a, 1970b) were scanned and registered to a UTM 12 projection with a datum of NAD83 using ArcInfo. An average error of 50 m is recorded for the registered surficial map when compared to the orthorectified satellite images. The scanned surficial geological maps are mosaicked, and a surficial geological map is a subset for the study area. This map is fused with the PC3 image to produce a map of surficial geological background (see Figure 3) for the present study.

5   Results

Although a number of image processing and statistical techniques have been proposed to assist in recognizing linear features and evaluating their significance, these have not come into widespread use. Some of the image enhancement techniques have been recast as automated digital procedures for lineament extraction. One of the examples is the Lineament Extraction Module of PCI Geomatica. It is
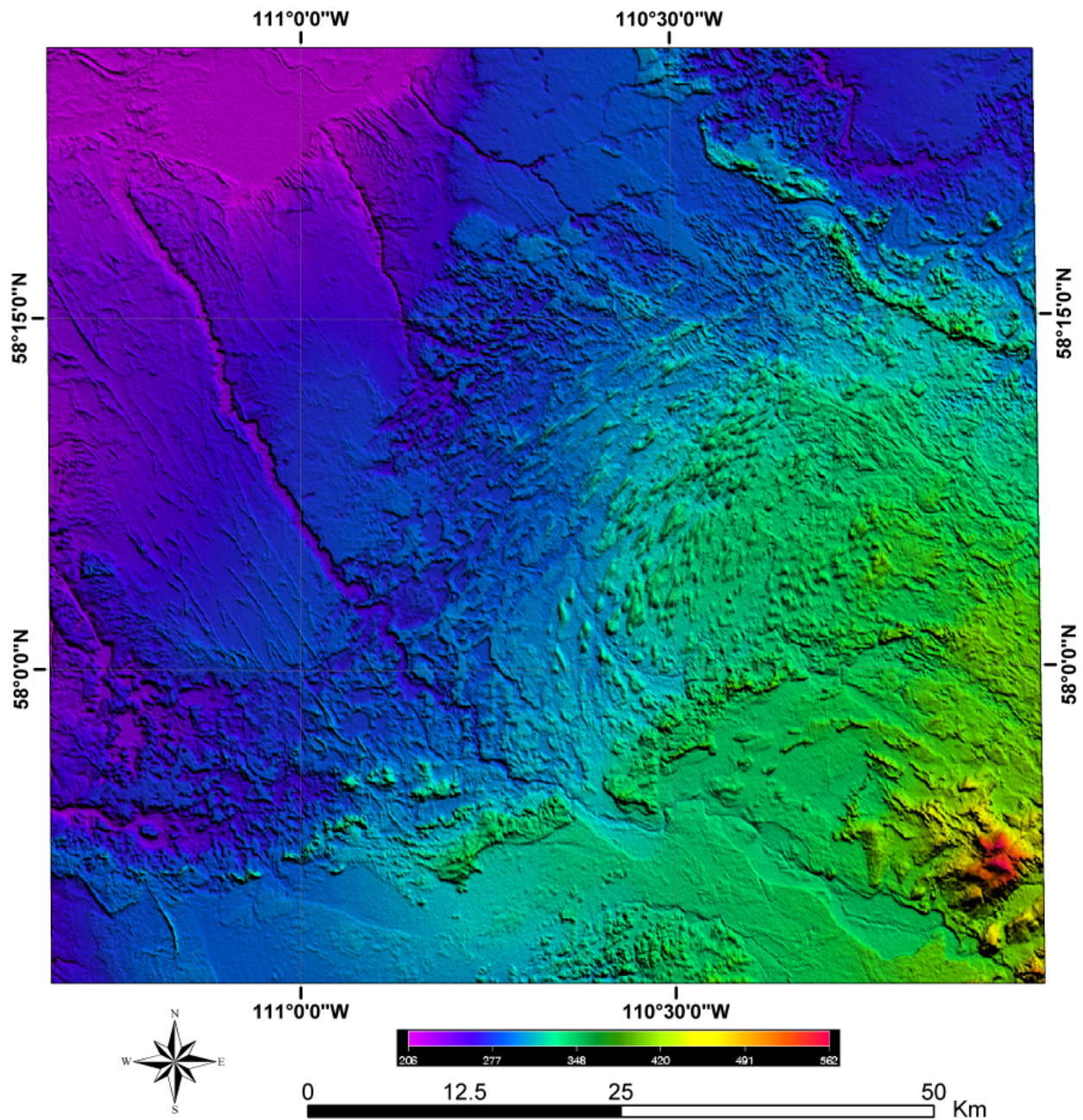
Figure 35. SRTM DEM displayed in pseudocolour combined with sunshade relief with an azimuth of 45 degrees and a sun elevation of 45 degrees.

a numerical method for lineament detection by applying an edge-detection filter to the image. As a test, this method was applied to the (S1A + S7A)-(S1D + S7D) image for automatic lineament extraction, and the result is shown in Figure 36. It appears this method tends to provide an excessive number of lineaments, with the probability that most are not related to underlying bedrock faults. Thus, this method is not as useful as the human visual system. The human visual system is very good at extrapolating linear features. To the eye, a lineament varying in intensity along its length may be viewed as a single long lineament, whereas to a numerical method this may appear as several short lineaments. In addition, the human interpreter, based on his knowledge and experience of the study area, can easily discriminate the interesting lineaments from those of no interest to the study purpose. In short, the automatically extracted lineaments (Figure 36) include those from linear sand dunes, drumlins, crevasse fillings, wetland boundaries, etc, and thus the pattern of the underlying bedrock and more interesting potential structural lineaments are obscured. As a result, the automatically extracted lineaments are used only for reference during the interpretation process.

It needs to be pointed out that the lineament interpretation carried out in this study was not biased by the known occurrence of the uranium zone at Maybelle River. However, for the reader's benefit the location of the Maybelle uranium zone, based on the uraniferous intersection in drillhole MR-39, is shown on the various maps of lineament interpretation as described in the following text.

Lineaments were visually interpreted separately for each of the processed false colour RADARSAT-1 images, DEM extracted from the RADARSAT-1 images, NTS DEM and SRTM DEM. Interpretation of the processed RADARSAT-1 images involved visual pattern recognition of surface linear features resulted from the combination of tone and textural variations. In the processed images (Figures 28–31), differences in surface roughness, moisture and topography have been highlighted. In several places, subtle differences are found between clearly identified lineaments, and they often represent the continuation of the clearly identified segments. Linear features that are obviously attributed to non-bedrock origins, such as linear sand dunes, crevasse fillings, flutings, fire tracks and some wetland boundaries, are excluded. Lineaments are interpreted from all four processed pseudocolour composite images (Figures 28–31), and RADARSAT-1 images, the principal component images and processed grey colour images (Figures 6–27); as a result, these images are frequently referenced during the process of interpretation that follows. Among the numerous recognizable lineaments, only those that can be recognized from at least three of the pseudocolour composite images are included. The result is those lineaments shown in Figure 37.

For the DEMs, two types of sunshade relief DEM images, one from a northeast-looking direction and the other from a northwest-looking direction, were created and used for interpretation. This is because the fact that the detection of linear structure is partially dependent on the look direction of the light source. If a linear feature is parallel to the look direction, then it may be nearly invisible (Harris, 1984; Lowman et al., 1987). Harris (1984) reported that the linear features show up as distinctive lines when the feature is within 20 degrees of the perpendicular to the look direction of the radar sensor. During the interpretation, different sun angles were interactively applied. The interpreted lineaments from different DEM images are shown in Figures 38 through 43.

An overlay of the lineaments (Figure 44) interpreted from all of the processed images and DEMs indicates that: a) the lineament patterns are different depending on the source images; and b) some of the lineaments are recognizable from different images and DEMs. All the interpreted lineaments are compiled into a single ArcView Shapefile, with necessary simplification to remove duplicate lineaments. As a result, 388 lineaments were identified, ranging in length from 0.8 km to 23 km, with a mean of 5.7 km (Figure 45). Each lineament is ranked based on its frequency of occurrence in the seven processed
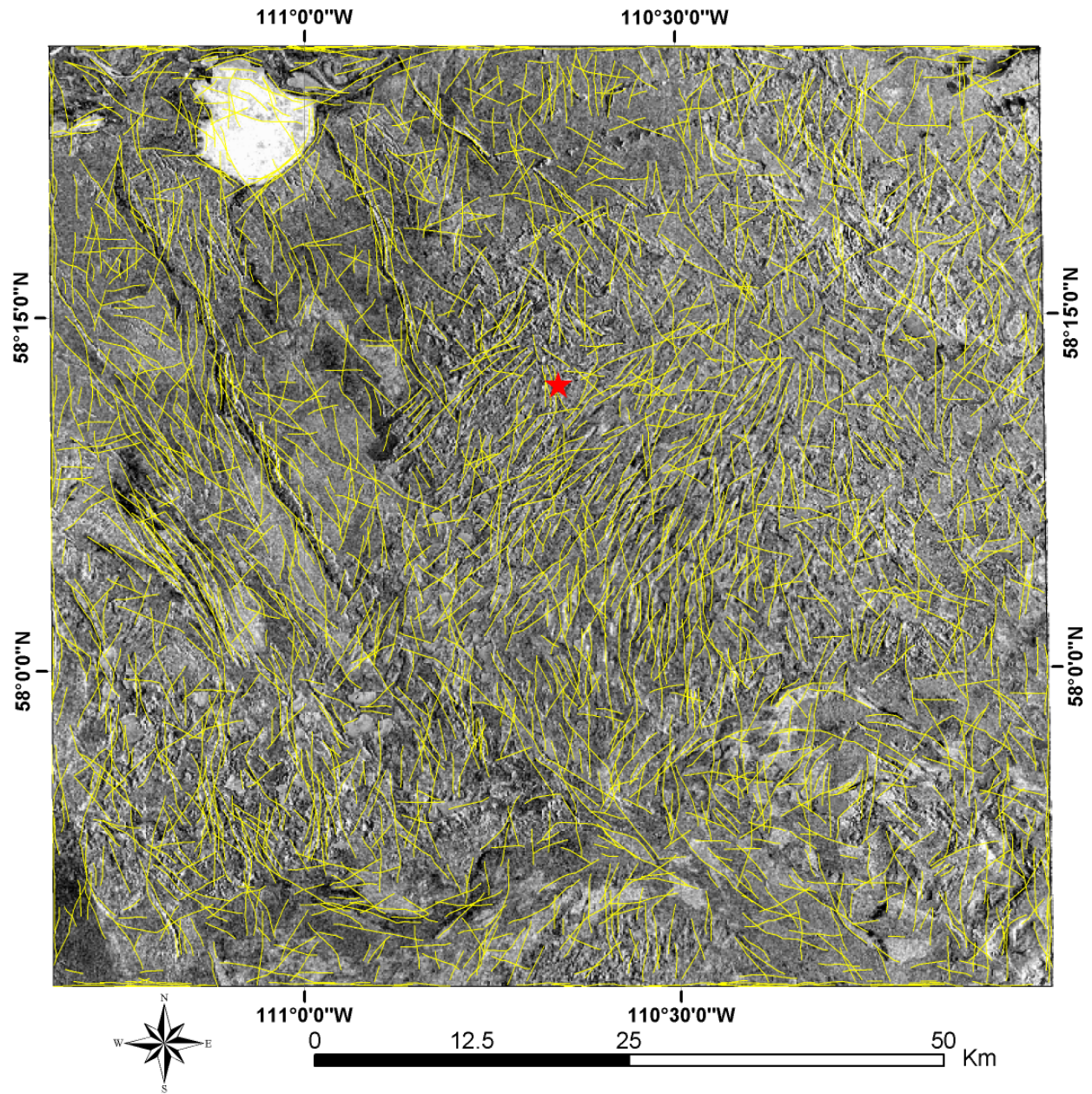
Figure 36. Lineaments automatically extracted from the (s1a+s7a)-(s1d+s7d) image using PCI Geomatica Lineament Extraction Module. The red star on this and subsequent figures identifies the approximate location of the Maybelle River uraniferous zone, which exists at depth near the unconformity between the Athabasca Group and the underlying basement granitoids and gneiss.
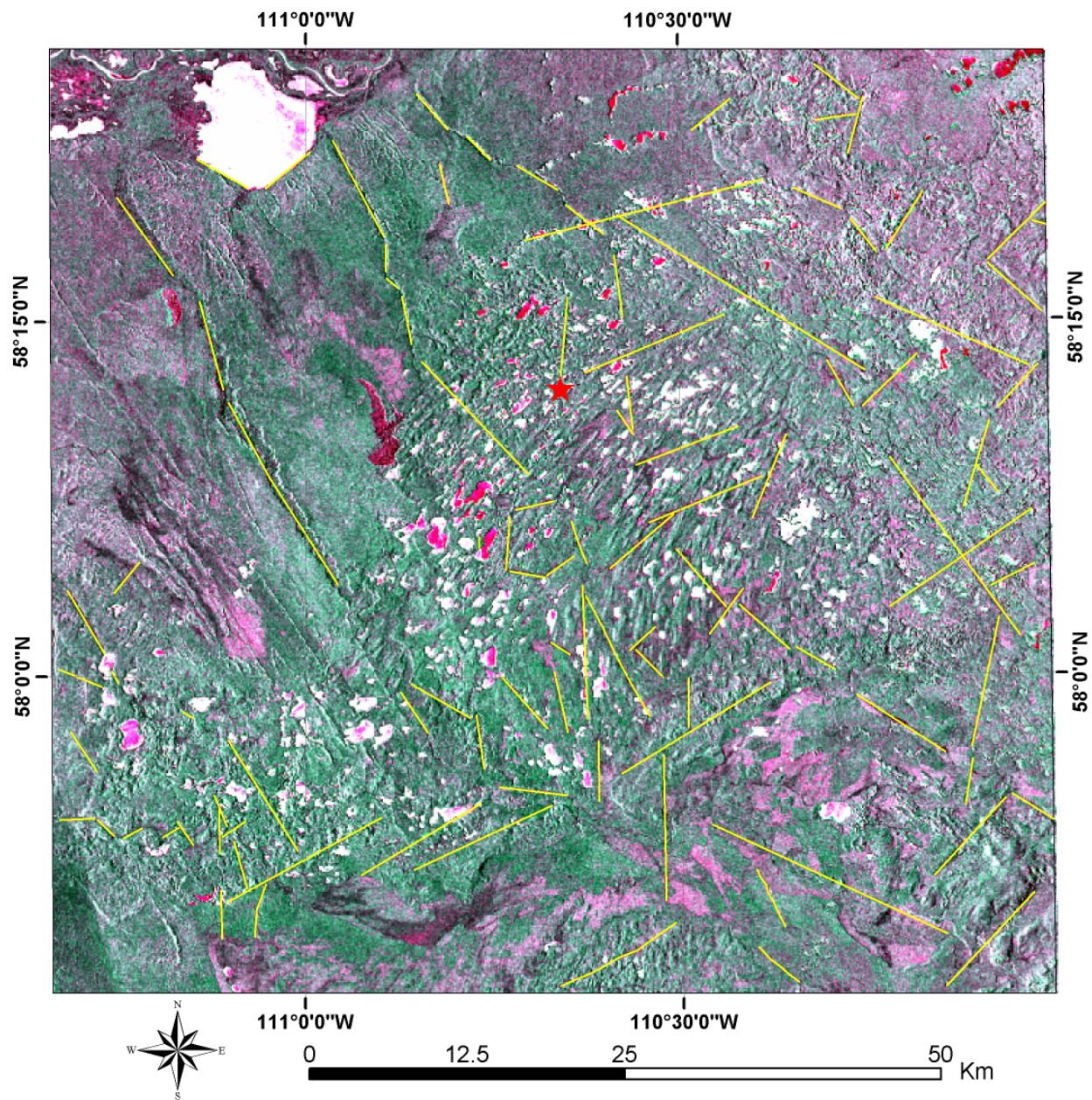
Figure 37. Lineaments interpreted from the processed RADARSAT-1 images. Lineaments are overlaid on top of the pseudocolour composite image using (S1A + S7A)/S7D as red, (S1A + S7A)/S1D as green, and (S1A + S7A)/(S1D + S7D) as blue.
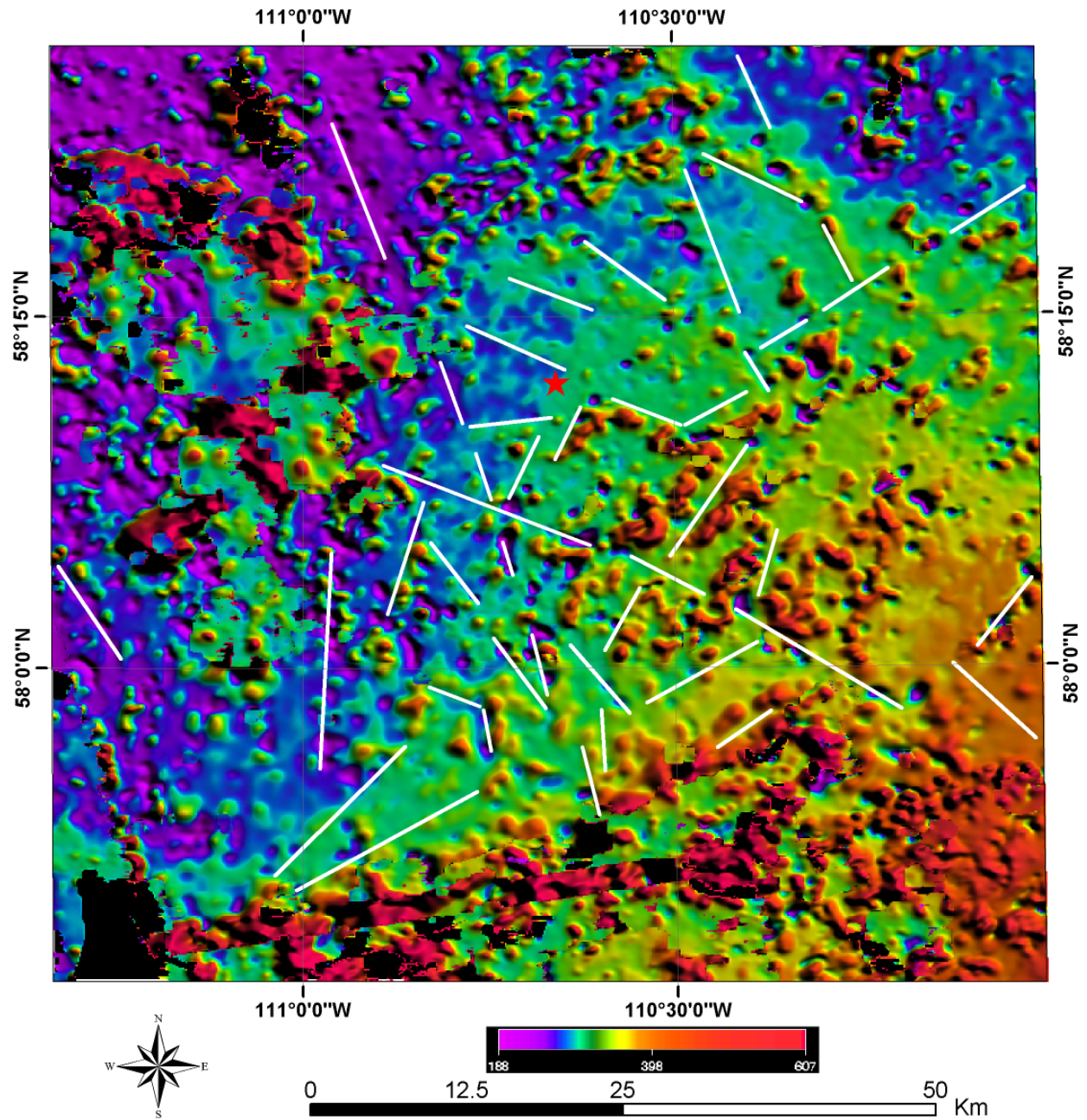
Figure 38. Lineaments interpreted from DEM extracted from RADARSAT-1 Standard Beam 1 and 7 image pairs from the ascending pass.
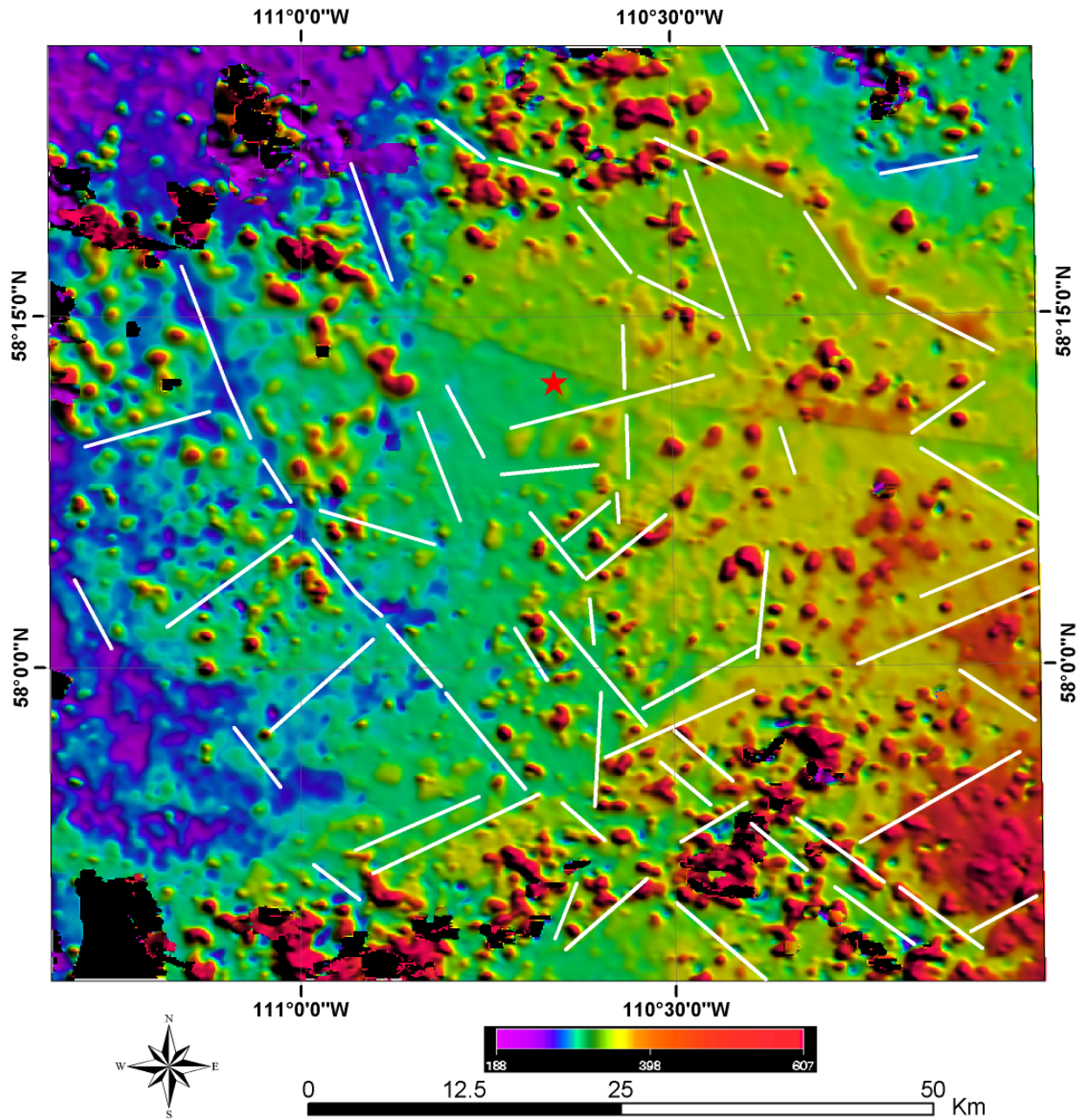
Figure 39. Lineaments interpreted from DEM extracted from RADARSAT-1 Standard Beam 1 and 7 image pairs from the descending pass.
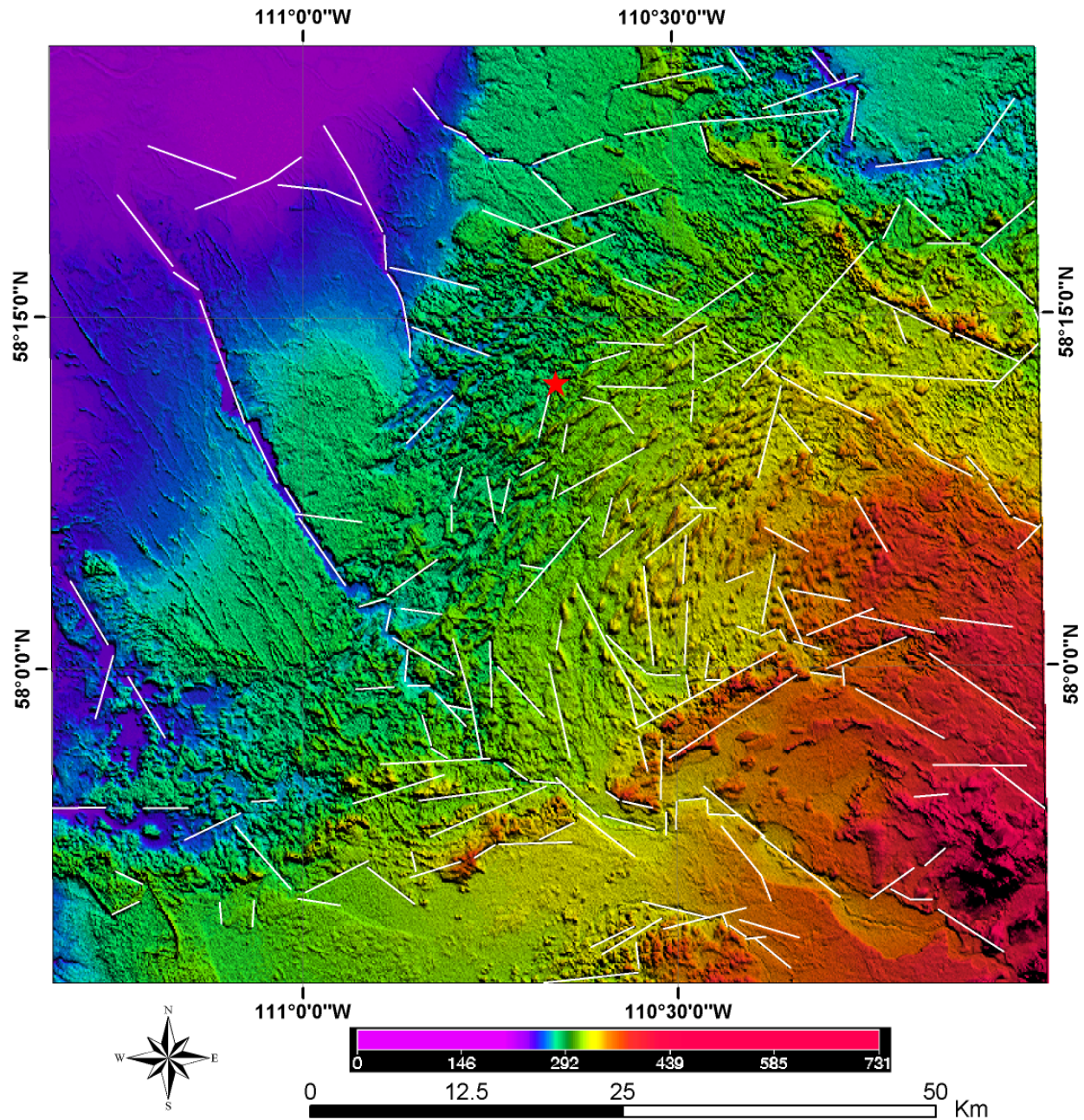
Figure 40. Lineaments interpreted from SRTM DEM displayed in pseudocolour and combined with sunshade relief effect with an azimuth of 45 degrees and a sun elevation of 45 degrees.
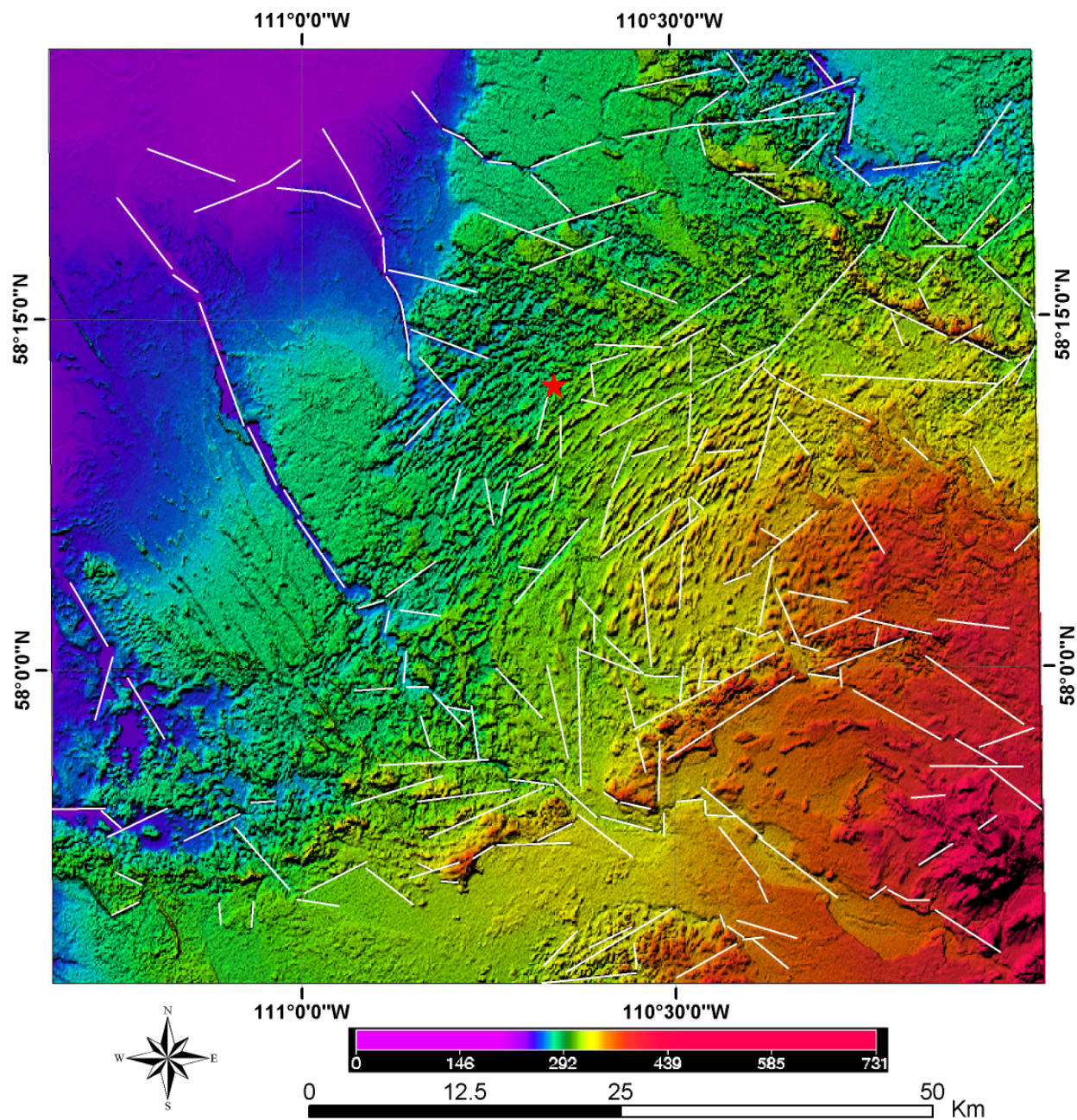
Figure 41. Lineaments interpreted from SRTM DEM displayed in pseudocolour and combined with sunshade relief effect with an azimuth of 315 degrees and a sun elevation of 45 degrees.
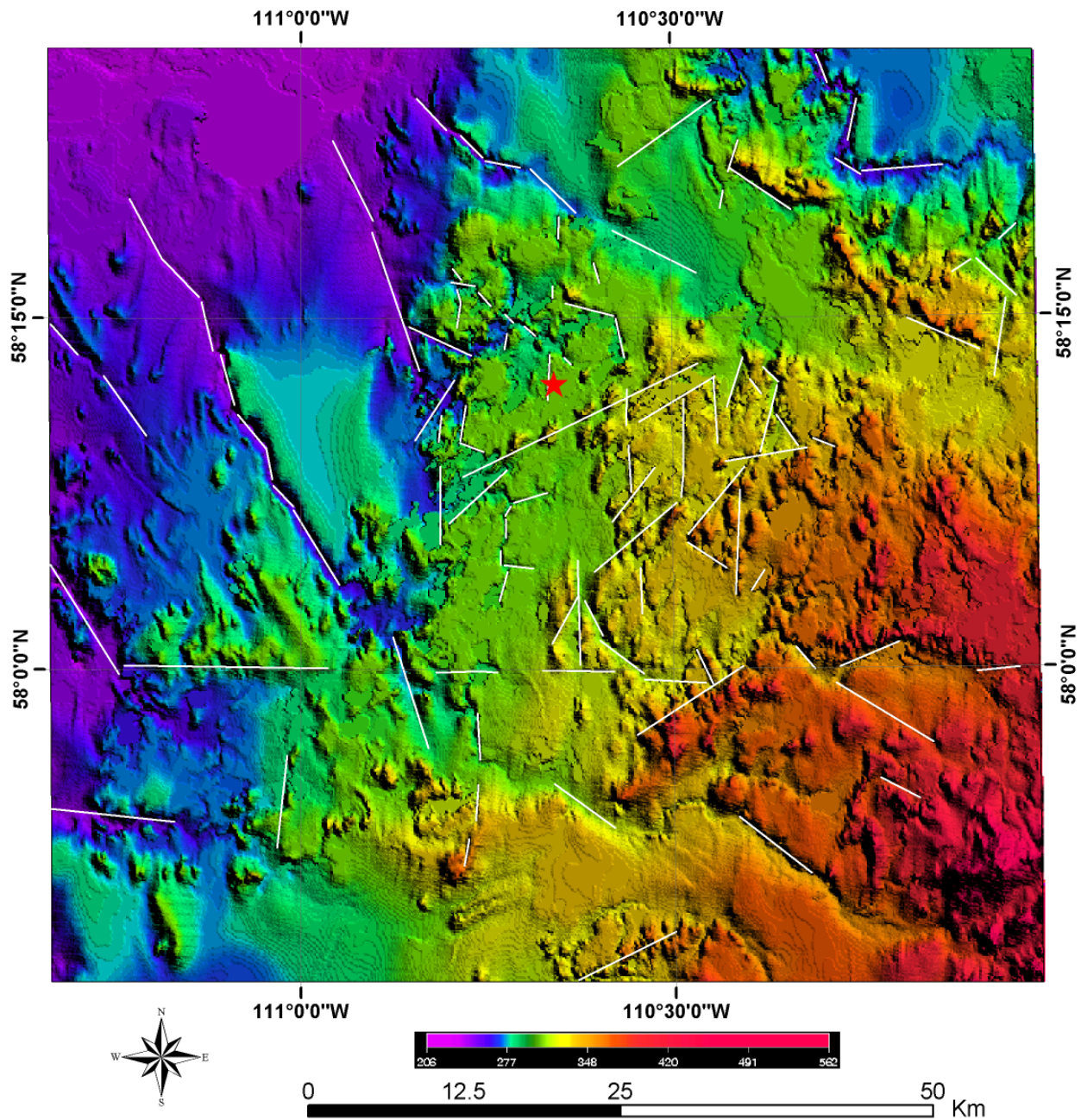
Figure 42. Lineaments interpreted from NTS DEM displayed in pseudocolour and combined with sunshade relief effect with an azimuth of 45 degrees and a sun elevation of 45 degrees.
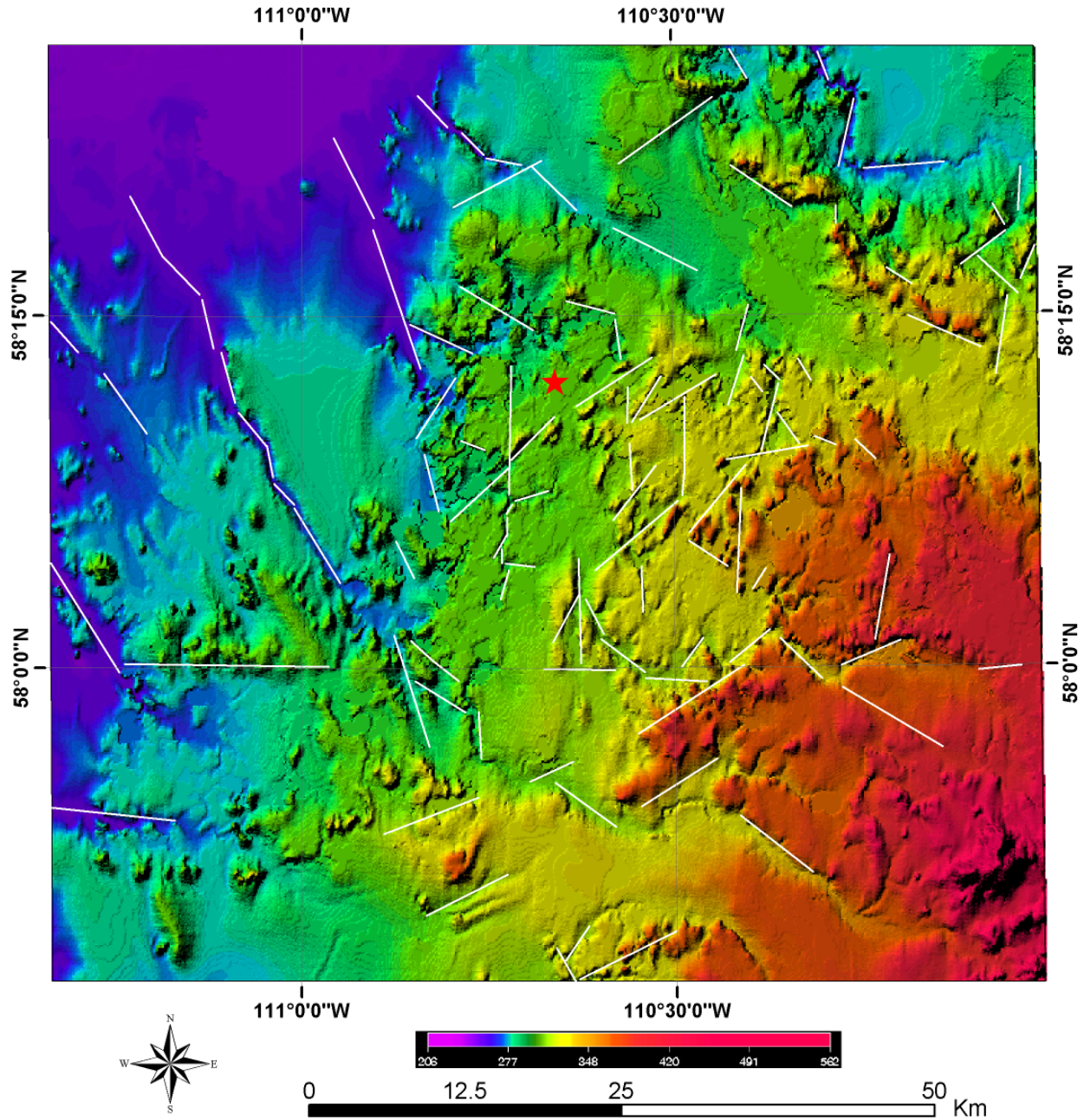
Figure 43. Lineaments interpreted from NTS DEM displayed in pseudocolour and combined with sunshade relief effect with an azimuth of 315 degrees and a sun elevation of 45 degrees.
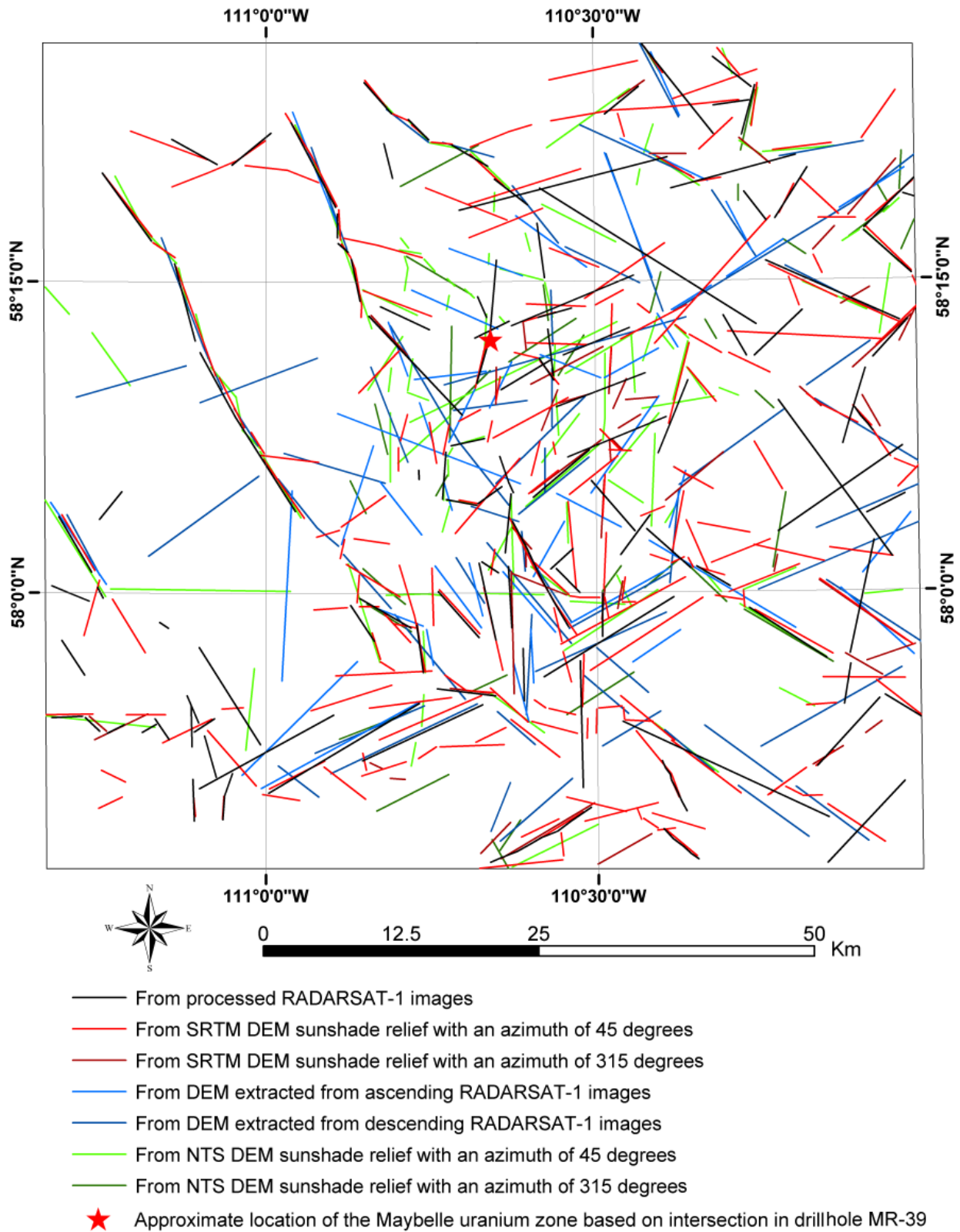
Figure 44. Lineaments interpreted from all seven images and DEMs.
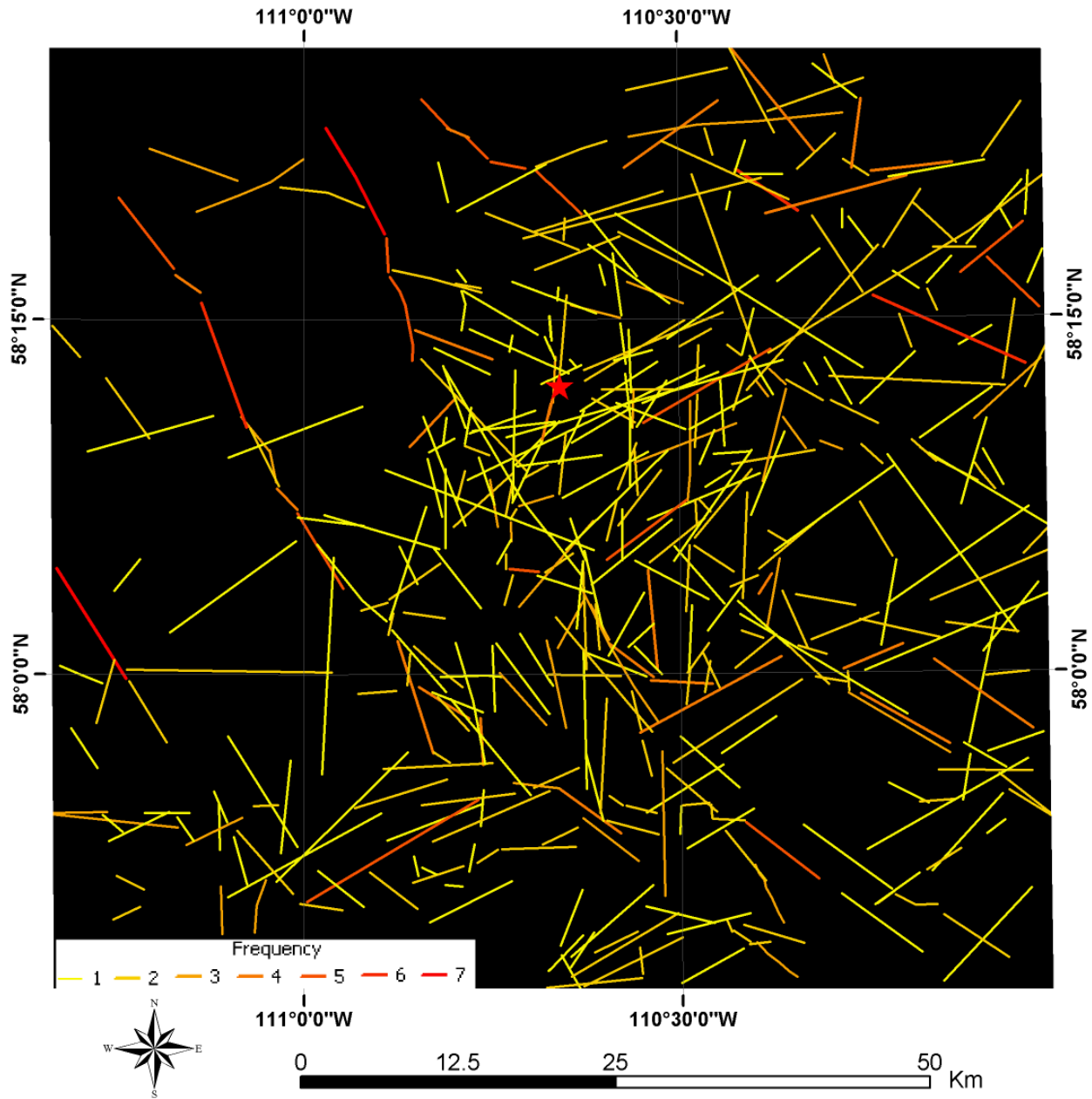
Figure 45. Interpreted lineaments displayed in frequency of occurrences in the seven images and DEMs used for interpretation. "1" means the lineament occurred once among the seven images and DEMs; "7" means the lineament occurred in all of the seven images and DEMs.

RADARSAT-1 and DEM images primarily used for lineament interpretation (Figure 45).

Rose diagrams were created for all interpreted lineaments, based on the total length of lineaments within each bin (Figure 46), and the number of lineaments within each bin (Figure 47). From the rose diagrams, it is clear the east-northeast, northwest and north to south-trending lineaments represent the most prominent linear trends in the study area. A close examination of the lineament pattern indicates that the north to south-trending lineaments often are intersected and offset by the east-northeast and northwest-trending lineaments. Thus, some of these north-south lineaments may represent the oldest structural features in the study area. In some places, the east-northeast trending lineaments intersect and offset the northwest trending lineaments, and in other places, vice versa. As a result, more detailed study needs to be done to determine their relative ages.

6 Discussion and Conclusion

A detailed discussion of the interpreted lineaments in relation to the bedrock geological structure and history is beyond the scope of the present study. Nonetheless, some summary observations and conclusions follow.

The present study indicates that surficial topographic information can be extracted from RADARSAT-1 Standard Beam 1 and 7 images in both ascending and descending passes by simple algorithms to contrast the difference between images from the different looking directions. The principal component 2 and 3 images are not necessarily superior to the images derived directly from the simple algebra algorithms such as (S1A + S7A)-(S1D + S7D) in highlighting the surficial topographic features.

Although RADARSAT-1 images have proven to be very effective in structural mapping in areas with no or thin surficial cover, such as the Canadian Shield, the use of them in such a thick drift-covered area as the Maybelle River area is limited and challenging. A close examination of a previous lineament study conducted by Paganelli et al. (2003) in the Buffalo Head Hills area, north-central Alberta, which is also covered by thick drift and highly vegetated, indicates that the surficial lineaments interpreted from the principal component 2 image (Paganelli et al., 2003, Figure 18B) seldom match the reported subsurface structural lineaments (Paganelli et al., 2003, Figure 18A). However, when proper methodology and suitable criteria for lineament recognition are carefully developed for a specific area, the RADARSAT-1 images are still useful for structural lineament mapping in those cases where seismic and geophysical investigations are not available. The processed RADARSAT-1 images contain information about surficial topography, moisture and land cover type, and thus are superior to the optical satellite images in lineament mapping in areas with thick drift cover and high vegetation (e.g., compare the Landsat image in Figure 1 with other processed RADARSAT-1 images in Figures 20 to 31). The methodology developed in the present study combines the use of RADARSAT-1 images, DEM derived from the RADARSAT-1 images, SRTM DEM and NTS DEM, and appears to be useful for lineament detection. This methodology is also potentially applicable to other parts of northern Alberta, as these areas are also covered by relatively thick drift and highly vegetated.

A comparison of the existing lineaments with those interpreted in the present study (compare Figures 2 and 48) indicates that the present study has considerably improved the detail and location accuracy of the lineaments for the study area. A comparison of the interpreted lineaments with the existing drillholes for uranium exploration indicates that considerable association exists (Figure 48). However, the association of interpreted lineaments with definite bedrock structures has not been fully investigated. Nonetheless, the lineaments interpreted in the present study can be used as basis for further investigation of selected bedrock structures and hopefully assist ongoing uranium exploration within the Maybelle River area.

TOTAL LINEAMENT LENGTH
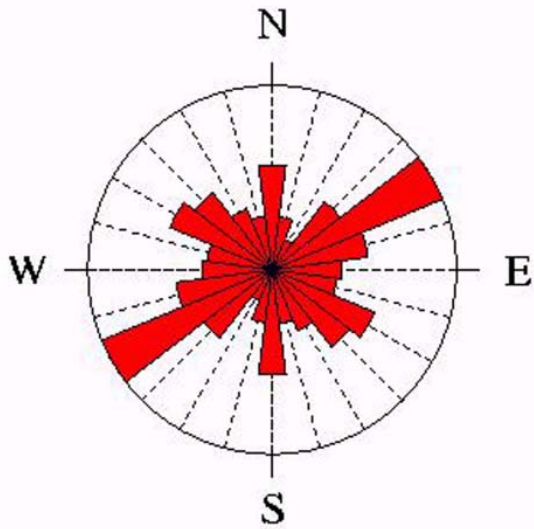
Total Lineaments: 388   Bin Size: 15.0 deg
Max Count: 53

Figure 46. Rose diagram of all interpreted lineaments, based on the total length of lineaments within each bin. The bin size is 15 degrees, and the total number of lineaments is 388.

NUMBER OF LINEAMENTS
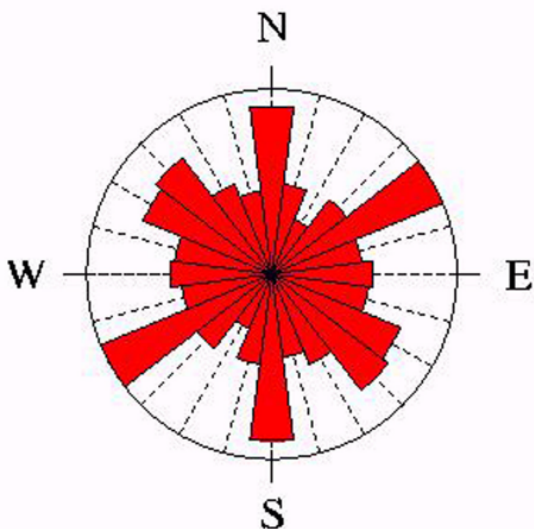
Total Lineaments: 388   Bin Size: 15.0 deg
Max Count: 53

Figure 47. Rose diagram of all interpreted lineaments, based on the number of lineaments within each bin. The bin size is 15 degrees, and the total number of lineaments is 388.
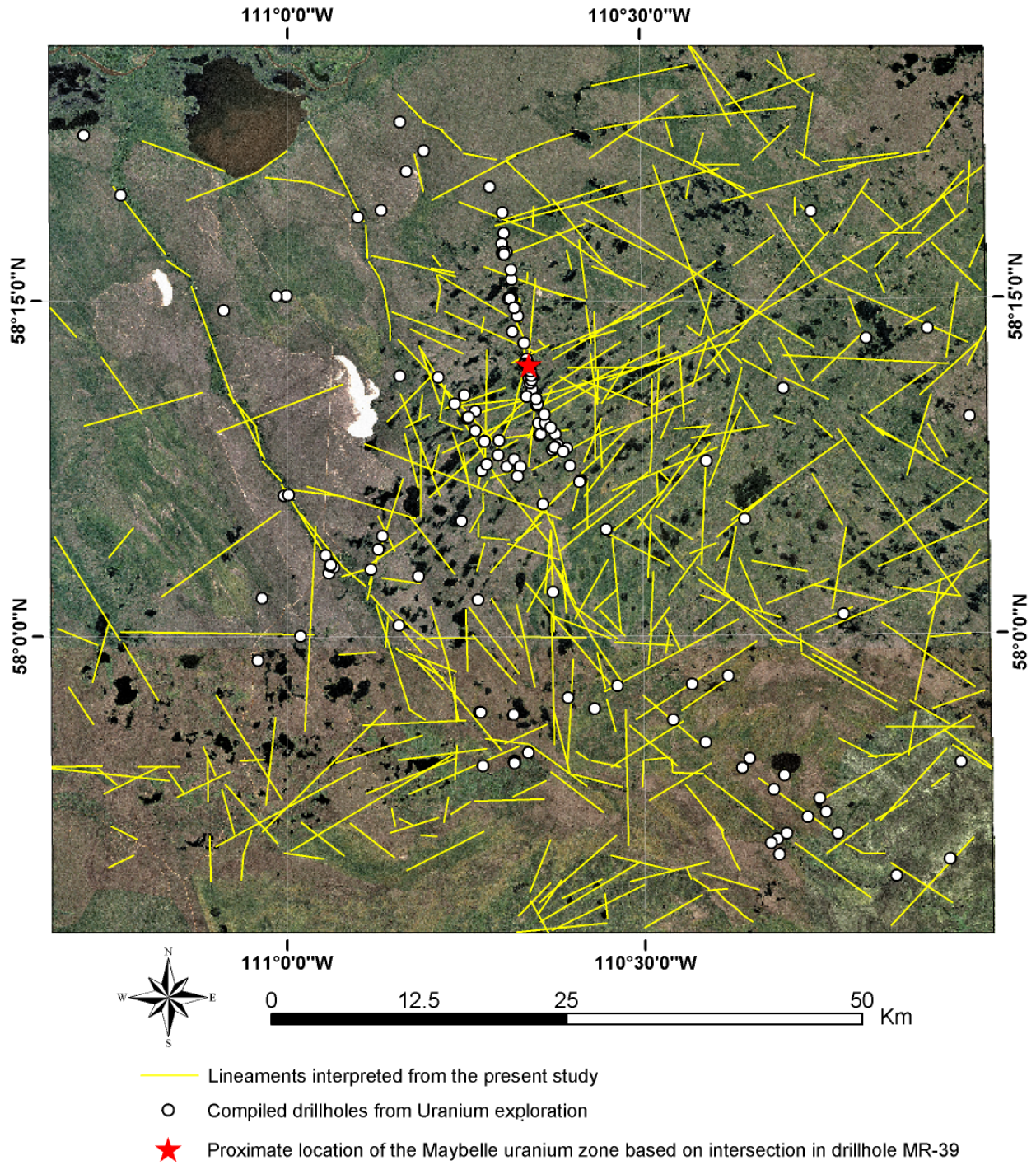
Figure 48. Comparison of interpreted lineaments with existing drillholes for Uranium exploration.

7 References

Alberta Geological Survey (AGS) (2003): Geology of Alberta; URL <http://www.ags.gov.ab.ca/GIS/gis_
and_mapping.shtml> April 7, 2004.

Bayrock L.A. (1970a): Surficial geology of the Fort Chipewyan area, Alberta, NTS 74L: Alberta Energy
and Utilities Board, EUB/AGS Map 141.

Bayrock L.A. (1970b): Surficial geology of the Bitumount area, Alberta, NTS 74E: Alberta Energy and
Utilities Board, EUB/AGS Map 140.

Card, C.D., Campbell, J.E. and Slimmon, W.L. (2003): Basement lithologic framework and structural
features of the western Athabasca basin; *in* Summary of Investigations 2003, volume 2,
Saskatchewan Geological Survey, Saskatchewan Industry resources, Misc. Rep. 2003-4.2, CD-ROM,
Paper D-3, 17 p.

Casas, A., Cortes, A., Maestro, A., Soriano, M.A., Riaguas, A. and Bernal, J. (2000): LINDENS: A
program for lineament length and density analysis; Computers and Geosciences, v. 26, p. 1011-1022.

Collier, B. (in press): Sequence stratigraphy and its use for uranium exploration in the western Athabasca
Basin of Alberta and Saskatchewan; Alberta Energy and Utilities Board, EUB/AGS Earth Sciences
Report 2004-01.

Pana, D.I., Creaser, R.A., Muehlenbachs, K. and Wheatley, K., (in press): Basement Geology in the
Alberta portion of the Athabasca Basin, context for the Maybelle River uranium prospect; in
EXTECH IV: Athabasca Basin Uranium Multidisciplinary Study, Saskatchewan and Alberta; C.W.
Jefferson and G. Delaney (ed.) Geological Survey of Canada Bulletin 588; Saskatchewan Geological
Society Special Publication 17; and Mineral Deposits Division of Geological Association of Canada
Special Publication 4.

Eccles, D.R., Grunsky, E.C., Grobe, M. and Weiss, J.(2001): Structural emplacement model for
kimberlitic diatremes in northern Alberta, Alberta Energy and Utilities Board, EUB/AGS, Earth
Sciences Report 2000-01, 103 p.

Graham, D.F. and Grant, D.R. (1994): Airborne SAR for surficial geologic mapping; Canadian Journal of
Remote Sensing, Special Issue on Radar Geology, v. 20, no. 3, p. 319-323.

Grunsky, E.C. (2002a): Satellite imagery catalogue; Alberta Energy and Utilities Board, EUB/AGS Geo-
Note 2002-18, 24 p.

Grunsky, E.C. (2002b): The application of principal components analysis to multi-beam RADARSAT-1
satellite imagery – a tool for land cover and terrain mapping; Canadian Journal of Remote Sensing,
v. 28, no. 6, p. 758-769.

Gupta, R.P. (1991): Remote Sensing Geology; Springer-Verlag, New York, 356 p.

Harris, J. (1984): Lineament mapping of central Nova Scotia using Landsat-MSS and SEASAT-
SAR imagery; *in* Proceedings of the 9th Canadian Symposium on Remote Sensing, St. John's,
Newfoundland, p. 359-373.

Harris, J.R., Bowie, C., Rencz, A.N. and Graham, D. (1994): Computer enhancement techniques for the
integration of remotely sensed, geophysical, and thematic data for the geosciences; Canadian Journal
of Remote Sensing, v. 20, no. 3, p. 210-221.

Heddi, M., Eastaff, D.J. and Petch, J. (1999): Relationships between tectonic and geomorphological linear features in the Guadix-Baza basin, southern Spain; Earth Surface Processes and Landforms v. 24, p. 931-942.

Leberl, F. (1990): Radargrammetric Image Processing; Norwood, MA, Artech House, 700 p.

Lowman, P.D., Harris., J. Masuoka, P.M., Singhroy, V.H. and Slaney, V.R. (1987): Shuttle imaging radar (SIR-B) investigations of the Canadian Shield: initial report; IEEE Transactions on Geoscience and Remote Sensing, v. GE-25, no. 1, January 1987, p. 55-66.

Masuoka, P.M., Harris. J., Lowman, P.D. and Blodget, H.W. (1988): Digital processing of orbital radar data to enhance geologic structure: examples from the Canadian Shield; Photogrammetric Engineering and Remote Sensing, v. 54, no. 5, May 1988, p. 621-632.

Mei, Shilong (2004a): Orthorectified and principal component RADARSAT-1 image dataset for NTS 73M, Alberta; Alberta Energy and Utilities Board, EUB/AGS Geo-Note 2003-11, 10 p.

Mei, Shilong (2004b): Orthorectified and principal component RADARSAT-1 image dataset for NTS 74D, Alberta; Alberta Energy and Utilities Board, EUB/AGS Geo-Note 2003-12, 10 p.

Mei, Shilong (2004c): Orthorectified and principal component RADARSAT-1 image dataset for NTS 74E, Alberta; Alberta Energy and Utilities Board, EUB/AGS Geo-Note 2003-13, 10 p.

Mei, Shilong (2004d): Orthorectified and principal component RADARSAT-1 image dataset for NTS 74L, Alberta; Alberta Energy and Utilities Board, EUB/AGS Geo-Note 2003-14, 10 p.

Mei, Shilong (2004e): Orthorectified and principal component RADARSAT-1 image dataset for NTS 74M, Alberta; Alberta Energy and Utilities Board, EUB/AGS Geo-Note 2003-15, 10 p.

Mei, Shilong (2004f): Orthorectified and principal component RADARSAT-1 image dataset for NTS 83M, Alberta; Alberta Energy and Utilities Board, EUB/AGS Geo-Note 2003-16, 10 p.

Mei, Shilong (2004g): Orthorectified and principal component RADARSAT-1 image dataset for NTS 83N, Alberta; Alberta Energy and Utilities Board, EUB/AGS Geo-Note 2003-17, 10 p.

Mei, Shilong (2004h): Orthorectified and principal component RADARSAT-1 image dataset for NTS 83O, Alberta; Alberta Energy and Utilities Board, EUB/AGS Geo-Note 2003-18, 10 p.

Mei, Shilong (2004i): Orthorectified and principal component RADARSAT-1 image dataset for NTS 83P, Alberta; Alberta Energy and Utilities Board, EUB/AGS Geo-Note 2003-19, 10 p.

Mei, Shilong (2004j): Orthorectified and principal component RADARSAT-1 image dataset for NTS 84A, Alberta; Alberta Energy and Utilities Board, EUB/AGS Geo-Note 2003-20, 10 p.

Mei, Shilong (2004k): Orthorectified and principal component RADARSAT-1 image dataset for NTS 84B, Alberta; Alberta Energy and Utilities Board, EUB/AGS Geo-Note 2003-21, 10 p.

Mei, Shilong (2004l): Orthorectified and principal component RADARSAT-1 image dataset for NTS 84C, Alberta; Alberta Energy and Utilities Board, EUB/AGS Geo-Note 2003-22, 10 p.

Mei, Shilong (2004m): Orthorectified and principal component RADARSAT-1 image dataset for NTS 84D, Alberta; Alberta Energy and Utilities Board, EUB/AGS Geo-Note 2003-23, 10 p.

Mei, Shilong (2004n): Orthorectified and principal component RADARSAT-1 image dataset for NTS 84E, Alberta; Alberta Energy and Utilities Board, EUB/AGS Geo-Note 2003-24, 10 p.

Mei, Shilong (2004o): Orthorectified and principal component RADARSAT-1 image dataset for NTS 84F, Alberta; Alberta Energy and Utilities Board, EUB/AGS Geo-Note 2003-25, 10 p.

Mei, Shilong (2004p): Orthorectified and principal component RADARSAT-1 image dataset for NTS 84G, Alberta; Alberta Energy and Utilities Board, EUB/AGS Geo-Note 2003-26, 10 p.

Mei, Shilong (2004q): Orthorectified and principal component RADARSAT-1 image dataset for NTS 84H, Alberta; Alberta Energy and Utilities Board, EUB/AGS Geo-Note 2003-27, 10 p.

Mei, Shilong (2004r): Orthorectified and principal component RADARSAT-1 image dataset for NTS 84I, Alberta; Alberta Energy and Utilities Board, EUB/AGS Geo-Note 2003-28, 10 p.

Mei, Shilong (2004s): Orthorectified and principal component RADARSAT-1 image dataset for NTS 84J, Alberta; Alberta Energy and Utilities Board, EUB/AGS Geo-Note 2003-29, 10 p.

Mei, Shilong (2004t): Orthorectified and principal component RADARSAT-1 image dataset for NTS 84K, Alberta; Alberta Energy and Utilities Board, EUB/AGS Geo-Note 2003-30, 10 p.

Mei, Shilong (2004u): Orthorectified and principal component RADARSAT-1 image dataset for NTS 84L, Alberta; Alberta Energy and Utilities Board, EUB/AGS Geo-Note 2003-31, 10 p.

Mei, Shilong (2004v): Orthorectified and principal component RADARSAT-1 image dataset for NTS 84M, Alberta; Alberta Energy and Utilities Board, EUB/AGS Geo-Note 2003-32, 10 p.

Mei, Shilong (2004w): Orthorectified and principal component RADARSAT-1 image dataset for NTS 84N, Alberta; Alberta Energy and Utilities Board, EUB/AGS Geo-Note 2003-33, 10 p.

Mei, Shilong (2004x): Orthorectified and principal component RADARSAT-1 image dataset for NTS 84O, Alberta; Alberta Energy and Utilities Board, EUB/AGS Geo-Note 2003-34, 10 p.

Mei, Shilong (2004y): Orthorectified and principal component RADARSAT-1 image dataset for NTS 84P, Alberta; Alberta Energy and Utilities Board, EUB/AGS Geo-Note 2003-35, 10 p.

Misra, K.S., Slaney, V.R., Graham, D. and Harris, J. (1991): Mapping of basement and other tectonic features using SEASAT and Thematic Mapper in hydrocarbon-producing areas of the Western Sedimentary Basin of Canada; Canadian Journal of Remote Sensing, v. 17, no. 2, p. 137–151.

Moon, W.M., Won, J.S., Singhryo, V. and Lowman, P.D. (1994): ERS-1 and CCRS C-SAR data integration for look-direction bias correction using wavelet transform; Canadian Journal of Remote Sensing, Special Issue on Radar Geology, v. 20, no. 3, p. 280-285.

Paganelli, F. and Rivard, B. (2002): Contribution of the synergy of RADARSAT-1 and seismic imagery interpretation in the structural geology of the central Alberta Foothills, Canada, as an aid for oil and gas exploration; Canadian Journal of Remote Sensing, v. 28, no. 5, p. 686–700.

Paganelli, F., Grunsky, E.C., Richards J.P. and Pryde R. (2003): Use of RADARSAT-1 principal component imagery for structural mapping: a case study in the Buffalo Head Hills area, northern central Alberta, Canada; Canadian Journal of Remote Sensing, v. 29, no. 1, p. 111–140.

Paillou, P. and Gelautz, M. (1999): Relief reconstruction from SAR stereo pairs: the "optimal gradient" matching method; IEEE Transactions on Geoscience and Remote Sensing, v. 37, p. 2099-2106.

PCI Geomatica (1997): Orthorectification and DEM extraction, Vol. 2, Chapter 13, "Using PCI Software," p.333-342.

Pryde, R. (2000): Buffalo Head Hills property AEC structural interpretation map, scale 1: 250 000; Ashton Mining of Canada Inc., North Vancouver, B.C.

RADARSAT International (RSI) (1999): RADARSAT Illuminated: Your Guide to Products & Services, RADARSAT user guide; RSI.

Ramaekers, P. (2004): Development, stratigraphy and summary diagenetic history of the Athabasca Basin, Early Proterozoic of Alberta and its relation to uranium potential; Alberta Energy and Utilities Board, EUB/AGS Special Report 62, 85 p.

Richards, J.A. (1986): Remote Sensing Digital Image Analysis; Springer-Verlag, New York, 281 p.

Ross, G.M. (1990): Deep crust and basement structure of the Peace River Arch: constraints on mechanism of formation; Bulletin of Canadian Petroleum Geology, v. 38A, p. 25–35.

Saskatchewan Geological Survey (1994): Geology and Mineral Resources of Saskatchewan; Saskatchewan Energy and Mines, Misc. Rep. 94-6, 99 p.

Toutin, T. (1999): Error tracking of radargrammetric DEM from RADARSAT images; IEEE Transactions on Geoscience and Remote Sensing, v. 37, no. 5, p. 2227-2238.

Toutin, T. and Gray, L. (2000): State-of-the-art of elevation extraction from satellite SAR data; ISPRS Journal of Photogrammetry and Remote Sensing, v. 55, p. 13-33.